LAFORA DISEASE: MECHANISMS INVOLVED IN PATHOGENESIS

Punitee Garyali

Submitted to the faculty of the University Graduate School
in partial fulfillment of the requirements
for the degree
Doctor of Philosophy
in the Department of Biochemistry and Molecular Biology
Indiana University

September 2014

Accepted by the Graduate Faculty, of Indiana University, in partial
fulfillment of the requirements for the degree of Doctor of Philosophy.

_____
Peter J. Roach, Ph.D., Chair

Doctoral Committee

_____
Anna A. DePaoli-Roach, Ph.D.

July 15, 2014

_____
Maureen A. Harrington, Ph.D.

_____
Nuria Morral, Ph.D.

_____
Amber Mosley, Ph.D.

DEDICATION

To my GrandMa,

who taught me to fight till the end and never give up.

ACKNOWLEDGEMENTS

Punitee Garyali

LAFORA DISEASE: MECHANISMS INVOLVED IN PATHOGENESIS

Lafora disease is a neurodegenerative disorder caused by mutations in either the *EPM2A* or the *EPM2B* gene that encode a glycogen phosphatase, laforin and an E3 ubiquitin ligase, malin, respectively. A hallmark of the disease is accumulation of insoluble, poorly branched, hyperphosphorylated glycogen in brain, muscle and heart. The laforin-malin complex has been proposed to play a role in the regulation of glycogen metabolism and protein degradation/quality control. We evaluated three arms of protein quality control (the autophago-lysosomal pathway, the ubiquitin-proteasomal pathway, and ER stress response) in embryonic fibroblasts from *Epm2a-/-*, *Epm2b-/-* and *Epm2a-/- Epm2b-/-* mice. There was an mTOR-dependent impairment in autophagy, decreased proteasomal activity but an uncompromised ER stress response in the knockout cells. These defects may be secondary to the glycogen overaccumulation. The absence of malin, but not laforin, decreased the level of LAMP1, a marker of lysosomes, suggesting a malin function independent of laforin, possibly in lysosomal biogenesis and/or lysosomal glycogen disposal. To understand the physiological role of malin, an unbiased diGly proteomics approach was developed to search for malin substrates. Ubiquitin forms an isopeptide bond with lysine of the protein upon ubiquitination. Proteolysis by trypsin cleaves the C-terminal Arg-Gly-Gly residues in ubiquitin and yields a diGly remnant on the peptides. These diGly peptides were immunoaffinity purified using anti-diGly antibody and then analyzed by mass spectrometry. The mouse skeletal muscle

ubiquitylome was studied using diGly proteomics and we identified 244 non-redundant ubiquitination sites in 142 proteins. An approach for differential dimethyl labeling of proteins with diGly immunoaffinity purification was also developed. diGly peptides from skeletal muscle of wild type and *Epm2b*-/- mice were immunoaffinity purified followed by differential dimethyl labeling and analyzed by mass spectrometry. About 70 proteins were identified that were present in the wild type and absent in the *Epm2b*-/- muscle tissue. The initial results identified 14 proteins as potential malin substrates, which would need validation in future studies.

Peter J. Roach, Ph.D., Chair

TABLE OF CONTENTS

LIST OF TABLES

LIST OF FIGURES

LIST OF ABBREVIATIONS

AGL	Amylo-1,6-glucosidase, 4-α-glucanotransferase
AMP	Adenosine monophosphate
AMPK	AMP activated protein kinase
ATG	Autophagy-related gene
ATP	Adenosine triphosphate
BE	Branching enzyme
BSA	Bovine serum albumin
C2	Carbon 2
C3	Carbon 3
C6	Carbon 6
$CaCl_2$	Calcium chloride
CAM	Carboxyacetamide
CBD	Carbohydrate-binding domain
Cys	Cysteine
Da	Dalton
DBE	Glycogen debranching enzyme
DSPD	Dual specificity phosphatase
DTT	Dithiothreitol
EDTA	Ethylenediaminetetraacetic acid
EGTA	Ethyleneglycol-O,O'-bis(2-aminoethyl)-N,N,N',N'-tetraacetic acid
Epm2a	Epilepsy progressive myoclonus type 2a

Epm2b	Epilepsy progressive myoclonus type 2b
ER	Endoplasmic reticulum
FBS	Fetal bovine serum
GAA	Lysosomal acid- α-glucosidase
GAPDH	Glyceraldehyde-3-phosphate dehydrogenase
GABARAP	γ-amino butyric acid receptor-associated protein
GABARAPL1	γ-amino butyric acid receptor-associated protein-like 1
GBE	Branching enzyme
G-1P	Glucose-1 phosphate
G-6P	Glucose-6 phosphate
Glc	Glucose
GLUT	Sodium independent glucose transporter
GN	Glycogenin
GP	Glycogen phosphorylase
GS	Glycogen synthase
GSK3	Glycogen synthase kinase-3
GSD	Glycogen storage disorder
GT	Glycosyl transferases
HEPES	4-(2-Hydroxyethyl)piperazine-1-ethanesulfonic acid
HCl	Hydrochloric acid
HK	Hexokinase
IAP	Immunoaffinity purification
LB	Lafora body

LC3	Microtubule-associated protein 1A/1B-light chain 3
LD	Lafora disease
MEFs	Mouse embryonic fibroblasts
$MgCl_2$	Magnesium chloride
MGSKO	Muscle glycogen synthase knockout
MS	Mass spectrometry
NaCl	Sodium chloride
NaOH	Sodium hydroxide
$NADP^+$	Nicotinamide adenine dinucleotide phosphate
NaOAc	Sodium acetate
NEM	N-ethylmalemide
ND	Not detectable
NH_4HCO_3	Ammonium bicarbonate
NHL	NCL-1, HT2A and LIN-41
NHLRC1	NHL repeat-containing protein 1
NH_4OH	Ammonium hydroxide
NMR	Nuclear magnetic resonance
OH	Hydroxyl
PAS	Periodic acid-Schiff
PBS	Phosphate buffer saline
PCR	Polymerase chain reaction
PFK	Phosphofructokinase
PGM	Phosphoglucomutase

Ph	Phosphorylase
PIP$_2$	Phosphatidylinositol (4,5) bisphosphate
PIP$_3$	Phosphatidylinositol (3,4,5) trisphosphate
PKA	cAMP dependent protein kinase/protein kinase A
PI3K	Phosphatidylinositol-3-kinase
PKB/Akt	Protein kinase B
PLP	Pyridoxal phosphate
PMSF	Phenylmethylsulfonylfluoride
PP1c	Protein phosphatase-1, catalytic subunit
PP1G	Glycogen associated phosphatase
PVDF	Polyvinylidene fluoride
PYGM	Glycogen phosphorylase, muscle
PYGL	Glycogen phosphorylase, liver
PTG	Protein targeted to glycogen
RING	Really interesting new gene
RIPA	Radioimmunoprecipitation assay buffer
RT	Room temperature
SDS	Sodium dodecyl sulphate
SDS-PAGE	Sodium dodecyl sulphate polyacrylamide gel electrophoresis
SEX4	Starch excess-4
SM	Skeletal muscle
STBD1	Starch-binding domain-containing protein 1

TBS	Tris-buffered saline
TBST	Tris-buffered saline containing tween-20
TCEP	(tris(2-carboxyethyl)phosphine)
TFA	Trifluoroacetic acid
TLCK	N-p-tosyl-1-lysine chloromethyl ketone
Tris	Tris(hydroxymethyl)aminomethane
TOF	Time of flight
Ub	Ubiquitin
UDP	Uridine diphosphate
UDPG	Uridine diphosphate glucose
UGP	UDP-glucose pyrophosphorylase
UGPPase	UDP-glucose pyrophosphatase
UMP	Uridine monophosphate
UTP	Uridine triphosphate
WT	Wild type

INTRODUCTION

1. Glycogen Structure

Glycogen is a branched polymer of glucose that serves as a means to store glucose in times of nutritional plenty for utilization in times of need. In mammals, the large majority of glycogen is found in skeletal muscle and liver but other tissues such as kidney, heart, adipose tissue and brain are also capable of synthesizing glycogen (1). Polymerization of glycogen occurs via α-1,4-glycosidic linkages between glucose residues. Branch points are introduced via α-1,6-glycosidic linkages at the C6 hydroxyl of a glucose residue in the chain (Figure 1). The glycogen structure has inner B-chains, which would normally contain two branch points, and outer A-chains, which are unbranched (Figure 2). A full-size glycogen molecule consists of 12 tiers with about 55000 glucose residues, a molecular mass of $\sim 10^7$ kDa and a diameter of ~44nm (2,3). The frequency of the branch point, about 1 every ~12 residues, determines the structure, topology and solubility of glycogen. Glycogen molecules cannot be detected by light microscopy but can be visualized under the electron microscope. They have been described as rosette-like β-particles in muscle and larger α-particles in liver (4), the latter being aggregations of the former.

Glycogen predominantly contains glucose residues but it also contains traces of glucosamine (5,6) and phosphate (7). Of the two, the covalent phosphate has been most studied. In the 1980s, phosphate was reported to be an integral part of glycogen (7). Recent work has shown the frequency of
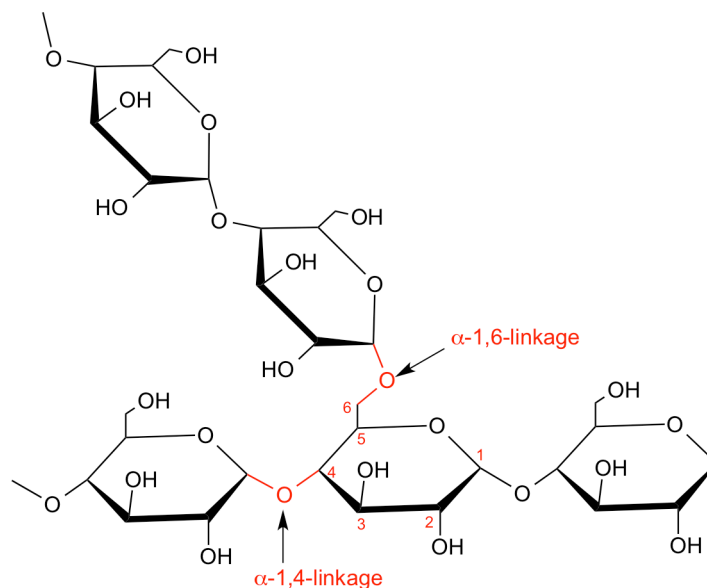
Figure 1. Glycosidic Linkages in Glycogen. Polymerization occurs at α-1,4 glycosidic linkages and branching occurs are α-1,6 glycosidic linkages. The numerical nomenclature of the carbons is represented in one of the glucose molecules.
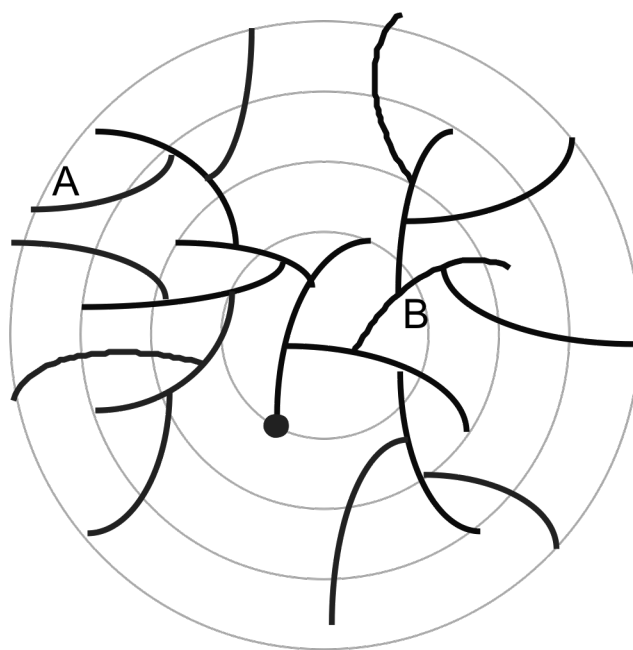
Figure 2. Glycogen Structure. A tiered model for glycogen organization in which the outer A-chains are unbranched and the inner B-chains carry an average of two branches. The black circle represents glycogenin.

glycogen phosphorylation as one phosphate for ~650 glucoses in rabbit skeletal muscle and one per ~2000 residues in mouse muscle glycogen (8,9). Furthermore, mass spectrometry (MS) and nuclear magnetic resonance (NMR) analyses have shown that the phosphate exists as C2-, C3 and C6-phosphomonoesters (10,11). A mechanism for the introduction of C2-phosphate via a side reaction of the normal synthetic enzyme glycogen synthase has been proposed (12). The origin of the other phosphates is less clear at this time. The physiological role, if any, of phosphate is not known; however excessive phosphorylation of glycogen is associated with a neurodegenerative disorder, Lafora disease (see section 5). Phosphate is also present as C3- and C6-phosphomonoesters in plant amylopectin, a complex carbohydrate similar in structure to mammalian glycogen (13). Introduction of phosphate into amylopectin is mediated by dikinase enzymes (14) and is thought to play a critical role in disrupting the semi-crystalline structure of the polymer during its degradation (15). Besides phosphate, there are also trace amounts of glucosamine in rabbit liver glycogen, but not in the skeletal muscle and heart glycogen (5). The role of glucosamine in glycogen is not well understood, although it is thought that glucosamine can be incorporated into glycogen by glycogen synthase using UDP-glucosamine as the glucosyl donor (5).

A glycogen molecule undergoes multiple cycles of expansion and contraction, potentially accumulating chemical and metabolic insults in each cycle. This results in an aberrant structure that sometimes escapes normal metabolism leading to formation of an insoluble material similar to other insoluble

deposits in various neurological diseases. In normal aging tissues, even in the absence of disease glycogen-like deposits are observed such as corpora amylacea in brain (16) and cardiac colloid in heart (17), which supports the idea that these chemical modifications in glycogen may reflect the age of the molecule and its need for disposal (18).

There are several proteins associated with glycogen (19-23) and glycogen along with the proteins and elements of the sarcoplasmic reticulum have been termed 'glycogen particles' (24,25) (Figure 3). The glycogen associating proteins bind to glycogen, sometimes to each other and to membranes. The known glycogen-associated protein include glycogenin, the initiator of glycogen synthesis, the metabolic enzymes glycogen synthase, glycogen phosphorylase, debranching enzyme AGL and regulatory proteins such as phosphorylase kinase and members of the protein phosphatase 1G family (26). The β-subunit of AMP-activated protein kinase (AMPK) has been shown to bind to glycogen (27,28) via its carbohydrate-binding module 20 domain (CBM20) (29,30). Recently, laforin (31,32) and starch-binding domain protein 1 (Stbd1) or genethonin (33,34) have been identified as glycogen-binding proteins via a CBM20 domain. The branching enzyme interacts with glycogen but it does not form a stable association (34). All glycogen-associating proteins have been shown to play a functional role in the metabolism of glycogen.
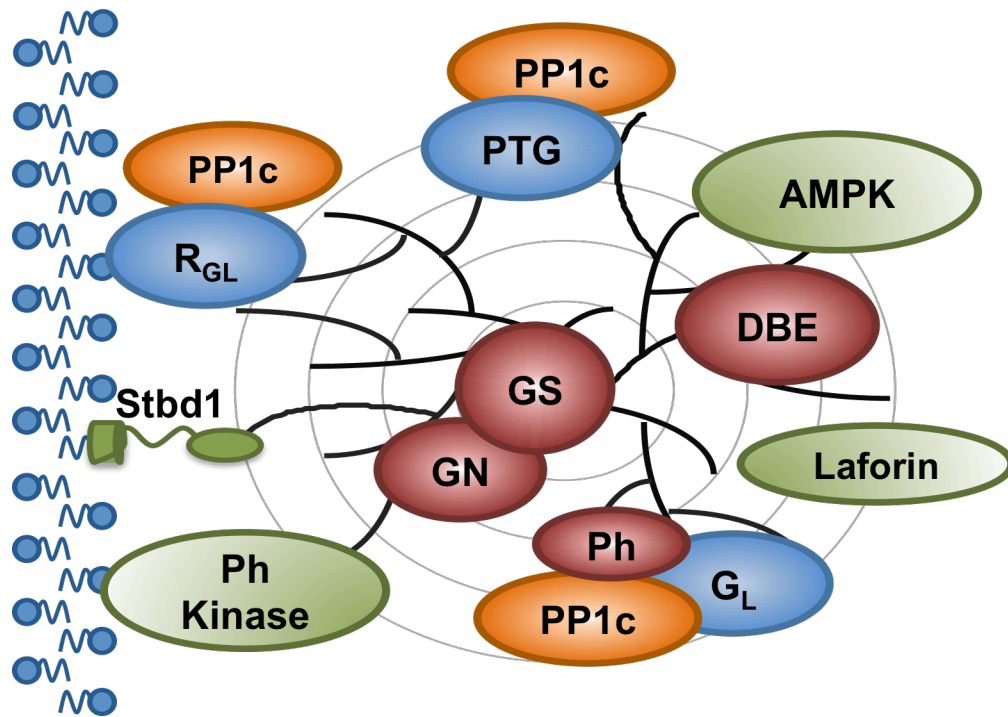
Figure 3. Glycogen Particles. Glycogen-associated proteins: the metabolic enzymes glycogenin (GN), glycogen synthase (GS), phosphorylase (Ph) and debranching enzyme (DBE); the phosphatases type 1 catalytic subunit (PP1c) and laforin; the protein kinases phosphorylase kinase and AMPK; the PP1 glycogen-targeting subunits R_{GL}, G_L and PTG; the membrance-anchoring protein Stbd1. Stbd1, R_{GL} and phosphorylase kinase anchor to membranes.

2. Glycogen Metabolism

Glycogen synthesis, glycogenesis, and breakdown, glycogenolysis, are both highly regulated processes. The precursors for glycogen synthesis are either glucose, derived from newly ingested carbohydrate, or gluconeogenic precursors, such as alanine or lactate in an indirect glyconeogenesis pathway (35). Glycogenesis (Figure 4) is triggered with the entry of glucose in the cell by one or more of the several glucose transporters (GLUTs) (36). The enzyme glucokinase/hexokinase converts glucose to glucose-6-phosphate (G6P). G6P is then converted to glucose-1-phosphate (G1P) by phosphoglucomutase (PGM) that is required for the formation of uridine diphosphoglucose (UDPG) by UDPG pyrophosphorylase (UGP). Glycogen synthesis is initiated by the specialized self-glycosylating protein glycogenin (37-39), a member of the family 8 retaining glycosyltransferases (GT8). Glycogenin forms a short glucose polymer by self-glycosylation reactions using UDPG as substrate. Glycogenin can interact directly with glycogen synthase via its C-terminus. Glycogen synthase (GS) then catalyzes the bulk formation of the glycogen molecule by adding new glucose residues via α-1,4-glycosidic linkages. The glycogen branching enzyme (GBE) introduces the branchpoints via α-1,6-glycosidic linkages every ~12 glucose residues. GBE cleaves an α-1,4-glycosidic linkage, excises a segment of the existing oligosaccharide and reforms an α-1,6-glycosidic linkage. The rate-limiting step in glycogenesis is the reaction catalyzed by glycogen synthase.

The initiation of glycogenolysis (Figure 4) occurs by the rate-limiting enzyme glycogen phosphorylase (GPh). GPh belongs to the family of retaining

glycosyltransferases (GT35). It catalyzes the phosphorolytic breakdown of the α-1,4-glycosidic linkages of glycogen to produce glucose-1-phosphate and glycogen$_{(n-1)}$ (1). GPh activity requires pyridoxal phosphate (PLP) as a cofactor involved in the acid/base catalysis by phosphorylase. GPh stalls four glucose residues from an α-1,6-glycosidic linkage necessitating the action of another enzyme, the glycogen debranching enzyme (AGL). There are two catalytic activities in two separate domains associated with AGL. The N-terminal domain has α-amylase-like activity which hydrolyzes an α-1,4-glycosidic linkage to leave a single branched residue in an α-1,6-glycosidic linkage and reforms an α-1,4-glycosidic linkage between the detached glucose residues and the main chain. The C-terminus of AGL contains a domain with amylo-1,6-glucosidase activity that removes the remaining branched glucose residue.

Glycogen metabolism is controlled hormonally via covalent modification and allosteric ligand binding of key enzymes involved in glycogen synthesis and degradation (Figure 5). Glycogen synthase is regulated by covalent phosphorylation of 9 or more sites at the N- and C-termini (1). Phosphorylation inactivates GS and dephosphorylation activates the enzyme. Glycogen synthase kinase-3 (GSK-3) phosphorylates four important regulatory sites of GS, thus inhibiting its activity (1). Type-1 protein phosphatase (PP1) associates with one of several glycogen-binding targeting subunits including RGL (G_M) and PTG and mediates dephosphorylation of GS. Phosphorylation and allosteric ligand binding also regulate glycogen phosphorylase, which is activated by phosphorylation and inactivated by dephosphorylation. Phosphorylase kinase phosphorylates and

activates GPh and PP1 catalyzes the dephosphorylation and inactivation of GPh (Figure 5).

In mammals, the postprandial rise in blood glucose triggers the secretion of insulin from β-cells of the pancreas into the bloodstream. Insulin binds to the insulin receptor of the peripheral tissues and triggers the uptake of glucose, raising the levels of intracellular glucose-6-phosphate, which activates glycogen synthase. Insulin receptor consists of two α- and two β-subunits. Binding of insulin to the extracellular domain of the α-subunit causes a conformational change that triggers activation of the β-subunit tyrosine kinase resulting in transphosphorylation of tyrosine residues in the β-subunit. The activated kinase then phosphorylates the insulin receptor substrates. The phosphorylated tyrosines in these substrates recruit signaling molecules containing SH2 domains. Recruitment of the p85 subunits of phosphatidylinositol-3-kinase (PI3K) leads to its activation. PI3K phosphorylates the membrane lipid phosphatidylinositol-4-5-bisphosphate (PIP$_2$) converting it to phosphatidylinositol-3,4,5-triphosphate (PIP$_3$). PIP$_3$ further binds and activates the protein kinase PDK1, which phosphorylates and activates protein kinase B PKB/AKT at catalytic T308 (40). AKT, in turn, phosphorylates an N-terminal serine of GSK3 to inhibit its ability to phosphorylate and inactivate GS (41). Insulin signaling thus regulates the activity of GS by preventing its phosphorylation through inactivation of GSK3 (Figure 5). In contrast to insulin, glycogenolysis is promoted by epinephrine and glucagon in muscle and liver, respectively. A signaling cascade is initiated activating adenyl cyclase that catalyzes the conversion of ATP to cAMP. cAMP

activates PKA that phosphorylates phoshorylase kinase which in turn phosphorylates and activates glycogen phosphorylase (Figure 5).
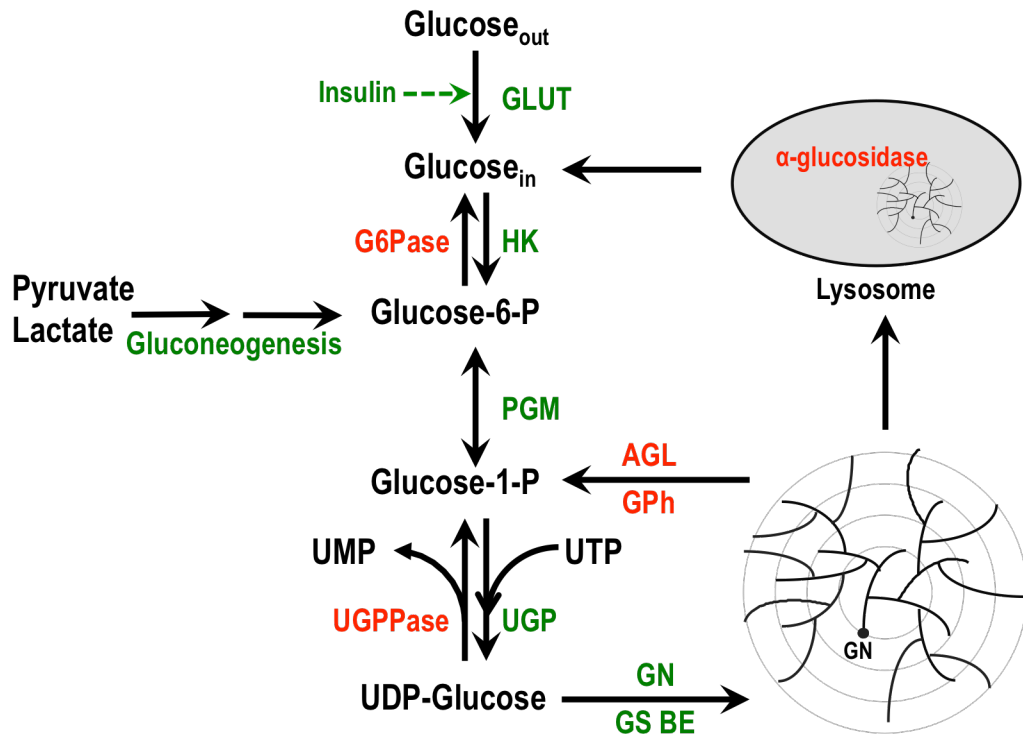
Figure 4. Glycogen Metabolism Overview. GLUT, glucose transporter; HK, hexokinase; G6Pase, glucose-6-phosphatase; PGM, phosphoglucomutase; AGL, debranching enzyme; GPh, glycogen phosphorylase; UGPPase, UDP-glucose pyrophosphatase; GN, glycogenin; GS, glycogen synthase; BE, branching enzyme.
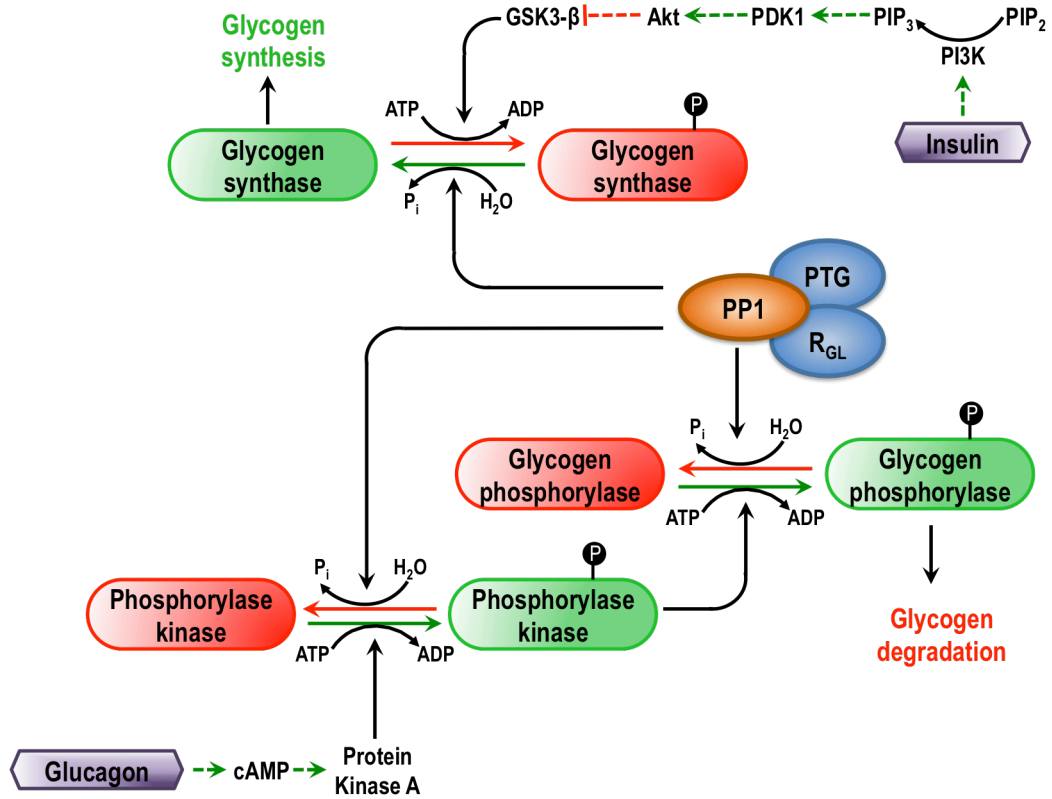
Figure 5. Regulation of Glycogen Metabolism. Schematic representation of major signaling pathways regulating glycogen metabolism. GSK3, glycogen synthase kinase 3; PIP2, phosphatidylinositol-4-5-bisphosphate; PIP3, phosphatidylinositol-3,4,5-triphosphate; PI3K, phosphotidyl inositol kinase; PP1, protein phosphatase 1.

3. Lysosomal Disposal of Glycogen

Glycogen is mainly broken down in the cytosol by glycogen phosphorylase and debranching enzymes. However, some glycogen is also transported to the lysosomes, where it is directly hydrolyzed to glucose by the action of lysosomal α-glucosidase (acid maltase, GAA) (Figure 4) (42). This is probably not the major degradation pathway, but defects in the enzyme GAA lead to accumulation of glycogen in lysosomes, causing a glycogen storage disorder, Pompe disease (OMIM 232300) (43) (see section 4.3). The exact mechanism by which glycogen is transferred to the lysosomes in unknown, but it is most likely to involve autophagy-like vesicular trafficking. Autophagy is a mechanism for recycling of cellular materials under conditions of nutritional deprivation or stress (44,45). Macroautophagy (hereafter called autophagy) is the most studied type and it involves engulfment of cargo within a double membrane to form autophagosomes that fuse with the lysosome where the cargo is ultimately degraded (46). A number of autophagy-related proteins (ATGs) are involved in the process of forming autophagosomes and eventually their fusion with lysosomes to form autophago-lysosomes (47) (Figure 6). There are variants of the basic autophagic process that have separate controls, specific cargo and different functions (48,49). 'Glycogen autophagy' has been described in the literature in livers of newborns (50). There is a prenatal accumulation of glycogen in several organs of the fetus, such as liver and heart, mainly to provide energy reserves for use during the immediate postnatal period (51), when gluconeogenesis is not well developed. Another connection of glycogen with

autophagy is provided by Pompe disease (52). The *Gaa-/-* mice show massive accumulation of glycogen in lysosomes, an increase in the glycogen containing autophagosomes and late endosomes, referred to as 'autophagic build up' (52). Raben et al. also generated mice that combined a homozygous null *GAA* mutation with muscle-specific disruption of the genes encoding autophagy-related proteins, Atg5 (53) or Atg7 (54). In both of these mice, there was a decrease in the autophagic build up in the muscle, but loss of autophagy worsened the clinical phenotype.

In *Saccharomyces cerevisiae* at the onset of nutrient deprivation, glycogen is accumulated as a carbon and energy reserve. The SNF1 gene is essential for regulation of gene expression by glucose repression and yeast mutated in SNF1 has diminished glycogen accumulation and concomitant inactivation of glycogen synthase. Analysis of an unbiased genetic screen for yeast glycogen metabolism showed that two yeast autophagy genes, *ATG1* and *ATG13* could restore the defective glycogen storage of *snf1* mutant strain (55). A genome-wide survey in yeast for genes affecting glycogen metabolism revealed ~60 genes involved in vesicular trafficking or vacuolar function, including genes encoding 13 of 17 proteins involved in structure or assembly of the vacuolar ATPase (56). These studies provide further evidence suggestive of vesicular transport of glycogen to the lysosome for degradation but the exact mechanism is not known. It is expected that glycogen would associate with membranes if it were to be involved in vesicular transport. There have been a few reports that show, using electron

microscopy, glycogen particles to be close to membranes, endoplasmic reticulum

in liver (57) or sarcoplasmic reticulum in muscle (20).
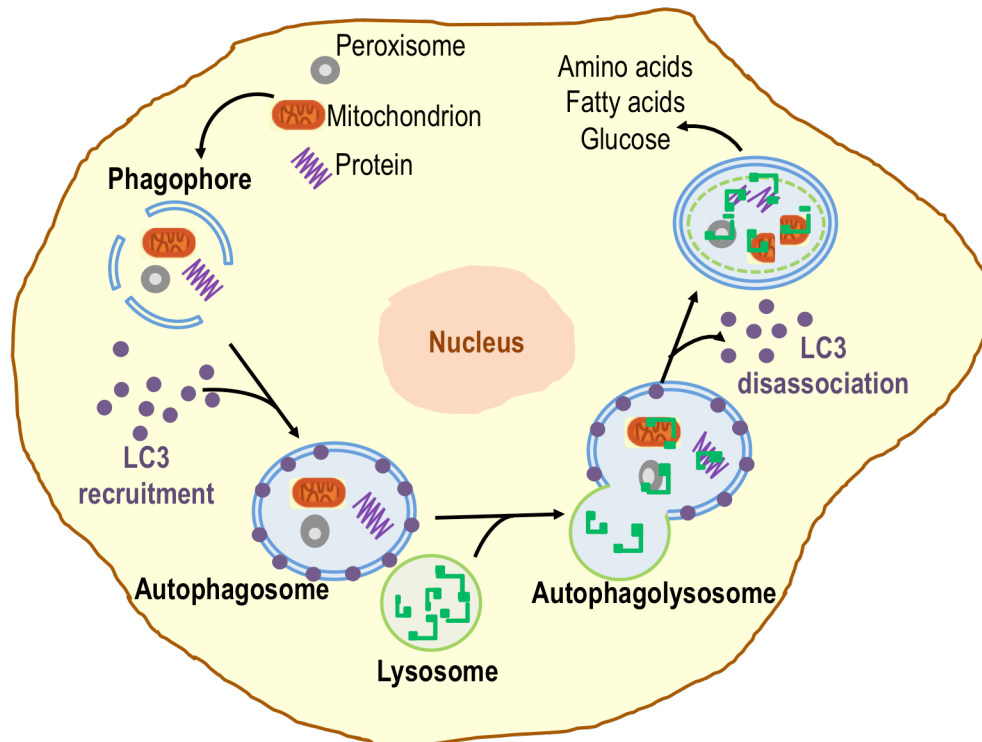
Figure 6. Autophagy. Schematic representation of the process of autophagy. Engulfment of the cargo within a double membrane leads to formation of autophagosomes that fuse with the lysosomes to form autophagolysosomes where the cargo is ultimately degraded. Microtubule associated protein 1 light chain 3 (LC3-I) is incorporated into the autophagosomes and is lipidated to LC3-II. Upon formation of the autophagolysosomes, LC3-II is recycled back to the cytosol.

In a proteomics study, starch-binding domain protein 1, Stbd1, was identified as a glycogen-associated protein and it was speculated to be involved in anchoring glycogen to membranes in different cell compartments (23). Stbd1 was first localized, as the novel human gene GENX-3414, at chromosome 4q24-q25 (58). It was proposed that the encoded protein is associated with T-tubules and sarcoplasmic reticulum (58). Janecek et al. identified the same protein in a bioinformatics study and referred to it as genethonin (59). Recent studies by Jiang et al. have shown that Stbd1 may anchor glycogen to membranes (33,60). Stbd1 has a C-terminal CBM20 domain (58) and a highly conserved N-terminal 24-residue hydrophobic sequence (Figure 7). Stbd1 binds to polysaccharides, preferentially with less branched structures such as amylopectin or glycogen isolated from mouse models of Lafora disease (33). In mice lacking glycogen, glycogen synthase knockout mice, *Gys1-/-*, Stbd1 levels are dramatically decreased, indicating a connection between glycogen metabolism and Stbd1 (33). Yeast two-hybrid studies with Stbd1 as bait identified two members of the mammalian ATG8 family of autophagic proteins; GABARAP (γ-aminobutyric acid type A receptor-associated protein) and GABARAPL1 (GABARAP-like 1) (33,60).
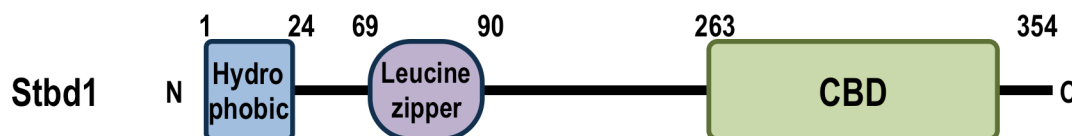
Figure 7. Starch-binding Domain Protein 1. Schematic representation of Stbd1 showing the N-terminal hydrophobic domain, the leucine zipper and the C-terminal carbohydrate-binding domain (CBD).

Co-immunoprecipitation assays confirmed the interaction of Stbd1 with GABARAPL1 (60). It was proposed that Stbd1 anchors glycogen to membranes and participates in lysosomal trafficking of glycogen, glycophagy with the help of GABARAPL1. Since Stbd1 preferentially binds to less branched glycogen, it is possible that Stbd1 plays a role in disposal of aberrant glycogen as part of quality control.

4. Glycogen Storage Diseases

Glycogen storage diseases (GSD) or glycogenoses are caused by inborn errors of metabolism involving either glycogen synthesis or degradation of the polysaccharide. As a result, glycogen is altered in quantity and/or quality.

4.1. Glycogen Storage Disease Type 0

GSD 0 is an autosomal recessive form of fasting hypoglycemia of infancy, caused by mutations in the *GYS2* gene, the liver isoform of glycogen synthase, resulting in an almost complete loss of liver glycogen. The patients have fasting hypoglycemia, high blood ketones, low levels of alanine and lactate and postprandial hyperglycemia, hyperlactatemia and hyperlipidemia (61).

4.2. Glycogen Storage Disease Type I: von Gierke's disease

It is the most common of all the glycogen storage diseases and is caused by mutations in the *G6PC* (glucose-6-phosphatase) and *G6PT* (glucose-6P translocase) genes that are required for delivery of hepatic glucose to the blood

stream. There is an accumulation of glycogen and fat in liver and kidneys and the patients suffer from hypoglycemic seizures, hepatomegaly, renomegaly, growth retardation and lactic acidosis (62,63).

4.3. Glycogen Storage Disease Type II: Pompe's disease

Pompe's disease is an autosomal recessive disorder caused by deficiency of lysosomal acid α-glucosidase enzyme resulting in an accumulation of glycogen in the lysosomes of heart and skeletal muscle as mentioned previously. Patients have mutations in *GAA* gene and present with cardiomegaly, cardiomyopathy, hypotonia, muscle weakness, failure to thrive and depending on the severity of the mutation death can ensue within the first year (43,64). Targeted disruption of the *Gaa* gene in mice reproduces the critical features of Pompe's disease, although the symptoms are milder and develop later relative to the onset of the human disease and the mice do not die (65). Studies on double *Gaa-/- Gys1-/-* mice showed a marked reduction in the heart and muscle glycogen levels, reduced lysosomal swelling and autophagic buildup and a complete reversal of cardiomegaly (66).

4.4. Glycogen Storage Disease Type III: Cori's disease

Cori's disease is an infantile autosomal recessive disorder caused by mutations in the *AGL* gene resulting in a deficiency of glycogen debranching enzyme (67). The disease is characterized by accumulation of glycogen in liver, muscles and heart presenting as infanitle hypoglycemia and failure to thrive (67).

4.5. Glycogen Storage Disease Type IV: Andersen's disease

Andersen's disease is the most severe form of glycogen storage disease with defects in the *GBE1* gene encoding the branching enzyme (68). Patients present with symptoms of hepatospleenomegaly, failure to thrive and cirrhosis of liver (69). The accumulated glycogen has long stretches of unbranched glucose chains resulting in a loss of solubility, leading to cellular dysfunction. Patients usually die within 5 years of disease onset because of liver failure.

4.6. Glycogen Storage Disease Type V: McArdle disease

McArdle disease is caused by deficiency of muscle phosphorylase because of mutations in the *PYGM* gene. Patients present in young adulthood with exercise intolerance, painful muscle cramps and early fatigue (70).

4.7. Glycogen Storage Disease Type VI: Hers' disease

Hers' disease is caused by deficiency of the liver phosphorylase due of mutations in the *PYGL* gene. Patients present with hypoglycemia, hyperlipidemia, hyperketosis, hepatomegaly and growth retardation (71).

4.8. Glycogen Storage Disease Type VII: Tarui's disease

Tarui's disease is caused by mutations in the *PFKM* gene, which encodes the muscle phosphofructokinase. The mutation causes impairment in the ability of phosphofructokinase to phosphorylate fructose-6P to fructose-1,6-bisphosphate. There is a build up of glycolytic intermediates, which are thought

to drive excessive glycogen synthesis mediated by elevation of allosteric activation of glycogen synthase by glucose-6-P. The patient presents with exercise-induced muscle cramps, myoglobinuria and hyperuricemia (72).

5. Lafora Disease

5.1. Preamble

Lafora progressive myoclonus epilepsy or Lafora disease (LD; OMIM 254780) is a fatal autosomal recessive neurodegenerative disorder. The onset of the disease is usually in the second decade of life with stimuli-sensitive grand mal tonic clonic, absence, visual and myoclonic seizures which progresses to dementia, psychosis, cerebellar ataxia, dysarthria, mutism, amaurosis and muscle wasting (73-77). Death occurs usually within 10 years of the onset because of respiratory failure. LD is diagnosed in patients by biopsy of sweat glands in the armpit that confirms the presence of pathognomonic Lafora bodies (Figure 8). Lafora bodies are composed of poorly branched, insoluble glycogen-like polymers that are periodic acid-Schiff-positive (PAS+). Lafora bodies are most commonly found in organs with the highest rates of glucose metabolism, including brain, skeletal muscle, heart and liver (73,78). LD is mostly found in parts of the world where the rate of consanguinity is high. This includes isolated ethnic populations in the Mediterranean basin of Spain, France, Italy, southern USA and Quebec, Canada, and in few regions of Central Asia, the Indian subcontinent, Africa and Middle East. There is no preventive or curative treatment available for LD yet (79).
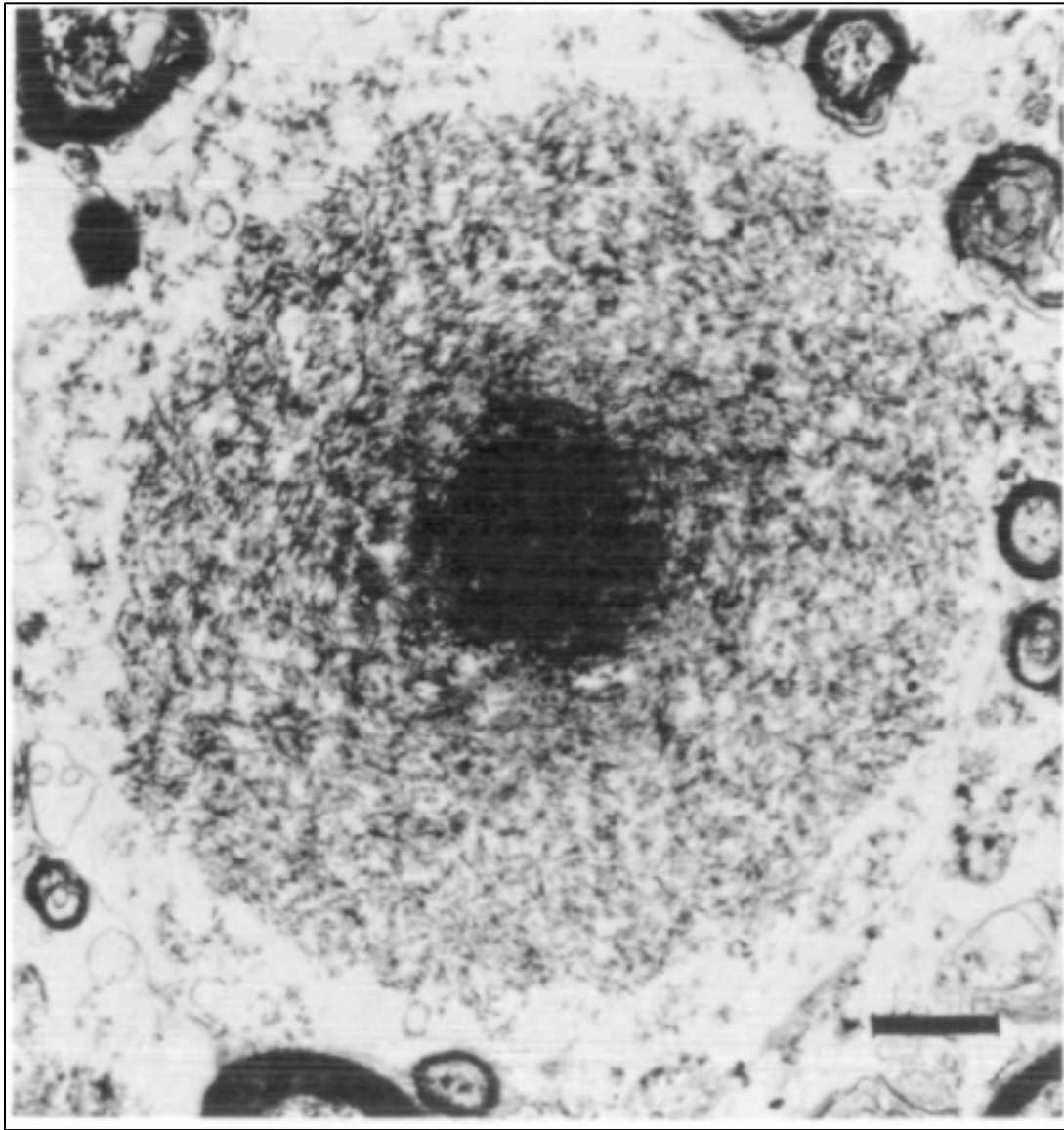
Figure 8. Lafora Body. An electron micrograph showing a layered polyglucosan Lafora body with dense center inside an unidentified cell process (80).

5.2. Clinical Homogeneity and Locus Heterogeneity in Lafora Disease

More than 95% of the cases of LD have mutation in either of the two genes Epilepsy progressive myoclonus 2A (*EPM2A*) and Epilepsy progressive myoclonus 2B (*EPM2B* or *NHLRC1*) (32,81,82). The remaining cases could result from mutations in the promoter or enhancer regions of the two known genes or from mutations in a third, as yet unidentified locus (83). To date more than 100 mutations have been reported to be associated with LD (The Lafora Progressive Myoclonus Epilepsy Mutation and Polymorphism Database, http://projects.tcag.ca/lafora/). In a meta-analysis about 100 distinct mutations were discovered in over 200 independent LD families (84). About half of the mutations were missense mutations and one-quarter were deletions. The analysis revealed that *EPM2A* mutations are more common in Spain and LD patients in Italy and France have predominantly *EPM2B* mutations. In the Indian subcontinent and Central Asia, the mutations are distributed evenly (84). Clinically, the symptoms in LD patients with mutations in either of the genes are indistinguishable. However, studies have shown that the course of disease was longer in *EPM2B* mutation patients who had a slower progression and slightly milder symptoms in comparison to patients with *EPM2A* mutation (85-88).

5.3. *EPM2A* gene

EPM2A, a 130 kb four-exon gene, was localized on chromosome 6q24 by linkage analysis and homozygosity mapping (89). LD patients are either homozygous or compound heterozygous for loss-of-function mutations (32).

EPM2A encodes a 331-residue dual-specificity phosphatase, laforin (82), which contains an N-terminal carbohydrate-binding domain (CBD) (residues 1-124) that can bind complex carbohydrates such as glycogen, amylopectin and polyglucosan (90,91). Laforin also has a C-terminal dual-specificity phosphatase domain (DSPD) (residues 157-326) with the signature motif HCXXGXXRS/T (Figure 9) and *in vitro* experiments have shown that laforin can dephosphorylate phospho-serine/threonine, phospho-tyrosine and p-nitrophenyl phosphate (pNPP) (92). Laforin is ubiquitous, with the highest expression in skeletal muscle, liver, kidney, heart and brain (93).

To date 64 different mutations have been described in the *EMP2A* gene (The Lafora Progressive Myoclonus Epilepsy Mutation and Polymorphism Database, http://projects.tcag.ca/lafora/). All the mutations are evenly distributed across the four exons of the gene affecting either the polysaccharide binding and/or the dual specificity phosphatase activity of laforin except one mutation that has no effect on polysaccharide binding or phosphatase activities but affects interaction with PTG (94). Despite remarkable allelic heterogeneity in *EPM2A*, there is a high prevalence of one mutation, R241X, in the Spanish population (40%), most likely due to a founder effect and recurrent events (95,96). Both functional CBD and DSPD are required for laforin function since loss-of-function mutations of either domain causes disease symptoms (84).
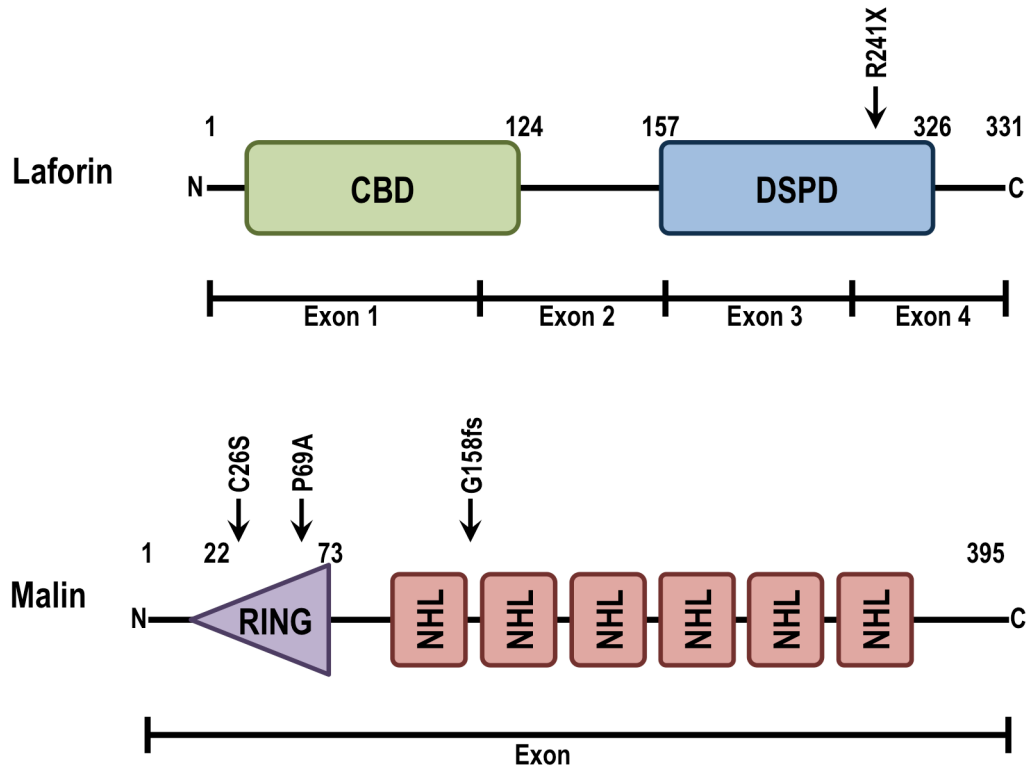
Figure 9. Laforin and Malin. Schematic representation of *A)* Laforin showing the four exons, the N-terminal carbohydrate binding domain (CBD) and the C-terminal dual-specificity phosphatase domain (DSPD). R241X is the most common mutation found in *EPM2A* in Lafora patients. *B)* Malin showing the exon, the N-terminal RING finger domain and the six NHL motifs. P69A, G158fs and C26S are the most frequent mutations in Lafora patients with *EPM2B* mutations.

5.4. *EPM2B* gene

Chan et al. (81) identified the second gene implicated in LD, *EPM2B* or *NHLRC1,* which is a single exon gene localized on chromosome 6p22 (97). *EPM2B* codes for a 395-residue protein malin, a putative E3 ubiquitin ligase with an N-terminal RING finger domain, common to all E3 ubiquitin ligases (98,99), followed by six NHL motifs, thought to be involved in protein-protein interactions (100) (Figure 9).

To date 61 different mutations have been described in the *EPM2B* gene (The Lafora Progressive Myoclonus Epilepsy Mutation and Polymorphism Database, http://projects.tcag.ca/lafora/). All the mutations are evenly distributed across the gene. The missense mutation P69A, affecting the RING finger domain, is the most frequent mutation observed in *EPM2B* followed by the G158fs mutation. Both of the mutations have been identified in several ethnic groups, indicating a recurrent mutational event. In French-Canadian isolates, the mutation C26S is prevalent and a founder effect for this mutation has been suggested (81,97). Nearly all mutations are predicted to cause loss of function of malin (81,86,87). Mutations in the RING domains abolished malin's ubiquitin ligase activity while those in the NHL motifs disrupted the interaction between malin and laforin (101).

5.5. Phylogeny

Laforin is conserved in all vertebrates, but it is absent from the genomes of most invertebrates, including *Saccharomyces cerevisiae*, *Drosophila*

melanogaster and *Caenorhabditis elegans* (102-104). Laforin is also conserved in five protozoans: *Cyanidioschyzon merolae, Toxoplasma gondii, Eimeria tenella, Tetrahymena thermophile* and *Plasmodium tetraurelia*, in the cephalochordate *Branchiostoma floridae* and in the cnidarian *Nematostella vectensis* (Figure 10) (103,104)*.* The evolutionary lineage of laforin is unique. The five protozoan species undergo hibernation at some point in their life cycle wherein they form an insoluble glucan that resembles Lafora bodies (105). Niittyla et al. (106) described a gene in plants; starch excess 4 (*SEX4*), which encodes a protein containing an N-terminal DSPD and a C-terminal CBD, the same domains as in laforin but in the opposite orientation. SEX4 is a starch phosphatase and hydrolyzes C3 and C6 phosphate from amylopectin and the genetic depletion of SEX4 causes starch accumulation (15,106). Laforin complements the SEX4 phenotype in Arabidopsis, thus providing evidence that laforin and SEX4 are functional equivalents (103). Malin is present in all vertebrates and a cephalochordate (Figure 10) (107). Malin does not correlate with laforin in species distribution. Laforin is present in the genomes of evolutionarily more basal organisms, suggesting that laforin probably has function(s) independent of malin (107).
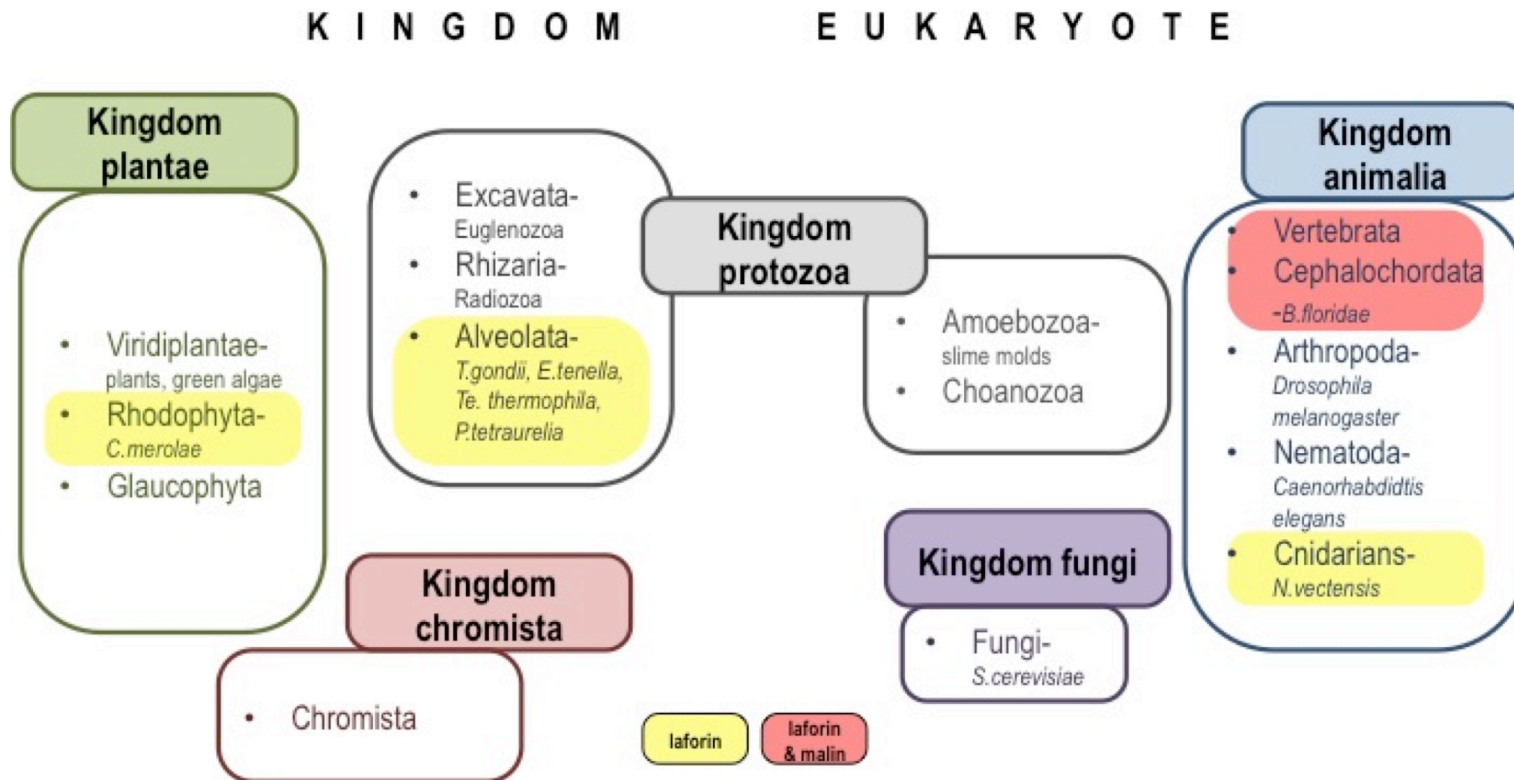
Figure 10. Phylogeny. Schematic representation of species distribution of laforin and malin. Laforin is present in the kingdoms plantae, protozoa and animalia whereas malin is present only in the kingdom animalia and is absent in the evolutionarily basal organisms.

6. Mouse Models of Lafora Disease

Three mouse models for Lafora disease have been developed (90,108-110). Targeted disruption of the mouse *Epm2a* gene resulted in viable null mice with most of the disease symptoms (109). It was initially reported that at two months of age, there was neuronal degeneration even in the absence of Lafora bodies. However, more recent work shows neuronal cell death at 11 days of age and type 1 Lafora bodies at 2 weeks of age (111). Type 1 Lafora bodies consist of granular, polymorphic, "dust-like", uniformly stained particles. Type 2 Lafora bodies, which have a heavily stained core with a less stained circular rim on PAS stain, are prominent at 3 months of age and are present in both neuronal and non-neuronal tissues, are positive for ubiquitin and advanced glycogen end products (109). By 12 months of age, the mice have widespread neuronal degeneration, impaired behavioral responses, ataxia, myoclonus epilepsy and EEG epileptiform activity (109). The second mouse model transgenically overexpressed a dominant negative form of laforin, generated by mutating Cys 266 to Ser, and thus inactivating the phosphatase (90). Lafora bodies were formed in the liver, muscle, neuronal perikarya and dendrites of these mice. Immunogold electron microscopy showed laforin in close proximity with endoplasmic reticulum and the surrounding polyglucosan accumulations (90). Mouse models with disruption of the *Epm2b* gene were generated by four independent studies (108,110,112,113). Targeted disruption of the gene resulted in viable mice that developed Lafora bodies in brain, heart and skeletal muscle by 3 months of age (108). The *Epm2b-/-* mice showed cognitive deterioration,

altered motor activity, impaired motor coordination, abnormal hind limp clasping and episodic memory deficits along with spontaneous single spikes, spike-wave, polyspikes, and polyspike-wave complexes with correlated myoclonic jerks (112,114).

7. Disease Mechanism of Lafora Disease

7.1. Laforin and Glycogen Metabolism

A prominent hypothesis in causation of Lafora disease has been that Lafora bodies are formed as a result of an imbalance between the activities of glycogen synthase and branching enzyme. Laforin has been reported to bind to several proteins involved in glycogen metabolism such as glycogen synthase, GSK3, PTG, malin and the α2 and β2 subunits of AMPK (94,101,115-117). Independent studies have proposed that laforin might increase the activity of glycogen synthase (115,118). Two groups proposed that the inhibitory kinase, GSK3, is a laforin substrate (115,118). Dephosphorylation of GSK3 activates GSK3 to phosphorylate GS at multiple sites, thus keeping glycogen synthesis in check (Figure 12) (115). However, several studies argue against GSK3 being a laforin substrate (8,9,108,116,119). The phosphorylation state of GSK3 remains unchanged in the three different mouse models of Lafora disease: *Epm2a-/-* mice (8,9), dominant-negative laforin overexpressing mice (119) and *Epm2b-/-* mice (108). Wang et al. found no difference in the activities of glycogen synthase and branching enzyme in the brain tissue of dominant-negative laforin overexpressing mice (119). Glycogen synthase activity state was also unchanged in skeletal

muscle and brain of *Epm2a-/-* and *Epm2b-/-* mice (8,108), thus arguing against the hypothesis of imbalance in glycogen synthesis and branching as a cause for Lafora body formation.

7.2. Laforin and Autophagy

Glycogen autophagy or glycophagy has been described as a mechanism for disposal of glycogen (see above in section 3). Autophagy has also been shown to be essential for the function of the central nervous system. Impairment of autophagy leads to neurodegeneration, behavioral changes and death in murine models of diseases (120). Recently, Aguado et al. (121) and Criado et al. (112) proposed defects in laforin-malin complex-regulated autophagy as the primary cause of Lafora disease (see section 7.5). Laforin would activate autophagy by acting upstream of tuberous sclerosis complex 2 (TSC2) and inhibit mammalian target of rapamycin (mTOR) to activate autophagy (Figure 12). Thus, in Lafora disease in the absence of laforin, mTOR would be activated inhibiting autophagy (121).

7.3. Laforin as a Glycogen Phosphatase

Worby et al. (116) demonstrated that laforin dephosphorylates amylopectin, the major component of plant starch. Amylopectin is similar to glycogen but with less frequent α-1,6 glycosidic linkages and contains phosphate in the form of C3- and C6-phosphomonoesters (13). Worby et al. (116) were unable to measure dephosphorylation of commercially available rabbit liver

glycogen by laforin. Tagliabracci et al. (9), however, showed that laforin can dephosphorylate rabbit muscle glycogen *in vitro* and was able to release ~25% of the phosphate from undigested rabbit muscle glycogen. Liver contains much lower levels of phosphate in glycogen as compared to muscle and this could explain why Worby et al. (116) were unable to measure dephosphorylation of glycogen in their experiment. Upon digestion with glucosidases, laforin released 90% of the phosphate. Mutation of laforin in the CBD eliminated its ability to dephosphorylate glycogen. Glycogen isolated from *Epm2a-/-* mice, had a 40% increase in phosphate in liver and a 4-fold elevation in muscle by three months of age suggesting that glycogen is a physiological substrate of laforin (9). Electron microscopic analysis of glycogen purified from 9-12-month-old *Epm2a-/-* mice revealed the presence of large conglomerated aggregates with less granularity, more defined boundary and a more even density (8). This abnormal appearance of glycogen was reversed by laforin-dependent hydrolysis of phosphate in the glycogen (Figure 12) (8).

7.4. Malin: an E3 Ubiquitin Ligase

Malin is a potential E3 ubiquitin ligase with an N-terminal zinc finger RING domain (101). During ubiquitination, ubiquitin monomers are attached to the substrate protein in a three-step reaction: 1) activation of ubiquitin by an E1 ubiquitin-activating enzyme in an ATP dependent manner; 2) E2 ubiquitin-conjugating enzyme catalyzes the transfer of ubiquitin from E1 to the cysteine of the E2; and 3) E3 ubiquitin ligase recognizes the substrate and catalyzes the

formation of an isopeptide bond between the lysine of the substrate and the C-terminal glycine of ubiquitin (Figure 11) (122,123). Ubiquitin is attached to the substrate at one lysine as mono-ubiquitination, at multiple lysines as multi-ubiquitination or several ubiquitins at one lysine as poly-ubiquitination. The type of ubiquitination determines the fate of the substrate; for example poly-ubiquitination at K48 of the ubiquitin targets the substrate for degradation by the ubiquitin proteasomal system whereas mono- or poly-ubiquitination at K63 of the ubiquitin controls gene transcription, DNA repair and intracellular trafficking (122,124) (Figure 11).

Gentry et al. (101) reported that malin interacts with laforin and promotes its polyubiquitination resulting in degradation via the ubiquitin proteasomal pathway (Figure 12). Based on this model, defective malin should increase laforin protein levels.
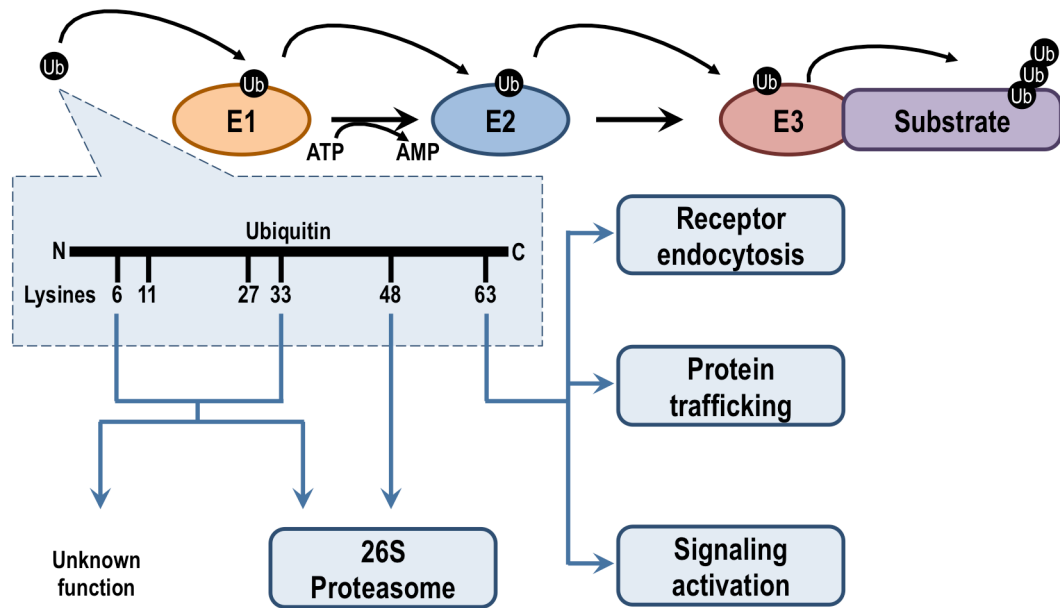
Figure 11. Ubiquitination. An ubiquitin moiety is attached to the lysine of the substrate in a three-step reaction involving the enzymes ubiquitin-activating enzyme, E1, ubiquitin-conjugating enzyme, E2 and ubiquitin ligase, E3. The site of ubiquitination decides the fate of the substrate.

Patients with mutations in *EPM2B (81)* and *Epm2b-/-* mice have increased levels of laforin (108,110,112). If the physiological role of malin is to mediate the degradation of laforin, then it is difficult to understand how patients develop Lafora disease with recessive mutations in either *EPM2A* or *EPM2B*. Malin has also been reported to ubiquitinate and cause degradation of glycogen debranching enzyme, AGL, via the ubiquitin proteasomal pathway (Figure 12) (125). As a result of mutations in malin, increased AGL protein would remove the α-1,6 glycosidic linkages and lead to polyglucosan formation in Lafora disease. Lohi et al. (115) reported that malin binds and ubiquitinates glycogen synthase, and degrades it via the ubiquitin proteasomal pathway (Figure 12). Therefore, in Lafora disease, it was suggested that in the absence of the inhibitory affect of malin on glycogen synthase, polyglucosan is formed. However, in 3 months old *Epm2b-/-* mice, there is no change in the protein levels of AGL or glycogen synthase in skeletal muscle arguing against AGL and glycogen synthase being substrates for malin (108).

7.5. Laforin-malin Complex

Laforin and malin have been described to have a complex relationship. While they are reported to function together as a complex, malin also ubiquitinates laforin and promotes its degradation (101). Vilchez et al. (126) reported that laforin increases the stability of malin in spite of laforin being a malin substrate, further increasing the complexity in the relationship of the two proteins. One of the first proposed substrates of the laforin-malin complex was

PTG, a glycogen targeting subunit of protein phosphatase 1 (94,126,127). PP1 activates glycogen synthase and inhibits glycogen phosphorylase. In this model, a laforin-malin complex would ubiquitinate and degrade PTG, thereby decreasing glycogen levels (Figure 12). In the absence of this complex due to mutations in either of the genes, *Epm2a-/-* or *Epm2b-/-*, glycogen synthase would be activated, thus forming polyglucosan. The protein level of PTG was unchanged in *Epm2a*-/- and *Epm2b*-/- mice, thus arguing against PTG being a malin substrate (108). Sharma et al. (128) reported neuronatin, a protein proposed to stimulate glycogenesis, as a novel substrate of the laforin-malin complex. The protein levels of neuronatin have not yet been evaluated in the mouse models.

Besides regulating proteins involved in glycogen metabolism, the laforin-malin complex has been proposed to play a role in protein clearance as well. Laforin and malin form a functional complex with the cellular chaperone Hsp70 to suppress the cytotoxicity of misfolded proteins, such as polyglutamine proteins and mutant α-synuclein (Figure 12) (129). It was proposed that laforin acts as a bridge between Hsp70 and malin, thus recruiting malin to ubiquitinate the misfolded proteins and target them for degradation via the proteasomal and/or autophagolysosomal pathway. The complex is suggested to function similar to other reported E3 ubiquitin ligases in protein clearance such as parkin (130), CHIP (carboxyl-terminal of Hsp70 interacting protein) (131), dorfin (132) and E6-AP (133). The laforin-malin complex has also been shown to play a role in the regulation of autophagy (Figure 12). In cellular and mouse models of Lafora disease, in the absence of laforin or malin, autophagosome formation is

33

impaired. It was proposed that the absence of laforin or malin causes an accumulation of autophagic substrates leading to stress and eventually cell death (112,121). These defects further draw similarities to other neurological disorders such as Parkinson, Alzheimer's or Huntington's diseases, which also present with defects in autophagy (134). Vernia et al. (135) reported that the absence of laforin enhances the ER stress response in cells leading to proteasomal dysfunction and increased apoptosis, which might be an important causative factor for the development of Lafora disease. Thus, defects in the protein quality control pathway have been speculated to be a primary cause of Lafora disease. However, these results are inconsistent with those reported by Puri et al. (136) who found no changes in LC3-II or other autophagy proteins in brain lysates of laforin-deficient mice arguing that autophagosome formation and function is not abnormal in the brain of laforin-deficient mice.

7.6. Malin as Transcriptional Regulator

Laforin and malin have been shown to form a complex with the co-chaperone CHIP, which improves the stability of malin (137). Sengupta et al. (138) demonstrated that the laforin-malin-CHIP complex translocates to the nucleus upon heat shock to interact with and activate HSF1 (heat-shock factor 1), a transcription factor that activates the transcription of heat-shock genes to protect cells against stress-induced cell death (Figure 12).

Malin has been reported to interact with dishevelled2, a key mediator of the Wnt signaling pathway (139). Malin promotes the K48- and K63- mediated

ubiquitination of dishevelled2, causes degradation via the proteasome and autophagy and thus, inhibits Wnt signaling in Lafora disease (Figure 12). An increase in Wnt signaling with malin mutations might lead to neurological defects such as synaptic plasticity and synaptic differentiation.

7.7. Lafora Bodies: Cause or Consequence

Lafora bodies are pathognomonic of Lafora disease, but there has been some debate as to whether Lafora bodies are the cause or consequence of Lafora disease. Turnbull et al. (140) generated the laforin-PTG-double knockout mice and analyzed the mice for phenotypes of Lafora disease. The PTG deficient mice, *Ppp1r3c-/-* mice have decreased glycogen synthase activity with 30% and 70% reductions in muscle and brain glycogen, respectively. In laforin-PTG-double knockout mice, glycogen accumulation and the number of Lafora bodies were dramatically decreased and the neurological symptoms due to the absence of laforin were alleviated (140). Further, recent studies by Pederson et al. (141) and Duran et al. (142) showed that inhibiting glycogen synthesis in laforin and malin knockout mice prevents the development of symptoms of Lafora disease (141). Taken together, these studies indicate that the primary defect in Lafora disease is the accumulation of insoluble, poorly branched polyglucosan.
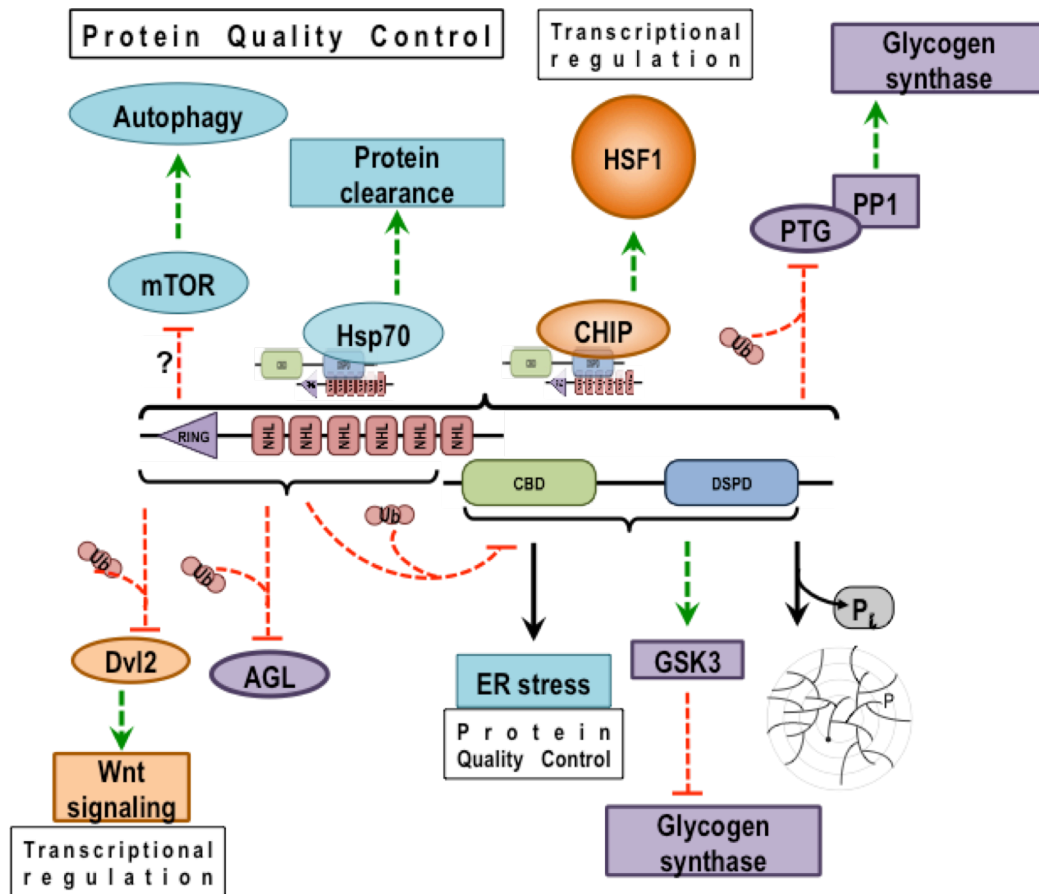
Figure 12. Mechanisms for Causation of Lafora Disease. Schematic representation of defects in glycogen metabolism (colored purple), protein quality control (colored blue) or transcriptional regulation (colored orange) in Lafora disease. AGL, debranching enzyme; CHIP, carboxyl-terminus of Hsp70 interacting protein; Dvl2, dishevelled 2; GSK3, glycogen synthase kinase 3; Hsp70, heat shock protein 70; HSF1, heat shock factor 1; mTOR, mammalian target of rapamycin; PTG, protein targeting to glycogen; PP1, protein phosphatase 1; Pi, phosphate.

RESEARCH OBJECTIVE

Lafora disease is a fatal neurodegenerative disorder with no cure available yet. The focus of Lafora disease research has been to understand the physiological role of the laforin phosphatase and the malin ubiquitin ligase in the etiopathogenesis of the disease, which might lead to identification of therapeutic targets. Previous work showed that laforin acts as a glycogen phosphatase and in the absence of laforin, in mouse models of Lafora disease, there is an increase in glycogen phosphorylation. Overall, it has been proposed that the laforin-malin complex plays a role in the regulation of glycogen metabolism and protein quality control. In this study, my focus was on two main aims:

1.   To understand the role of laforin and malin in the protein degradation/quality control process, I evaluated the three different arms: the autophagolysosomal pathway, the ubiquitin-proteosomal pathway and the ER stress response.

2.   To understand the precise role of malin in the causation of Lafora disease, I used an unbiased quantitative proteomics approach in an attempt to identify the physiological substrate(s) of malin.

EXPERIMENTAL PROCEDURES

1. Animals

The *Epm2a*-/- and *Epm2b*-/- mice have been previously described (108,143). *Epm2a*-/- and *Epm2b*-/- mice were intercrossed to generate double heterozygous *Epm2a*+/- *Epm2b*+/- mice, which were then crossed to generate the double *Epm2a*-/- *Epm2b*-/- mice. All mice were maintained in temperature- and humidity-controlled conditions with a 12:12-hour light-dark cycle, fed a standard chow (Harlan Teklad global diet 2018SX) and allowed food and water *ad libitum*. All studies were conducted in accordance with Federal Guidelines, and were approved by the Institutional Animal Use and Care Committee of Indiana University School of Medicine.

2. Generation of Mouse Embryonic Fibroblasts (MEFs)

On day 0 evening, breeders for each genotype were set up with one adult male and two adult females. The females were examined for the presence of a vaginal plug the following morning. The age of the embryo was recorded as day 0.5 when the plug was present. The male mouse was removed from the cage. The female mice were euthanized on day 13.5 by cervical dislocation and the uterus along with the embryos was dissected out. The embryos were harvested from the uterus under aseptic conditions. The head of the embryo was removed, the remainder was cut up into small pieces in 1 ml of 1X phosphate-buffered saline (PBS) (137 mM sodium chloride, 10 mM disodium phosphate, 2.7 mM potassium chloride, 1.8 mM monopotassium phosphate, pH 7.4) and a single-cell

suspension was created by sequentially passing the material through 16-, 18-
and 20-gauge needles using a 2 ml syringe. The cell suspension was centrifuged
at 2000 X g for 5 minutes at room temperature. The supernatant was saved for
genotyping (described below) and the cell pellet was washed once with 1X PBS
and then resuspended in 10 mL of Dulbecco's Modified Eagle Medium:Nutrient
Mixture F12 (DMEM-F12) (Hyclone) supplemented with 10% fetal bovine serum
(FBS) (Thermo Fisher Scientific), 100 units/ml of penicillin (Sigma) and 100 µg/ml
of streptomycin (Sigma). The cells were plated in 100 mm tissue culture dishes
and incubated at $37^{o}C$ with 5% CO_2 in a humidified incubator.

3. Genotyping of the MEFs

Embryos were generated by crossing appropriate homozygous parents;
Epm2a-/-, *Epm2b-/-* and double *Epm2a-/- Epm2b-/-* mice. The genotype of the
resulting MEFs was confirmed by PCR as described before (108) (Figure 13).
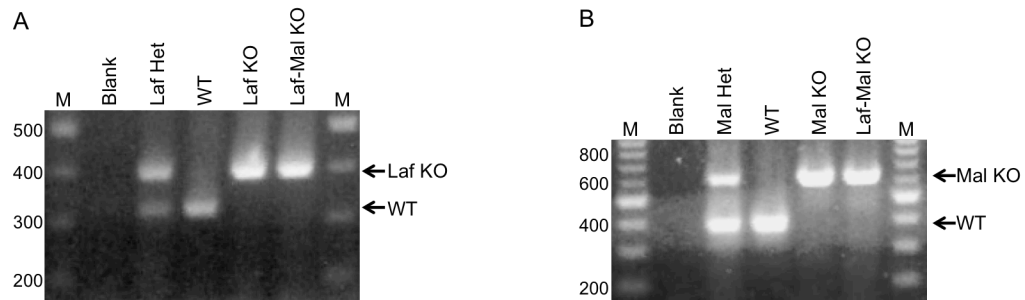
Figure 13. Genotyping of the Mouse Embryonic Fibroblasts.
Mouse embryonic fibroblasts (MEFs) derived from *Epm2a-/-* (Laf
KO), *Epm2b-/-* (Mal KO) and double *Epm2a-/- Epm2b-/-* (Laf-Mal
KO) mice were genotyped by PCR. *A)* "Laf Het" is the control
showing alleles for both wild type and mutant laforin loci. *B)* "Mal
Het" is the control showing alleles for both wild type and mutant
malin loci. WT; wild type, M; marker.

4. Mammalian Cell Culture

MEFs were seeded at a cell density of around 1.5×10^6 cells/100-mm plate, grown till 85-90% confluence and then passaged in a 1:3 ratio for propagation. MEFs between passage 3 and 8 were used for all experiments. Under basal conditions the MEFs were cultured in DMEM-F12 medium supplemented with 10% FBS, 100 units/ml of penicillin and 100 µg/ml of streptomycin (full medium) at 37^oC with 5% CO_2 in a humidified incubator.

To culture cells under starvation conditions, cells were washed twice with PBS at room temperature and switched from full growth medium to Earle's balanced salt solution (EBSS from Sigma) and incubated for 2 hours at 37^oC with 5% CO_2 in a humidified incubator. Cell extracts were prepared at the time of harvest as described below in section 10.

For inhibition of lysosomes, MEFs were incubated with medium that contained 20 µM chloroquine for 2 hours. For studies of autophagy, MEFs were treated with 10 nM rapamycin, an inhibitor of mTOR for 2 hours. For inhibition of proteasomal function, MEFs were incubated with medium that contained 20 µM MG132 for 2 hours. To measure ER stress responses, MEFs were incubated with medium that contained 1 µM thapsigargin or 2 µg/ml tunicamycin for 18 hours. In control experiments, MEFs were incubated in medium that contained vehicle, dimethyl sulfoxide or sterile distilled water as appropriate. Cell extracts were prepared at the time of harvest as described below in section 10.

5. Stable Isotope Labeling with Amino Acids in Cell Culture

MEFs from *Epm2b-/-* mice and their wild-type controls were grown in lysine- and arginine-free DMEM-F12 medium supplemented with 10% or 2% dialyzed FBS, 100 units/ml of penicillin and 100 µg/ml of streptomycin. The medium was also supplemented with either $[^{12}C_6{}^{14}N_2]$ lysine (K0) and $[^{12}C_6{}^{14}N_4]$ arginine (R0) (light medium) or $[^{13}C_6{}^{15}N_2]$ lysine (K8) and $[^{13}C_6{}^{15}N_4]$ arginine (R10) (heavy medium). The concentration of lysine (90 µg/ml) and arginine (148 µg/ml) was the same in both light and heavy medium. The cells were grown for at least for 5 passages in an effort to ensure complete labeling with heavy lysine and arginine. In most cases, the cells were grown for 7-8 passages over 4-5 weeks to obtain enough starting material (45-50 mg of protein). Cells, in both light and heavy medium, were incubated with medium containing 20 µM MG132 for four hours before the time of harvest. The cells were harvested as described below in section 14.1.

6. Culturing MEFs in Serum-free Medium

The cells were cultured in full medium and then adapted to serum-free media by either direct adaptation or sequential adaptation. FibroGRO™ Complete Media Kit (Millipore) was used as a serum-free alternative for growing mouse embryonic fibroblasts. The medium contains FibroGRO Basal Medium and supplements including 5 ng/ml of basic fibroblast growth factor, 5 ng/ml of epidermal growth factor, 30 pg/mL of transforming growth factor-β1, 500 µg/mL of human serum albumin, 0.6 µM linoleic acid, 0.6µg/mL of lecithin, 50 µg/ml of

ascorbic acid, 7.5 mM L-glutamine, 1 μg/ml of hydrocortisone hemisuccinate and 5 μg/ml insulin. The cells were initially grown in DMEM-F12 medium with 10% FBS and then switched directly to the serum-free alternative medium. For sequential adaptation, the cells were initially grown in DMEM-F12 medium with 10% FBS (Full medium) and then switched to the serum-free alternative medium (SFM) through several sequential steps. This involved increasing the ratio of SFM to Full medium at sequential passages from 0:100, 30:70, 50:50, 70:30, 80:20, 90:10 to 100:0.

7. Culturing MEFs in Low Serum Medium

The cells were initially grown in DMEM-F12 medium with 10% FBS (Full medium) and then switched to the DMEM-F12 medium with reduced serum through several sequential steps. This involved switching the concentration of FBS at sequential passages from 10%, 7.5%, 5%, 2% to 1%. The concentration of antibiotics was reduced from 100 units/ml of penicillin and 100 μg/ml of streptomycin to 20 units/ml of penicillin and 20 μg/ml of streptomycin.

8. Rinsing and Washing Techniques for MEFs

MEFs were cultured in DMEM-F12 medium supplemented with 10% FBS and 100 units/ml of penicillin and 100 μg/ml of streptomycin (full medium). At the time of harvest, the cells were rinsed by different techniques. The culture medium was removed completely by aspiration while the plates were on ice. The plates were then rinsed three times with either 10 ml of ice cold PBS on ice, on an

orbital shaker at 4°C for 5 minutes or with 10 ml of DMEM-F12 medium without FBS on an orbital shaker at 4°C for 5 minutes. The cells were also washed in suspension after tryspinization. The cells were detached from the plate surface and full medium was added to inactivate trypsin activity followed by centrifugation at 2000 X g for 5 minutes. The supernatant containing the medium was discarded and the cell pellet was washed three times for 5 minutes with 10 ml of ice-cold Dulbecco's phosphate buffered saline with calcium and magnesium on a nutator at 4°C. Following the washes, cell lysates were prepared as described below in section 10.

9. Chemicals, Antibodies and other Reagents

Chloroquine was from Sigma. Rapamycin was from LC Laboratories. Thapsigargin, tunicamycin and MG132 were from Cayman Chemicals. Antibody sources were as follows: Anti-LC3, anti-Phospho-S6K, anti-S6K, anti-Phospho-S6, anti-S6 were from Cell Signaling Technology; anti-GABARAPL1, anti-CHOP were from Protein Tech Group; anti-LAMP1, anti-S5a subunit of 26S Proteasome were from Iowa Hybridoma; anti-Ubiquitin was from Millipore; anti-glyceraldehyde-3-phosphate dehydrogenase was from Biodesign International; anti-Stbd1 has been previously described (33). HEPES, CAM, TCEP and NEM were from Sigma. Trypsin-Gold was from Promega. Lys-C was from Roche. Sep-Pak® C18 columns were from Waters. StageTips (C18) and trifluoroacetic acid were from Thermo Scientific. Acetonitrile was from Thermo Fisher Scientific.

Other chemicals and reagents were from Sigma, Bio-Rad, Invitrogen or New England Biolabs.

10. Western Blot Analysis

Cells were washed three times with ice-cold PBS and then lysed with ice-cold RIPA buffer (50 mM Tris-HCl, pH 7.5, 150 mM NaCl, 0.1% sodium dodecyl sulphate, 1% sodium deoxycholate and 1% nonidet-P40) for 15 minutes in presence of protease inhibitors (1mM phenylmethylsulfonyl fluoride (PMSF), 0.1 mM N-p-tosyl-1-lysine chloromethyl ketone (TLCK), 1 mM benzamidine, 1 µg/ml aprotinin, pepstatin and leupeptin). The cell lysates were centrifuged at 10,000 X g for 15 minutes at 4°C to pellet insoluble materials. For detection of LC3 and GABARAPL1, cells were lysed with ice-cold RIPA buffer with 0.5% sodium dodecyl sulphate for 15 minutes in the presence of protease inhibitors as described above. Protein concentration was determined by the Bradford method using bovine serum albumin as a standard (144). The supernatants of the lysates or total lysates (for LC3 and GABARAPL1) were diluted with 5 X loading buffer (62.5 mM Tris-PO$_4$ pH 6.8, 50% (w/v) glycerol, 6.25% (w/v) SDS, 0.1% (w/v) bromphenol blue and 5% β-mercaptoethanol) to 1 X and boiled for 10 minutes.

Samples of 10 µg protein from MEFs were separated on 10% SDS polyacrylamide gel electrophoresis (PAGE) and transferred onto a 0.45 µm nitrocellulose membrane (Biorad) at 15 V overnight. For detection of LC3, 10 µg protein were separated on 15% SDS-PAGE at room temperature and transferred onto a 0.22 µm polyvinylidene fluoride (PVDF from Millipore) membrane at 100 V

for 90 minutes at 4°C. After transfer, the nitrocellulose membranes were stained with Ponceau S (0.5% Ponceau S in 1% glacial acetic acid) to monitor loading followed by blocking in 5% non-fat milk powder in 1X tris-buffered saline (TBS) (50mM Tris-HCl, 150 mM sodium chloride, pH 7.6) with 0.1% Tween 20 or 5% BSA in 1X TBS with 0.1% Tween 20 (for anti-LC3, anti-phospho-S6K, anti-S6K, anti-phospho-S6 and anti-S6 antibodies). The membranes were probed with various primary antibodies (diluted in 2% non-fat milk powder in 1X TBS with 0.1% Tween 20 or 5% BSA in 1X TBS with 0.1% Tween 20 for PVDF) for 2 hours at room temperature or overnight at 4°C followed by three 10 minutes washes with 1X TBS with 0.1% Tween 20. Incubation with horseradish peroxidase-conjugated-secondary antibodies (diluted in 2% non-fat milk powder in 1X TBS with 0.1% Tween 20 or 5% BSA in 1X TBS with 0.1% Tween 20 for PVDF) was done for 1 hour at room temperature followed by three 15 minute washes with 1X TBS with 0.1% Tween 20. Detection was performed by enhanced chemiluminescence using Pierce ECL Western blot substrate or Millipore Immobilon Western substrate (for anti-ubiquitin antibody). The levels of proteins were quantitated by densitometric analysis of the autoradiograph using CareStream software. Phospho-specific antibodies were used first during immunoblotting. The membranes were treated with stripping buffer (62.5 mM TrisCl pH 6.8, 2% SDS, 0.7% β-ME) for 40 minutes at 55°C and then probed for the total protein of interest.

11. Staining of SDS-PAGE gel with Coomassie Blue

To prepare the Coomassie Blue stain, glacial acetic acid (100 mL) was added to 500 mL of water. To this, 400 mL of methanol was added and mixed well. Coomassie R250 dye (1 g) was added to the solution and mixed till completely dissolved. The stain solution was filtered to remove any undissolved particulates. Destaining solution consisted of 10% (v/v) acetic acid, 20% (v/v) methanol. After electrophoresis, the SDS-PAGE gel was removed from its glass plates and rinsed once in water. Coomassie blue stain was added such that the stain covered the gel completely. The gel was incubated for 20 minutes on an orbital shaker at room temperature. The Coomassie stain was poured off and the gel was rinsed twice with destaining solution. Destaining solution was added to cover the gel completely. Kimwipes®, which bind the Coomassie dye, were rolled up into small balls and placed in the destaining solution around the gel. The gel was incubated in the destaining solution overnight at room temperature.

12. Quantitation of Proteasomal Activity

Chymotrypsin-like activity of the proteasome was evaluated using the Proteasome-Glo™ Assay Reagent (Promega). The reagent contains a luminogenic substrate of the proteasome, Suc-LLVY-aminoluciferin (145). Incubation with soluble cellular protein extracts is used to measure proteasome activity. Substrate cleavage generates a "glow-type" luminescent signal produced by the luciferase reaction (Ultra-Glo™ recombinant luciferase) (Figure 14). The signal thus generated is proportional to the amount of activity of the proteasome.
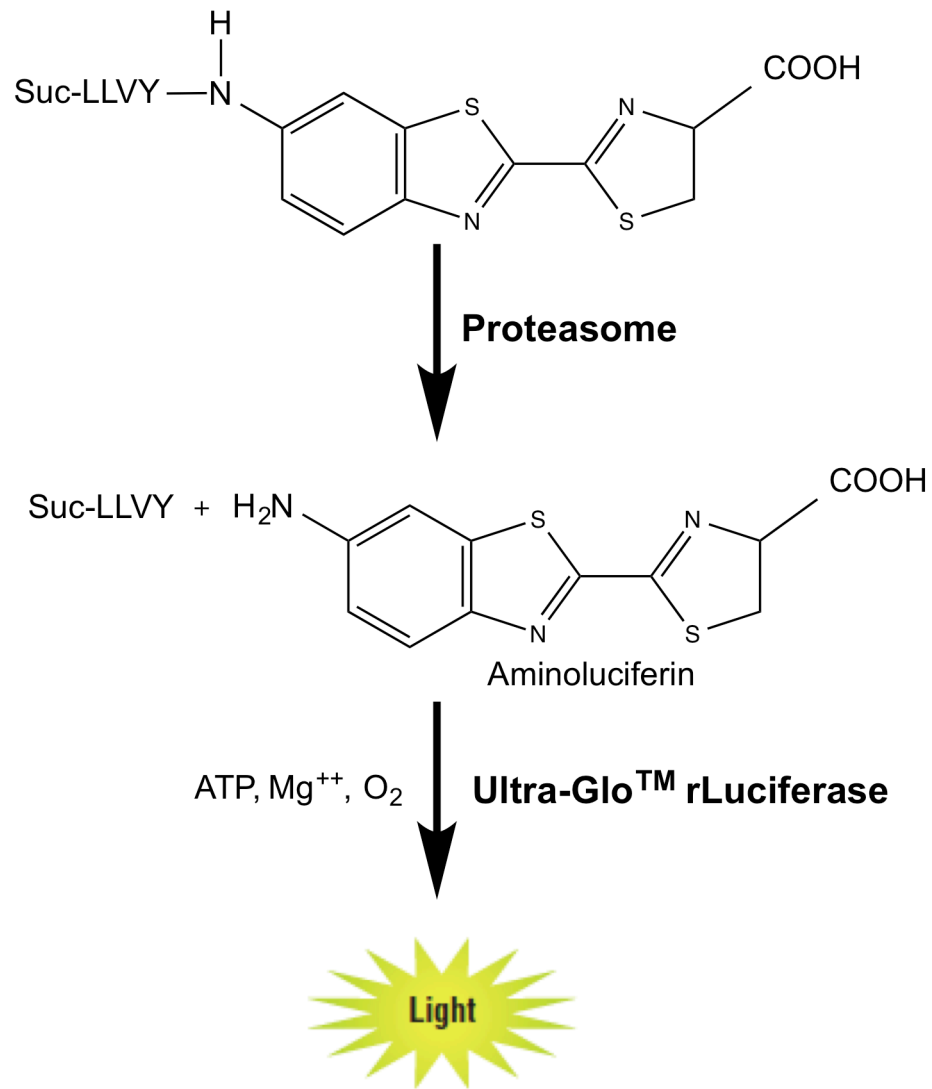
Figure 14. Proteasomal Activity. The luminogenic substrate contains the Suc-LLVY sequence that is recognized by the chymotrypsin-like activity of the proteasome. Upon cleavage by the proteasome, aminoluciferin generates the luminescent signal in a reaction catalyzed by luciferase enzyme.

Proteasome-Glo™ Buffer, the lyophilized Luciferin Detection Reagent and the Suc-LLVY-Glo™ Substrate were equilibrated to room temperature. The Luciferin Detection Reagent was reconstituted with 10ml of Proteasome-Glo™ buffer. The Proteasome-Glo™ Reagent was prepared by adding the Proteasome-Glo™ Substrate to the reconstituted Luciferin Detection Reagent. The Reagent was left at room temperature for at least 60 minutes before use. This allows the removal of any contaminating free aminoluciferin. MEFs from wild type, *Epm2a-/-*, *Epm2b-/-* and double *Epm2a-/- Epm2b-/-* mice were harvested and soluble protein extract was prepared as described above in section 10. The cell extracts were diluted in water such that 25 uL corresponded to 10 µg of soluble protein. Proteasome-Glo™ Reagent (25 µL) was added to each well of a white walled, clear-bottom, flat-bottom, half area 96-well plate. To each well, 25 µL of soluble protein extract was added. The contents of the plate were mixed using a plate shaker at 300-500 rpm for 30 seconds followed by incubation at room temperature for 15 minutes. Chymotrypsin-like proteasomal activity was detected by measuring the relative light units (RLU) using a SpectraMax M5 Luminometer (Molecular Devices).

13. Measurement of Glycogen Levels in MEFs

Total glycogen in the MEFs was assayed by slight modifications of the method described by Suzuki et al. (146). MEFs were seeded in 100-mm cell culture plates in DMEM:F12 medium (full medium) as described above and grown till 100% confluence. The cells were grown for 7 days and supplemented

with fresh medium every day. At the time of harvest, the total lysate was prepared as described above in section 10, collected in a 1.5 mL screw cap tube and freshly prepared hot 50% KOH was added to a final concentration of 30%. The lysate was boiled for 30 minutes, mixing by inverting the tubes every 5-10 minutes. The samples were cooled on ice 2% Na_2SO_4 (w/v) and 2 volumes of 100% ethanol were added and incubated at -20^oC overnight to precipitate the glycogen. After precipitation, the glycogen was collected by centrifugation at 17500 X g for 20 minutes, resuspended in 100 μL of water and precipitated again by addition of 2 volumes of 100% ethanol at -20^oC for 1 hour. This procedure was repeated one more time, the last and third precipitation going overnight. The glycogen pellet after each precipitation was dried in a SpeedVac. The glycogen was digested to glucose either enzymatically with amyloglucosidase or with hydrochloric acid as described below. For enzymatic digestion, the glycogen pellet was digested overnight with 100 μL of amyloglucosidase in 0.2 mM sodium acetate pH 4.8 (final concentration 0.3 mg/ml). For acidic digestion of glycogen, 100 μL of 2 N hydrochloric acid was added to the glycogen pellet, boiled for 2 hours and then cooled on ice. The acid was neutralized with 2 N NaOH in the presence of 0.1 M Tris HCl pH 7.0. After the digestion, the samples were centrifuged at 17500 X g for 5 minutes and the supernatant collected in a new tube. The supernatants were stored at -20^oC till use. Glucose equivalents were determined by a coupled reaction involving the conversion of glucose to glucose-6-phoshate by hexokinase and reduction of nicotinamide adenine dinucleotide phosphate ($NADP^+$) by glucose-6-phosphate dehydrogenase and measuring the

OD at 340 nm. Typically, 10 µL of digested glycogen was added to a 300 uL reaction mix (300 mM triethanolamine pH 7.6, 4 mM $MgCl_2$, 0.9 mM $NADP^+$, 2 mM ATP and 2 µg/mL glucose-6-phosphate dehydrogenase (Roche)). An aliquot (100 µL) was taken from the reaction mix and the OD at 340 nm was recorded (blank). To the remaining 200 µL, 5 µL of hexokinase (1 mg/mL stock, Roche) (diluted 1:10 in 3.2M $(NH_4)_2SO_4$) was added and the reaction was allowed to proceed at room temperature for 30 minutes. The OD at 340 nm was recorded (147). Glycogen content is expressed as µmol of glucose/mg of protein.

14. Sample Preparation for Mass Spectrometric Analysis

14.1.   Preparation of Cell Lysates

MEFs from *Epm2b-/-* mice and their wild-type controls were grown in light or heavy medium as described above in section 5. At least ten 150-mm cell culture plates grown to about 90% confluence were used for each genotype. The medium was aspirated from the each plate and the plate was kept tilted for 30 seconds so that the remaining medium flows to the bottom edge that was also aspirated. The plate was washed with at least 15 ml of cold PBS three times. During removal of medium and washes, the plate was kept on ice. After washing, the plate was brought to room temperature and 10 ml of denaturing lysis buffer, containing 20 mM HEPES pH 8.0, 9 M urea, 1 mM sodium orthovanadate, 2.5 mM sodium pyrophosphate, 1 mM β-glycerophosphate and 5 mM N-ethylmaleimide, was added. The lysis buffer was prepared fresh prior to each experiment. The cells were scraped into the buffer to the bottom edge of the

plate. The sample was transferred to the second plate and the process was repeated for all the plates of the same genotype. The same process of washing and lysis was repeated for all the plates of the second genotype. The yield for all genotypes was around 12-15 ml of lysate. Using a microtip, each lysate was sonicated three times for 30 seconds each using Ultrasonic Processor (from Misonix Incorporated). The lysate was centrifuged at 20,000 X g for 15 minutes at room temperature and the protein extract (supernatant) was transferred to a new tube. Protein concentration was determined by the Bradford method using BSA as standard (144). Extracts from cells labeled with light or heavy amino acids were mixed in a 1:1 ratio according to the protein concentration. About 20 µg of the total extract was saved for analysis by mass spectrometry as an internal control to determine the heavy:light ratio.

14.2.   Preparation of Tissue Homogenates

Random fed 6-month-old male wild type and *Epm2b-/-* mice were sacrificed by cervical dislocation. The animals were decapitated and the heads immediately dropped in liquid nitrogen, and skeletal muscles were dissected and immersed in liquid nitrogen. Frozen tissue was pulverized under liquid nitrogen and stored at -80°C until use. Around 800 mg of frozen muscle from mice of each genotype was homogenized in 20 volumes (w/v) of denaturing lysis buffer, containing 20 mM HEPES pH 8.0, 9 M urea, 1 mM sodium orthovanadate, 2.5 mM sodium pyrophosphate, 1 mM β-glycerophosphate and 5 mM N-

ethylmaleimide (NEM) with a tissue tearer for 30 seconds. Protein concentration was determined by the Bradford method using BSA as standard (144).

14.3.   Reduction and Alkylation of the proteins

To the tissue lysate 0.1 M Tris(2-carboxyethyl)phosphine (TCEP) was added to a final concentration of 5 mM and incubated at room temperature for 30 minutes. This was followed by addition of 0.5 M carboxyacetamide (CAM) to a final concentration of 10 mM and incubated for 30 minutes at room temperature in the dark to alkylate the cysteines.

14.4.   Protein Digestion

After reduction and alkylation, the lysate was diluted with 20 mM HEPES pH 8.0 to a final concentration of 2 M urea. Calcium chloride ($CaCl_2$) (1 M) was added to a final concentration of 2 mM and sequencing-grade trypsin (Promega) was added in an enzyme-substrate ratio of 1:200 and incubated overnight at 37°C with shaking. The enzymatic digestion was terminated by addition of 20% trifluoroacetic acid (TFA) to a final concentration of 1%. The pH of the peptide solution was checked (should be less than 3). The acidified peptide solution was kept on ice for 15 minutes to allow any precipitate to form. The precipitates were removed by centrifugation at 1800 X g at room temperature for 15 minutes and the supernatant was transferred to a new tube.

14.5.   Purification of Lysate Peptides

The acidified cleared peptides were purified using C18 Sep-Pak® columns (Waters). The column size was chosen such that the binding capacity of the SepPak® column is at least 2 times higher than the total amount of sample loaded to prevent any loss. All solutions were applied by gravity flow and the application of vacuum was avoided. For conditioning and washes, 5-10 column-volumes were used. The column was pre-wet with 100% acetonitrile and washed with 0.1% TFA. After washing, the acidified cleared peptides were loaded followed by sequential washes with 0.1% TFA and 5% acetonitrile, 0.1% TFA. The peptides were eluted with at least two column-volumes of 60% acetonitrile, 0.1% TFA. The eluate from each genotype was collected in a fresh tube and frozen on dry ice (or -80°C) for at least 2 hours or overnight. The frozen peptides were freeze-lyophilized for a minimum of 3 days to assure complete removal of TFA from the peptide sample using a Labconco lyophilizer.

14.6.   Immunoaffinity Purification of diGly Peptides

The lyophilized peptides were resuspended in 1.4 mL of immunoaffinity purification (IAP) buffer (50 mM MOPS/NaOH pH 7.2, 10 mM disodium phosphate, 50 mM NaCl) by pipetting repeatedly with a P-1000 micropipettor, avoiding introduction of excessive air bubbles into the solution. The resuspended peptides were transferred into a new 1.5 ml tube. The pH of the solution was maintained close to neutral or no lower than 6.0. If the pH was low, it was adjusted by addition of 1 M Tris base solution (10-20 µl). The resuspended

peptide solution was cleared by centrifugation at 10000 X g for 5 minutes at room temperature. The supernatant was collected in a fresh tube and cooled on ice.

The diGly antibody-bead slurry (80 µl) was sequentially washed with 1 ml 1X PBS four times and resuspended in 40 µl PBS. The peptide solution (1.4 mL) was transferred to the beads. The peptide-bead mix was incubated on a nutator for 3 hours at 4°C. Before incubation, the microfuge tube containing the peptide-bead mix was sealed with parafilm to prevent leakage. After 3 hours, supernatant was collected after centrifugation at 2000 X g for 30 seconds and transferred to a new tube. The beads were washed with IAP buffer twice followed by three washes with water. Each time 1 ml of IAP buffer or water was added and mixed by inverting tube 5 times followed by centrifugation at 2000 X g for 30 seconds. After the last wash, the beads were centrifuged for 5 seconds and all remaining supernatant was removed. Elution was performed by incubation with 100 µl of 0.15% TFA at room temperature for 10 minutes, mixing by tapping every 2-3 minutes followed by centrifugation at 2000 X g for 30 seconds. The step was repeated with 100 µl of 0.15% TFA and both eluates were combined.

14.7.　　　　On-column Labeling of Peptides.

For some samples, eluates from the IAP were immobilized and then labeled on C18 Sep-Pak® columns (Waters). The column was prepared as described above. After loading the sample (IAP eluate) the column was flushed with the respective on-column labeling reagents as described below. To ensure complete labeling, the labeling reagent was passed through the column over at

least 30 minutes. Labeling reagent (200 mL) was used for 200 µg of protein sample. The labeling reagents were prepared by an adaptation of the protocol of Boersema et al. (148). Sodium phosphate buffer pH 7.5 (50 mM) was prepared by mixing 40 mL of 50 mM NaH_2PO_4 with 140 mL of 50 mM Na_2HPO_4. To this, 10 mL of 4% (v/v) formaldehyde in water (CH_2O or CD_2O) and 10 mL of 0.6 M cyanoborohydride in water ($NaBH_3CN$) was added at a final concentration of 65 mM formaldehyde and 30 mM cyanoborohydride. It is important to note that the concentrations of the light and heavy formaldehyde as supplied by the manufacturer (Sigma) are different: 37% (w/v) light formaldehyde and 20% (w/v) deuterated formaldehyde. The labeling reagent mixtures were kept at 4^oC and used fresh (within 24 hours) to ensure complete labeling. After labeling, the columns were sequentially washed with 0.1% TFA and 5% acetonitrile, 0.1% TFA. The labeled peptides were eluted with 2 column volumes of 80% acetonitrile, 0.1% TFA and then freeze lyophilized overnight. The differentially labeled peptides were mixed and the sample was analyzed by mass spectrometry as described below.

14.8. Mass Spectrometry Analysis and Data Processing

14.8.1. Multidimensional Protein Identification Technology

Following diGly antibody immunoaffinity purification, optional dimethyl labeling and elution, peptides were analyzed using an adapted multidimensional protein identification technology (MudPIT) protocol in collaboration with the Mosley laboratory in the Department of Biochemistry and Molecular Biology at

IUSM, Indianapolis. MudPIT is the method of choice for analyzing complex protein samples. In brief, two different chromatographic resins are used to improve the resolving power of the chromatography since each separation methods uses different molecular properties as a basis for separation. A strong cation exchange resin (SCX), which binds positively charged compounds, is the first dimension of the separation, occupying approximately 2.5 – 3 centimeters in a 100 micron nanocolumn. The second dimension of separation is a reverse-phase C18 resin that will separate peptides based on their hydrophobicity (149,150). The peptides are eluted off the SCX resin using ammonium salts in sequential steps starting from low to high salt concentration. After each step, some peptides will be released from the SCX resin and will bind to the C18 resin. The salt step is followed by a gradient of acetonitrile (organic) buffer to elute the peptides from the C18 resin and directly into the mass spectrometer. Following previous studies in the Mosley laboratory (151), a 10-step MudPIT experiment was performed using 8 µL of the following concentrations of ammonium acetate in sequential steps to elute subsets of peptides from the strong cation exchange resin (Luna 5µM SCX, Phenomenex): 5 mM, 10 mM, 25 mM, 50 mM, 100 mM, 150 mM, 200 mM, 250 mM, and 300 mM (performed twice) followed by a 120-minute gradient of 5-60% acetonitrile. Considering that ubiquitination reduces the likelihood of trypsin cleavage at the modified lysine residue and that the N-terminus of the diGly remnant retains a positive charge, the majority of the diGly modified peptides have a net charge of ≥ +3. During the initial pilot experiments for this study, we determined that the diGly remnant peptides eluted late in the

56

standard 10-step MudPIT. To provide greater chromatographic resolution for these peptides and to allow for their complete elution, we employed a modified MudPIT experimental protocol for these analyses using 8 µL of the following concentrations of ammonium acetate in sequential steps to elute subsets of peptides from the strong cation exchange resin: 25 mM, 50 mM, 75 mM, 100 mM, 150 mM, 200 mM, 250 mM, 300 mM, 350 mM, 400 mM. Additionally, the organic gradient of 5-60% acetonitrile was increased to 140 minutes. This approach, henceforth referred to as diGly MudPIT, was used to analyze dimethyl-labeled and unlabeled samples.

14.8.2.   Mass Analysers

Using the diGly MudPIT approach, technical replicates of the samples were analyzed on a LTQ Velos Pro ion trap, a LTQ Velos Pro Orbitrap, or a Q-Exactive mass spectrometer as indicated. Ion trap mass spectrometers are high-throughput instruments that feature fast scan rates, high sensitivity and reasonable resolution and mass accuracy (100 ppm) (152). Orbitrap uses orbital trapping of ions in its electrostatic fields (153) in which ions orbit around a central electrode and oscillate in the axial direction. The Orbitrap mass analyzer has high resolution, high mass accuracy (2-5 ppm), a mass-to-charge range of 6000 and a dynamic range greater than 10^3. The Q-Exactive mass spectrometer is the combination of a quadrapole mass filter with the Orbitrap analyzer and has better than 1 ppm mass accuracy (154). Peptides are traditionally fragmented by collision induced dissociation (CID) fragmentation (155) and this method was

employed on both the Velos Pro instruments. The data acquired on the Q-Exactive instrument all used higher-energy collision induced dissociation (HCD) fragmentation for MS/MS peptide analysis. The fragmentation events normally occur at the peptide bonds and some fragmentations occur more frequently than others as a consequence of individual amino acid characteristics resulting in variation in the abundance of the peaks in MS/MS spectra. The fragment peaks that contain the amino-terminus of the starting peptide (parent) are termed b-ions while those containing the carboxy-terminus are called y-ions. In Figure 15, the b-ion series is in red and the y-ion series is in blue. The amino acid sequence of sections of the fragmented peptide can be inferred by the mass difference between the fragment peaks, for example the mass difference between y10 and y11 is the mass of glutamic acid (Figure 15 B). The mass of the precursor ion is also used to identify the sequence of the peptide when compared to a protein database. MS/MS data were collected during the MudPIT separation as outlined above using Xcalibur software (Thermo Scientific). For each sample, data was collected using data dependent acquisition with the top 20 most intense ions being selected for MS/MS analysis following collision induced dissociation (CID) or higher-energy collision induced dissociation (HCD) fragmentation. Dynamic exclusion settings were as follows: LTQ Velos Pro = 90 seconds, LTQ Velos Pro Orbitrap = 75 seconds, Q-Exactive = 50 seconds; with a repeat count of 1. MS1 data were collected on the LTQ Velos Pro Orbitrap and the Q-Exactive with a resolution of 60,000. MS/MS analysis in the Q-Exactive was analyzed in the Orbitrap with a resolution of 7,500. The use of high-resolution instruments for

some technical replicates of each sample was performed to aid in confirmation of the peptide identification.

14.8.3.   Peptide Identification

Peptide identification is performed by correlating the acquired MS/MS spectra from the experiment with theoretical spectra predicted for each peptide in a protein sequences database using a number of available computational tools. The program takes the experimental MS/MS spectrum as the input and generates a score after comparison against the theoretical fragmentation spectra. The search score calculated by the program measures the number of fragment ion matches between the experimental and theoretical spectra for peptides from the FASTA database with similar precursor ion masses. All RAW files from the respective mass spectrometers were used for FASTA database searches using Proteome Discoverer 1.4, which is licensed for use of SEQUEST HT as the database search algorithm. A beta version of Percolator 64 was used for target-decoy based false discovery rate calculations as previously described (156). All searches were performed using the mouse Uniprot FASTA proteome for peptide-spectrum matching. A peptide-spectrum match (PSM) scoring function counts the number of times a peptide-spectrum pair matches the fragmentation pattern of a peptide in the database (157). The database also contained ~150 common contaminant proteins including keratins, IgGs, and proteolytic enzymes. In all searches, modification of cysteine by NEM was included as a static modification (+125.13 dalton). Dynamic modifications applied

in every search included methionine oxidation (+15.999 dalton) and diGly remnant on lysine (+114.1 dalton). Specific modifications included for dimethyl labeling experiments include: static N-terminal light methylation (+28 dalton) with dynamic heavy labeling (+4 dalton), lysine light methylation (+28 dalton), lysine heavy methylation (+32 dalton), diGly remnant with light labeling of the free glycine N-terminus (+142 dalton), and heavy labeling of the glycine free N-terminus (+146 dalton). The precursor mass tolerance is used to identify candidate peptides for MS/MS comparison from the FASTA database digested *in silico*. The fragment mass tolerance is the distance allowed between experimental and theoretical fragments to still be identified as a match. Relevant specific settings for the database search for LTQ-Velos Pro ion trap data were: precursor mass tolerance = 1.4 dalton, fragment mass tolerance = 0.8 dalton, and average masses were used. Relevant specific settings for the database search for LTQ-Velos Pro Orbitrap and Q-Exactive data were: precursor mass tolerance = 50 ppm, fragment mass tolerance = 1.0 dalton, and monoisotopic masses were used (these are the settings previously used by the Gygi and Harper groups for diGly remnant studies (158,159)). Protein inference challenges were resolved by applying parsimony rules; however assignment for protein families such as mouse myosins and actins were challenging given the high levels of redundancy of these protein families. For instance, myosin 4 was our top candidate for the myosin family peptide because all myosin family peptides matched to the myosin 4 sequence. Scaffold 4 (Proteome Software) was used in addition to Proteome Discoverer 1.4 for PSM viewing and figure preparation.
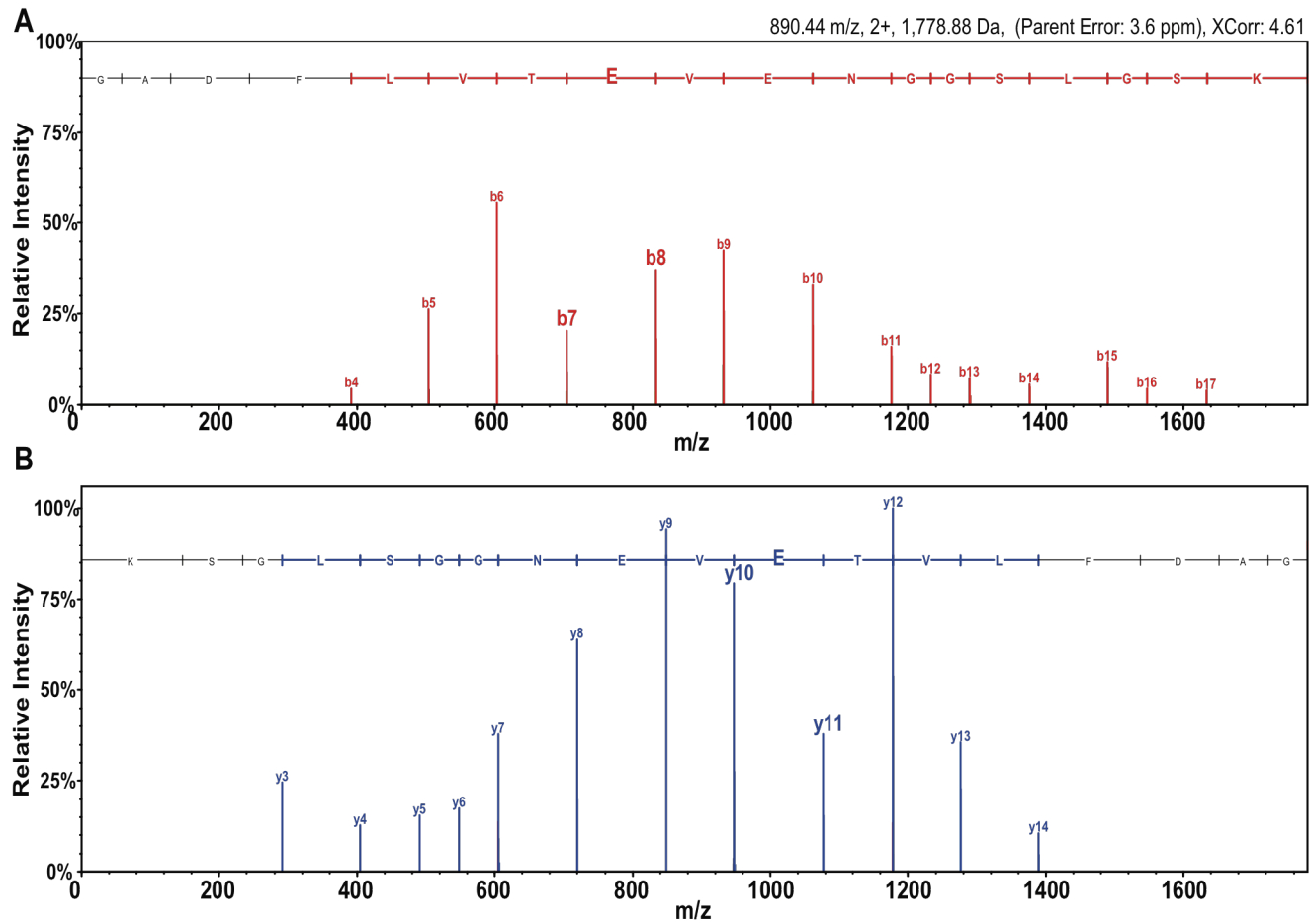
Figure 15. Simplified MS/MS Spectrum. Simplified fragment ion spectra for (K)GADFLVTEVENGGSLGSK(K) peptide from Pyruvate kinase. The b-ion series (red) is displayed in (A) while the y-ion series is displayed in blue (B).

RESULTS

1. Glycogen in MEFs from Mouse Models of Lafora Disease

1.1. Preamble

Lafora bodies are the hallmark of Lafora disease and in the different mouse models (32,81,108,109) of the disease, there is an over accumulation of abnormal hyperphosphorylated and poorly branched glycogen. Therefore, we analyzed the glycogen content in the MEFs derived from wild type (WT), *Epm2a-/-* (LKO), *Epm2b-/-* (MKO) and *Epm2a-/- Epm2b-/-* (DKO) mice. The method used to determine glycogen levels in animal tissues (146) was adapted in order to measure the glycogen levels in mouse embryonic fibroblasts.

1.2. Glycogen Levels in MEFs from Muscle Glycogen Synthase *Gys1-/-* Mice

The *Gys1-/-* mice, which are deficient in the muscle isoform of glycogen synthase, were generated in our laboratory as previously described (160). We derived MEFs from *Gys1-/-* mice and their wild type littermates as described in section 2 of Experimental Procedures. This experiment was performed as a positive control to determine that the biochemical measurement of glycogen is in fact representative of the cellular condition. As seen in Figure 16, the glycogen content in the *Gys1-/-* MEFs was close to zero in comparison to the wild type controls. There is very little or no glycogen present in the *Gys1-/-* mice (161) and therefore the MEFs have similar phenotypes to the mouse with regard to

glycogen accumulation thus, validating the method for determination of glycogen in MEFs.

1.3. Glycogen Levels in MEFs from Mouse Models of Lafora Disease

Upon enzymatic digestion of glycogen by amyloglucosidase, both *Epm2a-/-* and *Epm2b-/-* MEFs had ~50% more glycogen as compared to the wild type controls. The double *Epm2a-/- Epm2b-/-* MEFs, on the other hand, had unexpectedly less glycogen than even the wild type MEFs (Figure 17 A). It is possible that the distinct abnormal insoluble structure of glycogen in double *Epm2a-/- Epm2b-/-* MEFs could resist enzymatic degradation by amyloglucosidase and, therefore the partial/incomplete digestion of glycogen could give a lower value.

In order to circumvent the problem, glycogen was hydrolyzed with HCl. Under these conditions, glycogen was ~70% higher in all the knockout cells as compared to the wild type control cells (Figure 17 B) similar to the results of tissues from the animal models (162). The double knockout cells showed the same increase as the single knockout consistent with the involvement of a similar pathway.
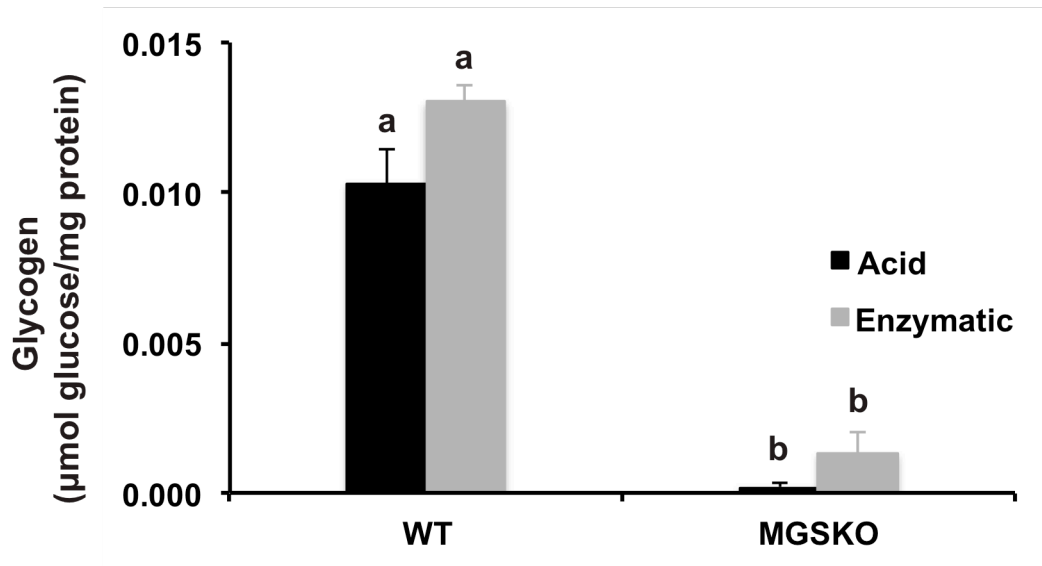
Figure 16. Glycogen in MEFs from Mice Lacking Muscle Glycogen Synthase. Glycogen levels in MEFs of wild type (WT) and *Gys1-/-* (MGSKO) mice were analyzed. The levels are expressed as glucose equivalents per mg protein. Values represent the average of three independent experiments ± SEM. Values marked by the same letter are not statistically significant, different letters indicate p<0.05.
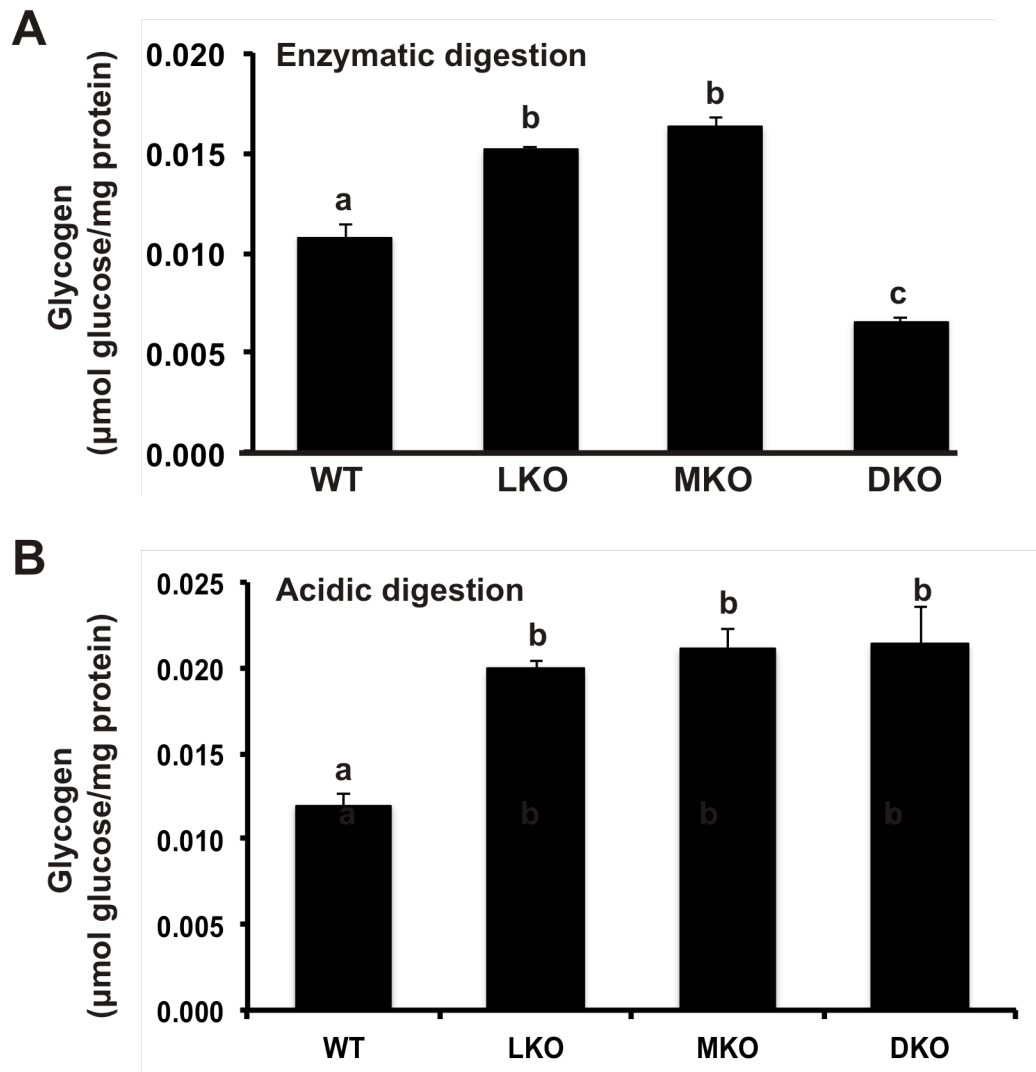
Figure 17. Glycogen in MEFs from Mouse Models of Lafora Disease. Glycogen levels in MEFs of wild type (WT), *Epm2a-/-* (LKO), *Epm2b-/-* (MKO) and double *Epm2a-/- Epm2b-/-* (DKO) mice were analyzed. Glycogen was digested by *A)* amyloglucosidase or *B)* hydrochloric acid. The levels are expressed as glucose equivalents per mg protein. Values represent the average of three independent experiments ± SEM. Values marked by the same letter are not statistically significant, different letters indicate p<0.05.

2. Protein Quality Control Process in MEFs from Mouse Models Lafora Disease

2.1. Preamble

Protein quality control processes play a critical role in maintaining intracellular homeostasis. Misfolded proteins are either refolded with the help of cellular chaperones or are degraded via the ubiquitin-proteasomal pathway or the autophago-lysosomal pathway (163). The proteasome tends to clear short-lived proteins while long-lived proteins are degraded by autophagy. Proteins are ubiquitinated before being targeted for degradation. While degradation via the proteasome is specific to ubiquitinated proteins, autophagy involves bulk degradation of various proteins, lipid droplets, damaged organelles, which may cause cellular stress upon accumulation (164-166). Under conditions of stress due to accumulation of non-degradable material, the proteolytic machinery is saturated which results in formation of aggregates (167). Under normal conditions, a certain amount of protein misfolding occurs in the endoplasmic reticulum, ER, which is ameliorated by retrograde transport of the misfolded proteins into the cytosol for degradation via the proteasomal pathway. Impairment of the function of the proteasome can lead to induction of ER stress to enhance the protein folding capacity of the ER. Excessive and prolonged ER stress along with impaired proteasomal function results in accumulation and aggregation of unfolded proteins (168), eventually leading to cell death.

We evaluated the three arms of the protein degradation/quality control process, the ubiquitin-proteasomal pathway, the autophago-lysosomal pathway

and the ER-stress response using primary embryonic fibroblasts (MEFs) derived from wild type, *Epm2a-/-*, *Epm2b-/-* and double *Epm2a-/- Epm2b-/-* mice.

2.2. Proteasomal Activity in MEFs from Mouse Models of Lafora Disease

Using MEFs from wild type (WT), *Epm2a-/-* (LKO), *Epm2b-/-* (MKO) and double *Epm2a-/- Epm2b-/-* (DKO) mice, the proteasomal function was assessed by measuring the chymotrypsin-like activity using the Suc-LLVY-aminoluciferin substrate. The absence of laforin and/or malin significantly decreased proteasomal activity in the knockout MEFs as compared to the wild type controls (Figure 18 A). However, the protein level of the S5a subunit of the 26S proteasome was not different between genotypes (Figure 18 B) suggesting that the observed difference in the chymotrypsin-like activity is not due to a difference in the levels of proteasome but rather intrinsic activity. Thus, proteasomal function is impaired in cells from mouse models of Lafora disease.

2.3. Autophago-lysosomal Pathway in MEFs from Mouse Models of Lafora Disease

Upon induction of autophagy, microtubule associated protein 1 light chain 3 (LC3-I) is lipidated to LC3-II, which displays increased electrophoretic mobility. LC3-II is then incorporated into the inner and outer membranes of the newly formed autophagosomes, which fuse with the lysosomes to form autolysosomes where the engulfed components are degraded by the lysosomal enzymes (Figure

6). Thus, LC3-II is commonly used as a marker to evaluate autophagosome levels (169).

MEFs were cultured in complete medium to assess basal autophagy or in serum-free and amino acid-free medium (EBSS) to induce autophagy by starvation (170). Under both basal and starved conditions, there was a significant decrease in the levels of LC3-II in knockout MEFs compared to the wild type controls (Figure 19 A, B). Starvation induced a significant increase in the LC3-II levels in the wild type cells but the effect was much smaller in the knockout cells. A decrease in the levels of LC3-II could either be due to impairment in the formation of autophagosomes or an increase in the degradation by autolysosomes. To differentiate between the two, MEFs were treated with 20 µM chloroquine, a lysosomal inhibitor, for 2 hours to block the degradation of LC3-II. The changes in the levels of LC3-II upon lysosomal inhibition should, thus, reflect changes in the rate of formation of autophagosomes (169). In the presence of chloroquine, there was still a significant decrease in the levels of LC3-II in knockout MEFs indicating impairment in the formation of autophagosomes (Figure 19 C, D). Combined starvation and chloroquine treatment still resulted in a small increase in the levels of LC3-II even in knockout MEFs but the increase was significantly lower than in the wild type MEFs (Figure 19 C, D). This small increase was further decreased in the double knockout cells. Thus, the absence of either laforin or malin dampens the autophagic process.
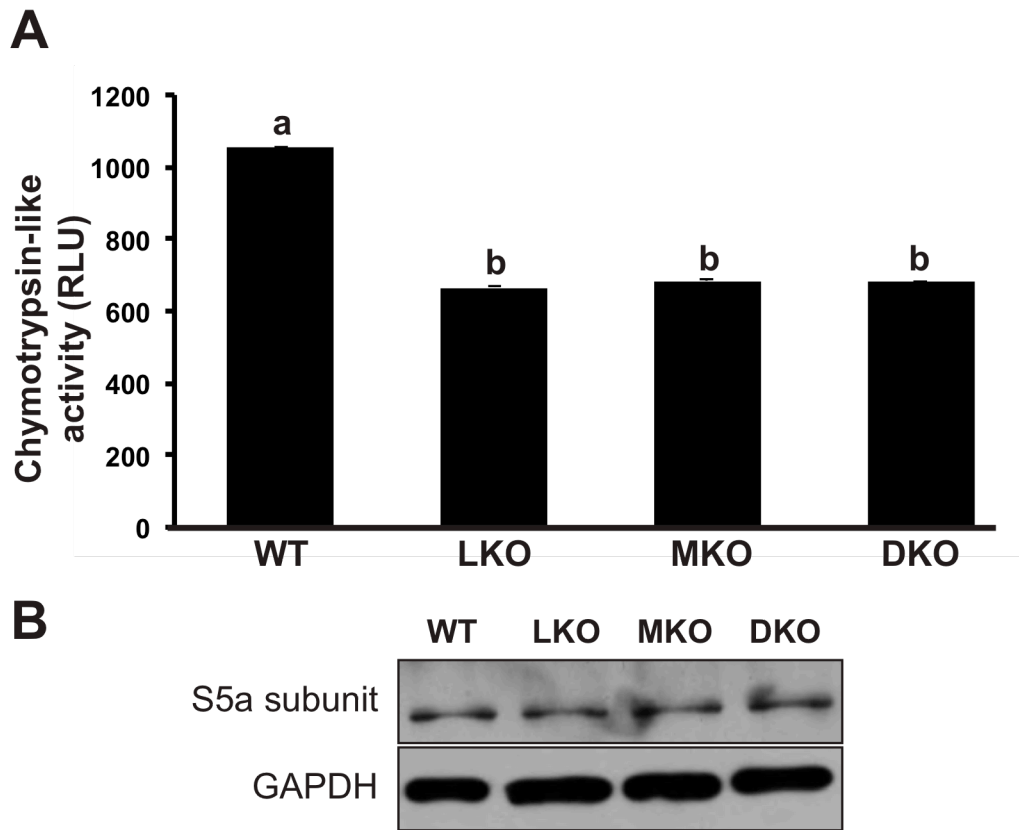
Figure 18. Proteasomal Activity in MEFs from Mouse Models of Lafora Disease. Soluble extracts derived from MEFs of wild type (WT), *Epm2a-/-* (LKO), *Epm2b-/-* (MKO) and double *Epm2a-/-Epm2b-/-* (DKO) mice were analyzed. *A)* Proteasomal activities were measured in soluble lysates (10 µg) using Proteasome-Glo™ Chymotrypsin-like assay. Values represent the average of three independent experiments performed in duplicates ± SEM. RLU-relative luminescence unit. Values marked by the same letter are not statistically significant, different letters indicate p<0.05. *B)* Representative Western blots using antibody against S5a subunit of the 26S proteasome. Loadings were 10 µg of protein. *GAPDH*, glyceraldehyde-3-phosphate dehydrogenase.

Figure 19. Autophagy in MEFs from Mouse Models of Lafora Disease. MEFs from wild-type (WT), *Epm2a-/-* (LKO), *Epm2b-/-* (MKO) and double *Epm2a-/- Epm2b-/-* (DKO) mice were incubated without and with 20 µM chloroquine for 2 hours under basal (NS) or starvation (S) conditions. Total lysates (10 µg) from MEFs were analyzed. *A, C)* Representative Western blots using antibody against LC3 in the absence and presence of chloroquine, respectively. The positions of LC3-I and LC3-II are indicated on the left. *GAPDH*, glyceraldehyde-3-phosphate dehydrogenase. *B, D)* LC3-II bands were quantitated by densitometry and normalized to the corresponding GAPDH bands. Values represent the average of three independent experiments ± SEM. Values marked by the same letter are not statistically significant, different letters indicate p<0.05.

2.4. mTOR Signaling Pathway in MEFs from Mouse Models of Lafora Disease

mTOR, mammalian target of rapamycin, negatively regulates autophagy. Nutritional deprivation inhibits mTOR and thus induces autophagy. Conversely, nutrient replenishment activates mTOR and suppresses autophagy (171,172). Activation of mTOR causes phosphorylation of downstream targets such as ribosomal protein S6 kinase (p70S6K) and its substrate ribosomal protein S6. Analysis of the levels of phosphorylated p70S6K and S6 protein indicated increased phosphorylation (Figure 20 A, B and Figure 20 A) under basal conditions in the knockout MEFs. Upon starvation, although there was a decrease in the phosphorylation of the S6 protein compared to the basal state, the phosphorylation in knockout MEFs was still higher than in the wild type control cells (Figure 20 B and Figure 21 A, high exposure). When MEFs were treated with 10 nM of rapamycin for 2 hours, the level of phosphorylated S6 protein in all MEFs decreased significantly as compared to the basal levels (Figure 21 A). Taken together, these observations suggest that mTOR signaling is upregulated in knockout cells and impairment of autophagy may be mTOR dependent.

Consistent with inhibition of mTOR, upon rapamycin treatment, LC3-II was increased in the wild type cells to a level similar to that of starvation. LC3-II in the knockout MEFs was also increased to the same level in the starved and rapamycin treated cells, although the effect did not reach the levels of the wild type cells (Figure 21 B, C). These observations suggest that either the autophagy

defect in knockout MEFs is only partly mTOR-dependent or that the maximum capacity of the cells to form new autophagosomes is impaired in the absence of laforin and/or malin.
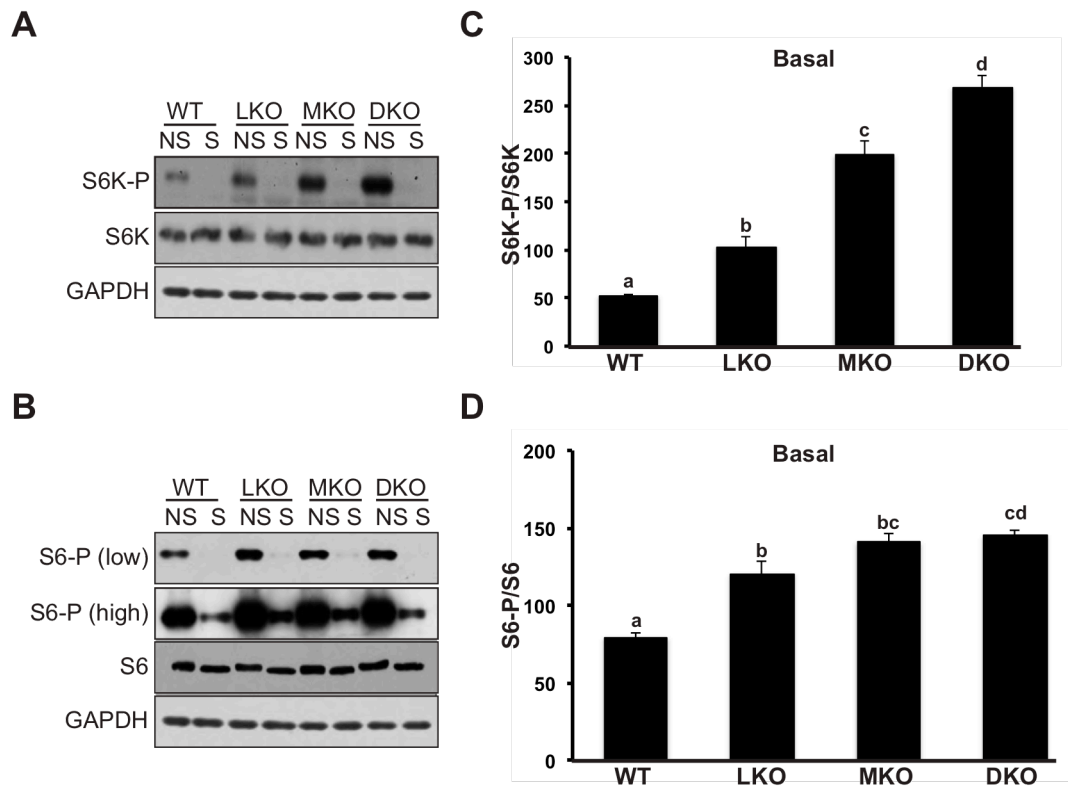
Figure 20. mTOR Signaling Pathway in MEFs from Mouse Models of Lafora Disease. MEFs from wild-type (WT), *Epm2a-/-* (LKO), *Epm2b-/-* (MKO) and double *Epm2a-/- Epm2b-/-* (DKO) mice were incubated under basal (NS) or starvation (S) conditions for 2 hours. Soluble extracts (10 µg) from MEFs were analyzed. Representative Western blots are shown against different antibodies; *A)* phosphorylated Thr[389] p70S6 kinase and total S6K, *B)* phosphorylated Ser[235/236]S6 and total S6 protein. *GAPDH*, glyceraldehyde-3-phosphate dehydrogenase. *C, D)* P-S6K and P-S6 bands were quantified by densitometry and normalized to the corresponding total S6K and total S6 bands, respectively. Values represent the average of three independent experiments ± SEM. Values marked by the same letter are not statistically significant, different letters indicate p<0.05.
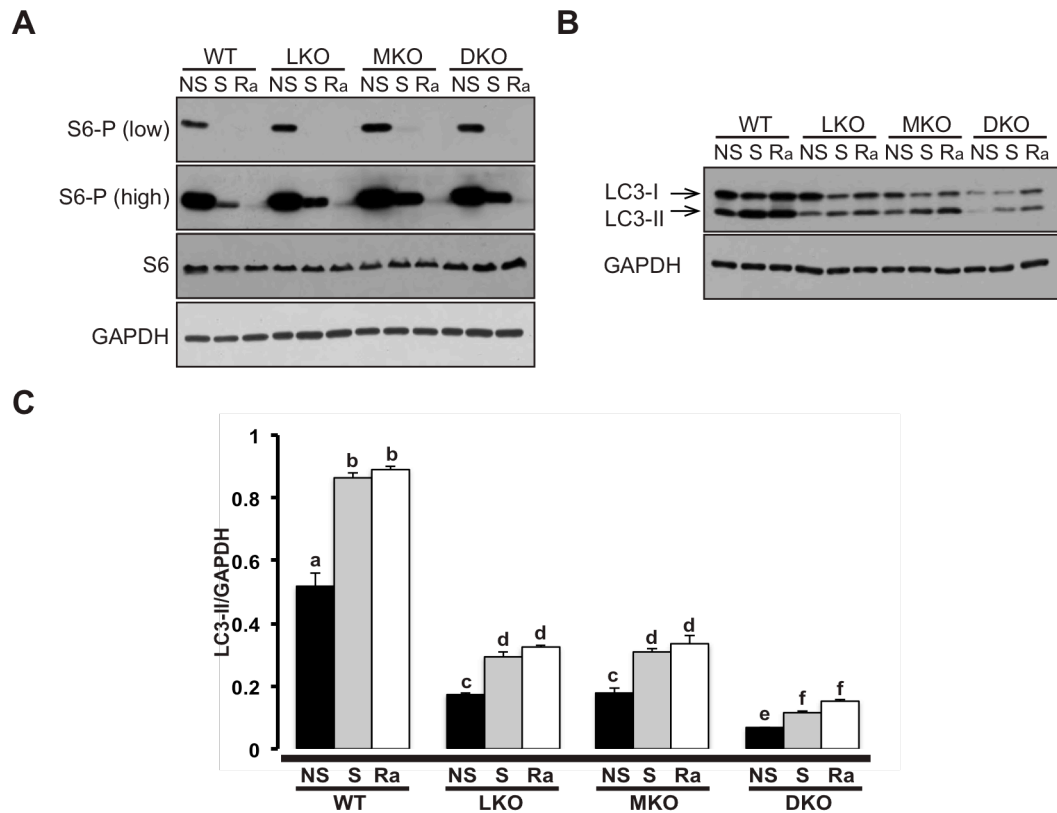
Figure 21. mTOR Signaling Pathway upon Rapamycin Treatment in MEFs from Mouse Models of Lafora Disease. MEFs from wild-type (WT), *Epm2a-/-* (LKO), *Epm2b-/-* (MKO) and double *Epm2a-/- Epm2b-/-* (DKO) mice were incubated under basal (NS) or starvation (S) conditions or with 10 nM rapamycin (Ra) for 2 hours. Soluble extracts (10 µg) from MEFs were analyzed. Representative Western blots are shown against different antibodies; *A)* phosphorylated $Ser^{235/236}$S6 and total S6 protein, *B)* LC3. *GAPDH*, glyceraldehyde-3-phosphate dehydrogenase. *C)* LC3-II bands were quantified by densitometry and normalized to the corresponding GAPDH bands. Values represent the average of three independent experiments ± SEM. Values marked by the same letter are not statistically significant, different letters indicate p<0.05.

2.5. Effect of Malin Deficiency on Lysosome and Late Endosome Markers

LC3 belongs to the autophagy-related genes 8 (Atg8) family, which includes γ-amino butyric acid receptor-associated protein-like 1 (GABARAPL1). Starch-binding domain protein 1 (Stbd1 or genethonin 1), a membrane and glycogen-binding protein, has been shown to interact with GABARAPL1 and abnormal glycogen and might be involved in the transfer of abnormal glycogen to lysosomes (33,60). We observed no difference in Stbd1 protein in the knockout MEFs as compared to the wild type controls (Figure 22 A). We also analyzed the levels of GABARAPL1 and interestingly, the levels of GABARAPL1 in the LKO MEFs were similar to the wild type controls whereas GABARAPL1 was much lower in MKO cells as compared to the wild type or to the LKO cells (Figure 22 A, B). Similar to GABARAPL1, LAMP1, a marker of late endosomes and lysosomes, was unchanged in LKO but significantly lower in the MKO cells (Figure 22 A, C). Additional loss of laforin in the DKO cells did not cause any further decrease in either GABARAPL1 or LAMP1 levels (Figure 22 A). These results suggest that there may not be a complete overlap in the functions of malin and laforin, as proposed by previous studies (115,125,127), and that a unique function of malin might be related to lysosome biogenesis or lysosomal trafficking of glycogen.
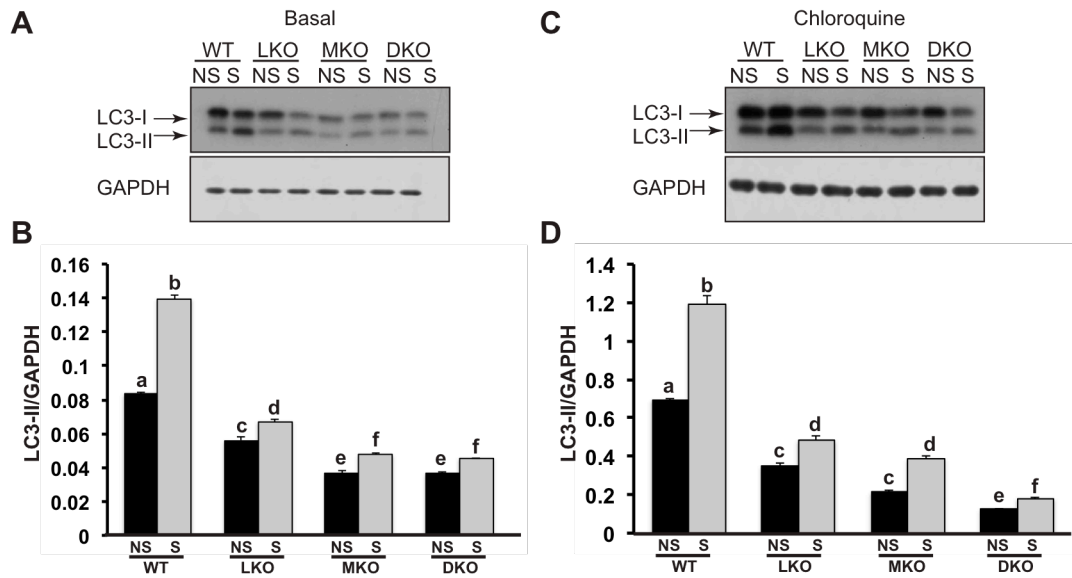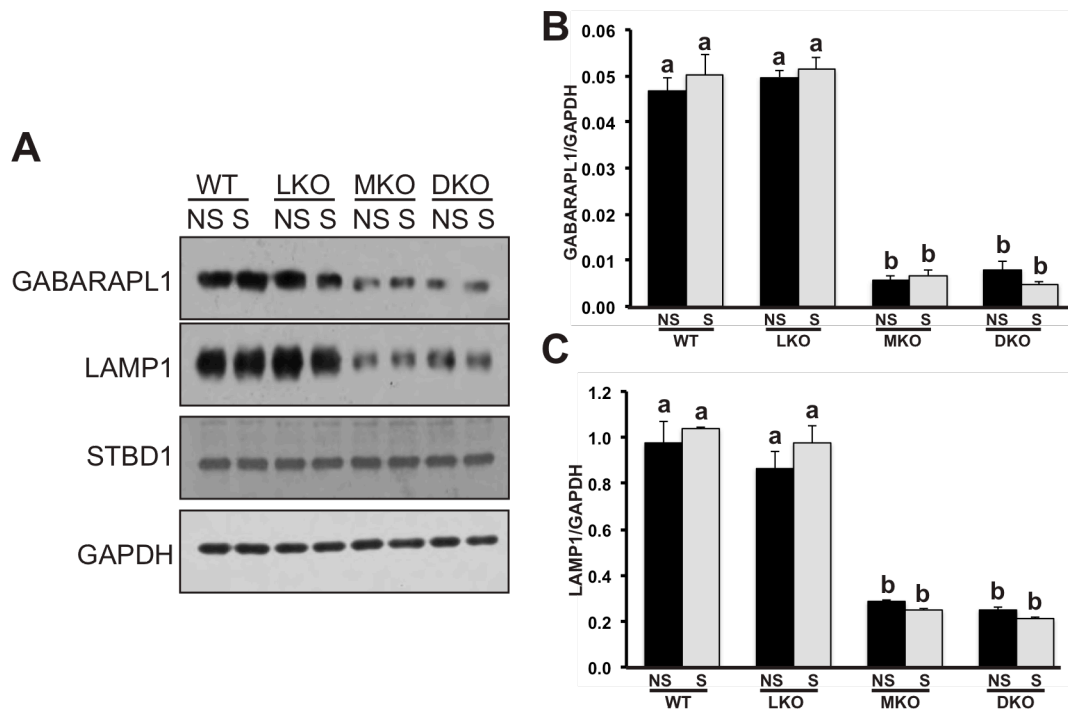
Figure 22. Lysosome and Late Endosome Markers in MEFs from Mouse Models of Lafora Disease. MEFs from wild-type (WT), *Epm2a-/-* (LKO), *Epm2b-/-* (MKO) and double *Epm2a-/-Epm2b-/-* (DKO) mice were incubated under basal conditions (NS) or starvation (S) for 2 hours. Total lysates (10 µg) from MEFs were analyzed. Representative Western blots using antibodies against *A)* GABARAPL1, LAMP1 and Stbd1. *GAPDH*, glyceraldehyde-3-phosphate dehydrogenase. *B, C)* GABARAPL1 or LAMP1 bands were quantified by densitometry and normalized to the corresponding GAPDH bands. Values represent the average of three independent experiments ± SEM. Values marked by the same letter are not statistically significant, different letters indicate $p<0.05$.

2.6. Degradation of Ubiquitinated Proteins in Laforin and/or Malin Deficient Cells

Ubiquitinated proteins are degraded either via the ubiquitin-proteasomal or the autophago-lysosomal pathway depending on the lysine involved in the formation of the polyubiquitinated chains (122,124). We compared the levels of ubiquitinated proteins in the knockout MEFs with the wild type controls. Under basal conditions, there was no difference in the level of ubiquitinated proteins. However, upon starvation, there was a significant decrease in ubiquitinated proteins in wild type cells while in the knockout MEFs the levels were no different than the basal state (Figure 23 A, D). When the MEFs were treated with the lysosomal inhibitor chloroquine (Figure 23 B, E) or the proteasomal inhibitor MG132 (Figure 23 C, F), even under starvation conditions, neither the wild type nor the knockout MEFs showed any decrease in levels of ubiquitinated proteins. These results indicate that loss of laforin and/or malin impairs the starvation- or stress-induced degradation of the ubiquitinated proteins and that the degradation could be either via the ubiquitin-proteasomal or the autophago-lysosomal pathway.
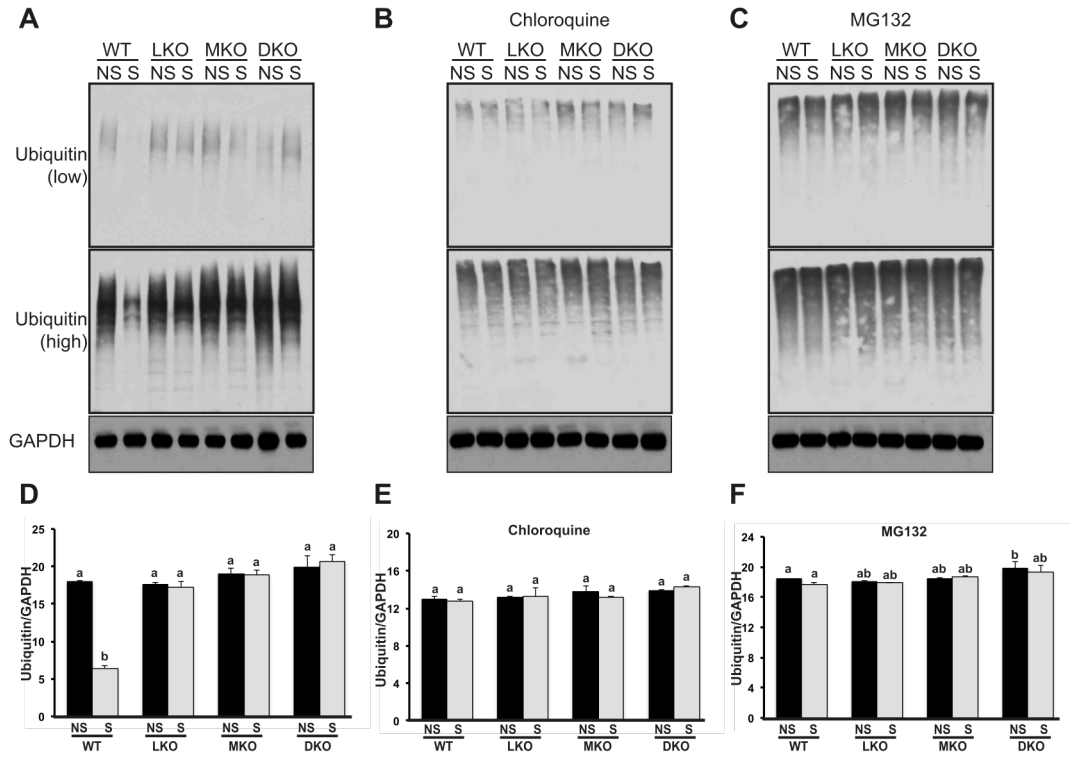
Figure 23. Degradation of Ubiquitinated Proteins in MEFs from Mouse Models of Lafora Disease. MEFs from wild-type (WT), *Epm2a-/-* (LKO), *Epm2b-/-* (MKO) and double *Epm2a-/- Epm2b-/-* (DKO) mice were incubated under basal conditions (NS) or starvation (S) without or with 20 µM chloroquine or 20 µM MG132 for 2 hours. Soluble extracts (10 µg) from MEFs were analyzed. Representative Western blots using anti-ubiquitin antibody against ubiquitinated proteins *A)* without and *B)* with chloroquine or *C)* with MG132. *GAPDH,* glyceraldehyde-3-phosphate dehydrogenase. *D, E, F)* Bands for ubiquitinated proteins were quantified by densitometry and normalized to the corresponding GAPDH bands. Values represent the average of three independent experiments ± SEM. Values marked by the same letter are not statistically significant, different letters indicate p<0.05.

2.7. ER Stress Response in MEFs from Mouse Models of Lafora Disease

Impairment of proteasomal function might lead to induction at the endoplasmic reticulum, ER stress. An earlier study by Vernia et al. (135) suggested that laforin deficiency leads to an increased sensitivity to ER stress-inducing agents. Therefore, we investigated the third arm of protein quality control, the ER stress response in MEFs by analyzing the expression of the transcriptional factor CHOP (173), a widely used ER stress marker. MEFs were treated with two known ER stress-inducing agents, thapsigargin, an inhibitor of the ER calcium pump and tunicamycin, an inhibitor of ER glycosylation. The levels of CHOP were higher upon treatment with thapsigargin or tunicamycin by comparison to the basal condition both in wild type and in the knockout MEFs with no differences between genotypes (Figure 24 A, B). Thus, the ER stress response is not compromised in the absence of malin and/or laforin.
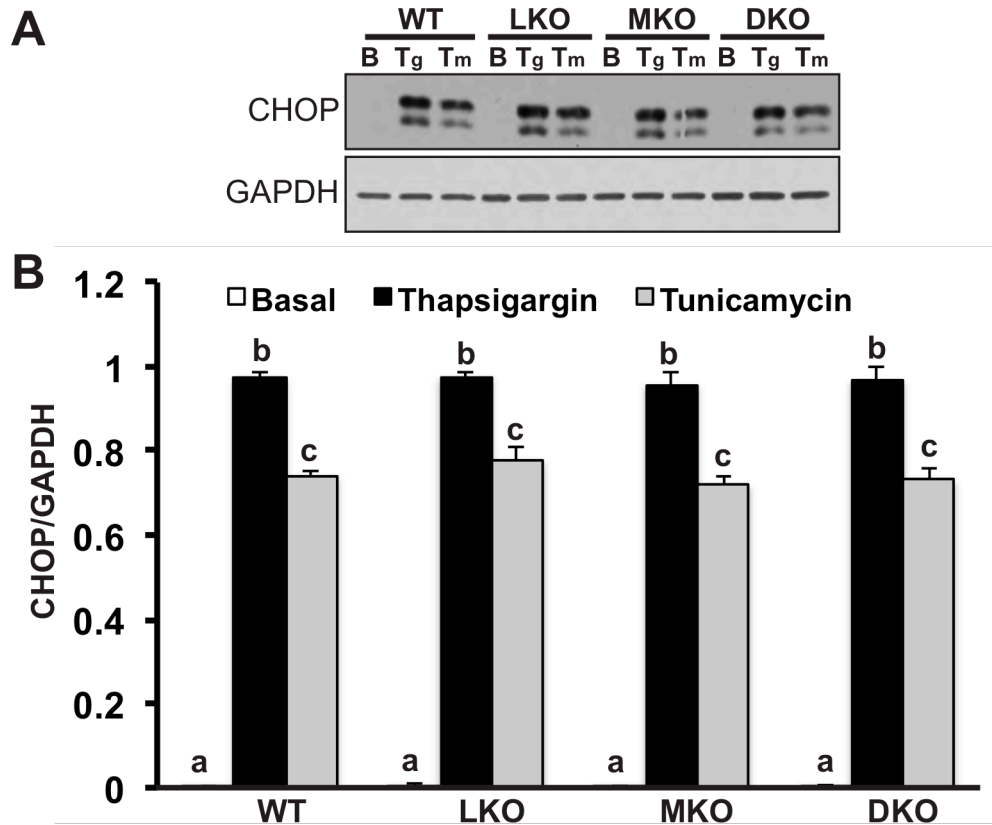
Figure 24. ER Stress Response in MEFs from Mouse Models of Lafora Disease. MEFs from wild-type (WT), *Epm2a-/-* (LKO), *Epm2b-/-* (MKO) and double *Epm2a-/- Epm2b-/-* (DKO) mice were incubated without or with 1 µM thapsigargin or 2 µg/ml tunicamycin for 18 hours. Soluble extracts (10 µg) from MEFs were analyzed. *A)* Representative Western blots using antibody against CHOP. *GAPDH*, glyceraldehyde-3-phosphate dehydrogenase. *B)* Bands for CHOP were quantified by densitometry and normalized to the corresponding GAPDH bands. Values represent the average of three independent experiments ± SEM. Values marked by the same letter are not statistically significant, different letters indicate p<0.05.

3. Malin-dependent Ubiquitylome in Lafora Disease

3.1. Preamble

Malin contains a RING finger domain characteristic of an E3 ubiquitin ligase (81). A number of different studies have attempted to identify the substrates of malin and several proteins involved in glycogen metabolism, laforin (101), glycogen synthase (115), protein targeted to glycogen (PTG) (127) and the debranching enzyme (AGL) (125) have been proposed to be malin substrates. However, most of these conclusions are based on either *in vitro* or cell culture overexpression systems. Moreover, results in our laboratory with *Epm2b-/-* mice did not provide any evidence for alterations in levels of PTG and AGL or in glycogen synthase activity (108) arguing against them being malin substrates.

In this study, we present the development of an unbiased proteomics approach to identify potential substrates of malin. Ubiquitination of proteins involves a chain of three reactions as described in section 7.4 of the Introduction (Figure 11). An isopeptide bond is formed between the C-terminal glycine and the ε-amino group of the lysine residue in the substrate. Trypsinolysis of proteins cleaves the C-terminal Arg-Gly-Gly sequence of ubiquitin and yields a characteristic diGly remnant on the lysine of the substrate (Figure 25). The diGly remnant provides a method for detection of ubiquitinated peptides by mass spectrometry. The approach was developed to systematically identify malin-dependent ubiquitination targets using quantitative diGly proteomics. This involved anti-diGly antibody-based capture of diGly ubiquitin-remnant containing peptides (158) from wild type and *Epm2b-/-* mice (Figure 26), that are

differentially labeled. In the absence of malin in the *Epm2b-/-* mice, the potential

malin substrate might not be ubiquitinated and the absence of the peptide from

Epm2b-/- lysates on mass spectrometry would identify candidate malin

substrates.
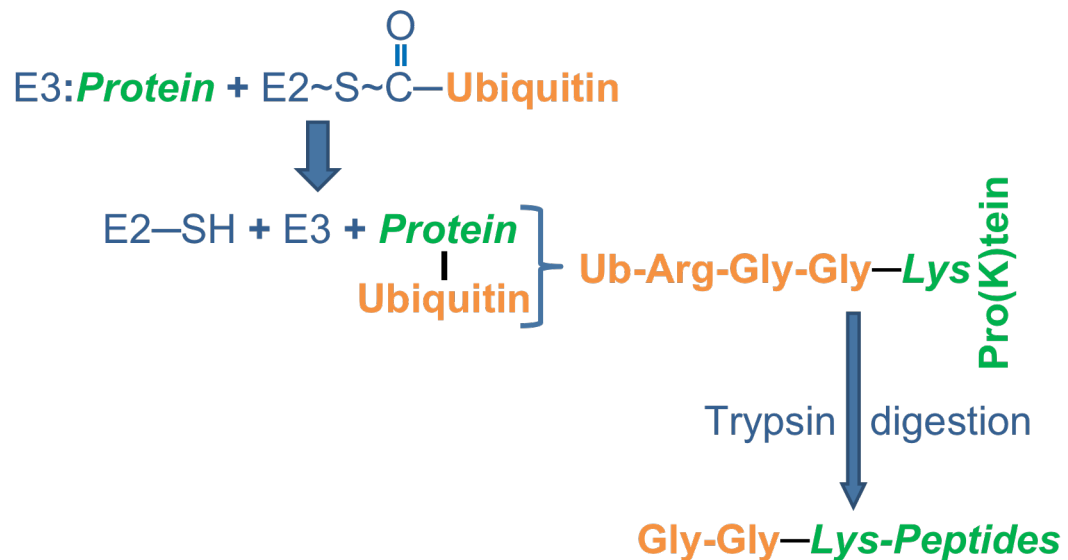
Figure 25. Ubiquitination reaction. An isopeptide bond is formed between C-terminal glycine and the ε-amino group of the lysine residue in the protein. Trypsinolysis of the proteins cleaves the Arg-Gly-Gly sequence of ubiquitin and yields a Gly-Gly remnant on the lysine of the protein.
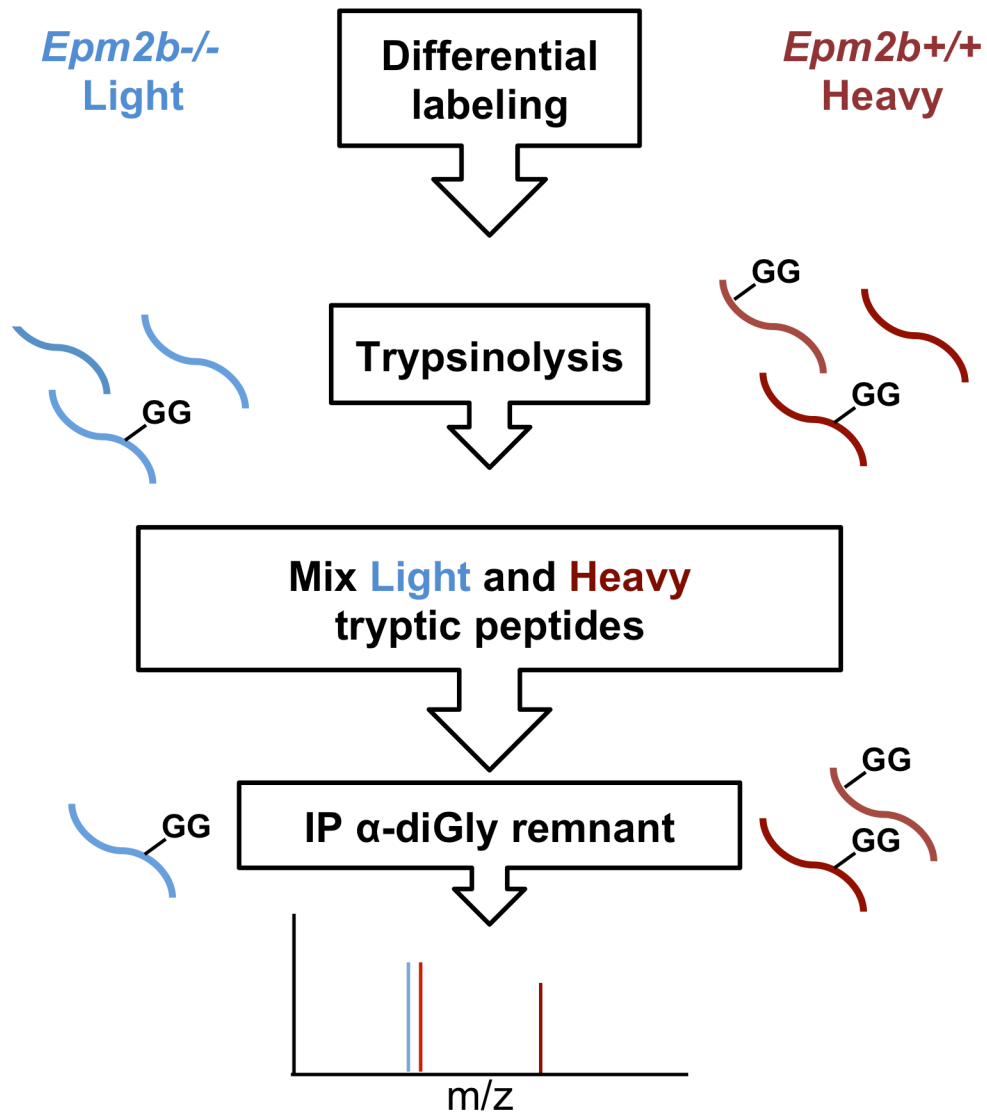
Figure 26. Quantitative diGly Proteomics Approach. It involves anti-diGly antibody-based capture of the diGly ubiquitin remnant containing differentially labeled peptides from wild type and *Epm2b-/-* mice.

3.2. Quantitative diGly Proteomics using SILAC

To investigate the ubiquitin proteome, MEFs derived from wild type and *Epm2b-/-* mice were cultured in lysine and arginine-free medium supplemented with either $[^{12}C_6^{14}N_2]$ lysine (K0) and $[^{12}C_6^{14}N_4]$ arginine (R0) (light medium) or $[^{13}C_6^{15}N_2]$ lysine (K8) and $[^{13}C_6^{15}N_4]$ arginine (R10) (heavy medium). Proteolysis by Lys-C and trypsin generated diGly remnants on the lysine on the peptides. In the absence of malin, the potential substrate might not be ubiquitinated and might not be immunoprecipitated by the diGly antibody and therefore not detected by mass spectrometry (Figure 27).

The cells (twelve 150 mm culture plates for each genotype) were incubated in either light or heavy medium that contained 20 µM MG132 for four hours before the time of harvest. MG132 should prevent the degradation of the substrate in the wild type cells by blocking the proteasomal activity. The cells were harvested and lysates were prepared as described in section 14.1 of Experimental Procedures. The lysates from the light and heavy cells were mixed in a 1:1 ratio based on protein concentration and then digested overnight with Lys-C followed by overnight digestion with Trypsin-Gold. The digestion was quenched by addition of 20% TFA to a final concentration of 1%. The acidified peptides were purified using a C 18 Sep-Pak column and then lyophilized for 3 days. The lyophilized peptides were then immunoaffinity-purified using the diGly antibody, concentrated using C18 StageTips followed by mass spectrometry.
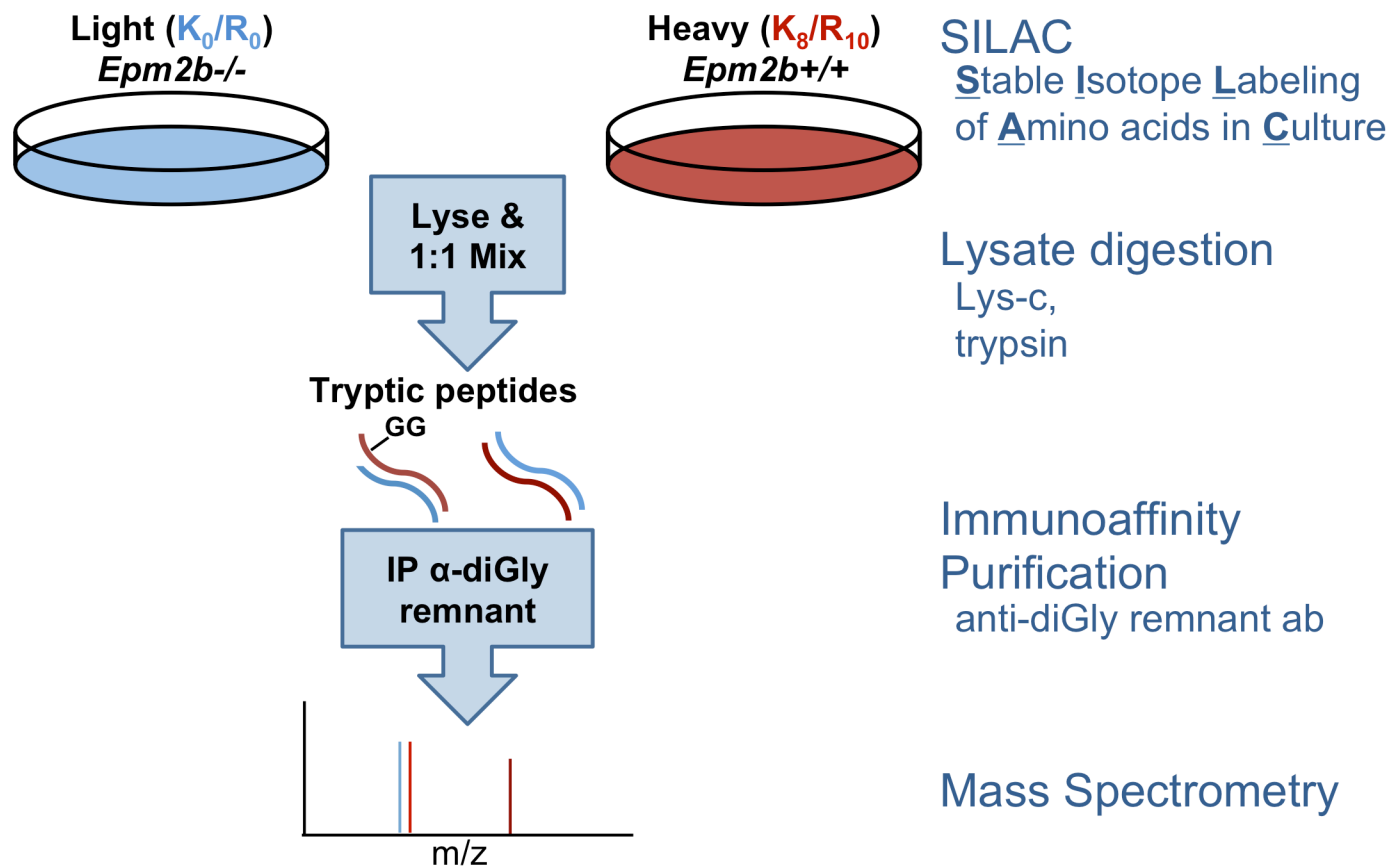
Figure 27. Quantitative diGly proteomics using SILAC. MEFs from wild type and *Epm2b-/-* mice were cultured in medium containing heavy and light amino acids, respectively. The cells were lysed and mixed in 1:1 ratio followed by proteolysis by Lys-C and trypsin yielding diGly remnants, which were immunoprecipitated using anti-diGly antibody. The final eluate from the immunoprecipitation is analyzed by mass spectrometry.

3.2.1. Serum Contaminants in Cell Lysates

The presence of serum proteins, in particular bovine albumin, interfered with the detection of the murine peptides. Albumin was present at levels much higher than the most abundant murine peptide, vimentin (Table 1). It is difficult to avoid contamination by albumin because it adheres not only to the cells in culture but also to the cell culture plates (174). Table 1 shows the list of the top 12 proteins obtained from MudPIT-LC/MS analysis. About 50% of the proteins were of bovine origin. Furthermore, there is a considerable homology between proteins from *Bos taurus* and *Mus musculus*; for example, myosin 9 from *Mus musculus* had homology to myosin 10 from *Bos taurus*. This makes it difficult to distinguish between bovine and murine peptides because of the overlap of identical tryptic peptide sequences. Subsequent experiments were focused on removal of serum contaminating proteins, mainly albumin, at the time of harvest and cell lysis.

Table 1. diGly Proteomics using SILAC. Proteins identified by quantitative diGly proteomics approach using SILAC in MEFs derived from wild type and *Epm2b-/-* mice.

Description	Source	Coverage	#Peptides	#PSMs	MW
Albumin	Bos taurus	54.86	26	247	69.2
Alpha-1-antiproteinase Precursor	Bos taurus	24.52	8	77	46.1
Alpha-2-HS-glycoprotein precursor	Bos taurus	31.75	9	66	38.4
Vimentin	Mus musculus	33.69	12	56	53.7
Myosin-9	Mus musculus	11.12	16	49	226.2
Serotransferrin precursor	Bos taurus	31.39	15	38	77.7
Serum albumin precursor	Mus musculus	4.77	2	33	68.6
Actin, cytoplasmic 2	Bos taurus	40.80	10	31	41.8
Tubulin alpha-1B chain	Bos taurus	20.40	6	31	50.1
Alpha acitinin-1	Mus musculus	14.13	10	26	103.0
Myosin-10	Bos taurus	6.43	9	26	229.0
Prelamin-A/C isoform A	Mus musculus	18.35	10	25	74.2

Coverage: The percentage of amino acid sequence identified by matching tryptic peptides
PSMs: The number of peptide spectral matches
#Peptides: The number of peptides that were detected
MW: The molecular weight of protein in kilodaltons

3.2.2. Modified Washing Techniques to Avoid Albumin Contamination

At the time of harvest, the culture medium was removed by aspiration and the cells were washed three times with 10 ml of ice cold PBS. The washes were modified to three 5-minute washes with PBS on an orbital shaker at 4°C or three 5-minute washes with serum-free medium on an orbital shaker at 4°C or three 5-minute washes of cells in suspension with PBS as described in section 8 of Experimental Procedures. Figure 28 shows that the cross contamination with albumin was present even after extended washes with PBS or serum-free medium.

3.2.3. Culturing Cells in Serum-free Medium (SFM)

Since it was difficult to remove albumin by extended washes, we tried to culture the cells in serum-free conditions. The FibroGRO™ Complete Media Kit from Millipore was used as an alternative to DMEM:F12 medium with 10% FBS. The cells were adapted to grow in the serum-free media (SFM) either by direct adaptation or by sequential adaptation as described in section 6 of Experimental Procedures. The cells failed to survive after direct adaptation from full medium to SFM. Therefore, the cells were cultured by sequential adaptation that involved serial switching to medium with different ratios of Full medium:SFM: 100:0, 70:30, 50:50, 30:70, 20:80 and 0:100. Figure 29 A represents the cell morphology at each step. There was no change in the morphology of the cells till a 50:50 ratio of Full:SFM. At a 30:70 ratio, there was a change in the morphology

of the cells with a lower number of cells surviving after each passage. There was a significant increase in the number of cells with altered morphology and increased cell death at 20:80 ratio of Full:SFM (Figure 29 A).

M: Prestained protein marker
+ :BSA protein as positive control
1 :Three washes with PBS
2 :Extended washes with PBS
3 :Washes in suspension
4 :Extended washes with serum-free medium
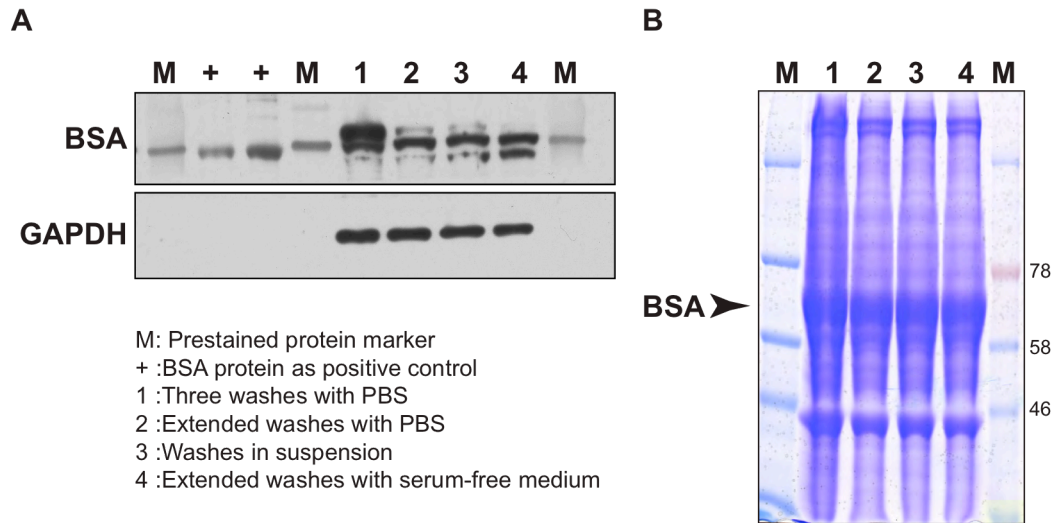
Figure 28. Modified Washing Techniques for Removal of Albumin. After removing the medium, cells were washed by four different methods. 1. Three washes with PBS, 2. Extended washes with PBS, 3. Washes in suspension after trypsinization and 4. Extended washes with serum-free medium. Soluble extracts (20 μg) from the cells were analyzed. *A)* Representative western blot using antibody against BSA. *BSA*, bovine serum albumin; *GAPDH*, glyceraldehyde-3-phosphate dehydrogenase. *B)* SDS-PAGE analysis with Coomassie staining showing BSA.

3.2.4. Culturing Cells in Low Serum Medium

While growing in SFM, the cells could maintain normal morphology only up to a Full:SFM ratio of 30:70. Since the cells failed to survive in the absence of serum, we tried to culture the cells under low-serum conditions. The cells were initially cultured with 10% serum and then switched to medium with reduced serum as described in section 7 of the Experimental Procedures. The cells were able to survive with 2% serum without a change in morphology; however at 1% serum the majority of the cells either failed to grow or had altered morphology (Figure 29 B). The antibiotics used in culture tend to bind to various serum proteins, thus reducing the effective concentration of the antibiotics (175). Therefore, in low serum medium, the concentration of antibiotics was reduced to avoid cell death due to antibiotic toxicity. The cells were cultured in DMEM-F12 with 2% dialyzed FBS and reduced antibiotic concentrations (20 units/ml of penicillin and 20 μg/ml of streptomycin) for SILAC. The cell lysate was analyzed by mass spectrometry for the presence of contaminant serum proteins. Table 2 lists the most abundant proteins obtained from MudPIT-LC/MS analysis. In contrast to Table 1, the majority of the proteins in Table 2 are of murine origin.

A

Full Medium (10%FBS)

70:30-Full:SFM

50:50-Full:SFM

30:70-Full:SFM

20:80-Full:SFM

B
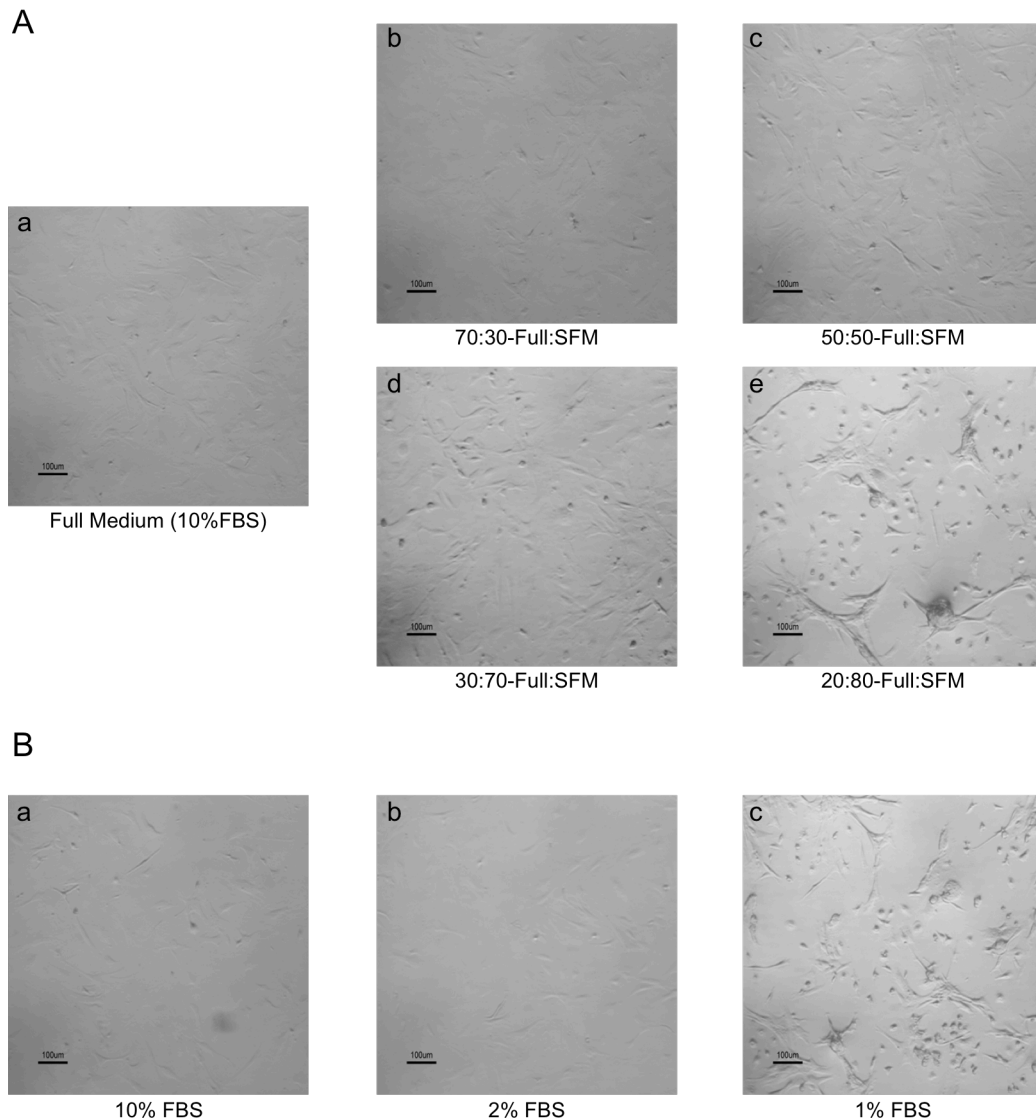
10% FBS

2% FBS

1% FBS

Figure 29. Cell Culture in Serum-free and Low Serum Conditions. *A)* Cells were cultured in full medium (a) and then sequentially adapted from Full:SFM ratio of 70:30 to 20:80 (b-e). *B)* Cells were cultured in full medium that contained 10% FBS (a) or 2% FBS (b) or 1% FBS (c). SFM, serum-free medium; FBS, fetal bovine serum. All pictures were taken using a stereoscopic microscope (Nikon Corporation).

Table 2. diGly Proteomics using SILAC with Low Serum Medium. Proteins identified by quantitative diGly proteomics approach using SILAC in MEFs derived from wild type and *Epm2b-/-* mice cultured in medium with 2% serum.

Description	Source	Coverage	#Peptides	#PSMs
Fibronectin	Mus musculus	29.79	48	1027
Actin	Mus musculus	38.40	12	613
Vimentin	Mus musculus	52.58	21	515
Fibulin-2 isoform b	Mus musculus	28.36	23	494
Myosin-9 isoform 1	Mus musculus	35.77	61	403
Vimentin	Bos Taurus	38.63	16	333
Actin, alpha cardiac muscle 1	Mus musculus	45.89	13	325
Galectin-1	Mus musculus	31.85	3	295
Tubulin beta-5 chain	Mus musculus	27.25	10	286
Tubulin alpha-1 B chain	Mus musculus	29.71	9	274

Coverage: The percentage of amino acid sequence identified by matching tryptic peptides
PSMs: The number of peptide spectral matches
#Peptides: The number of peptides that were detected

3.2.5. Difficulties in SILAC Labeling and Cell Culture

The labeling of MEFs with heavy lysine and arginine was very poor. Even after culturing the cells in heavy medium for 4-6 weeks, close to 100% labeling efficiency could not be obtained as verified by mass spectrometric analysis. Figure 30 represents a MS/MS spectrum for the tryptic peptide KGVNLPGAAVDLPAVSEK, which contains an N-terminal lysine, a possible missed cleavage site, even after proteolysis by trypsin. The C-terminal lysine of the tryptic peptide is heavy whereas the N-terminal lysine is light, thus representing an incomplete labeling with heavy amino acids. Moreover, to obtain higher starting amounts of protein from cells, at least 20-150 mm cell culture plates were needed. It was difficult to culture cells in 2% FBS to obtain higher number since the cell growth was slower as compared to 10% FBS.
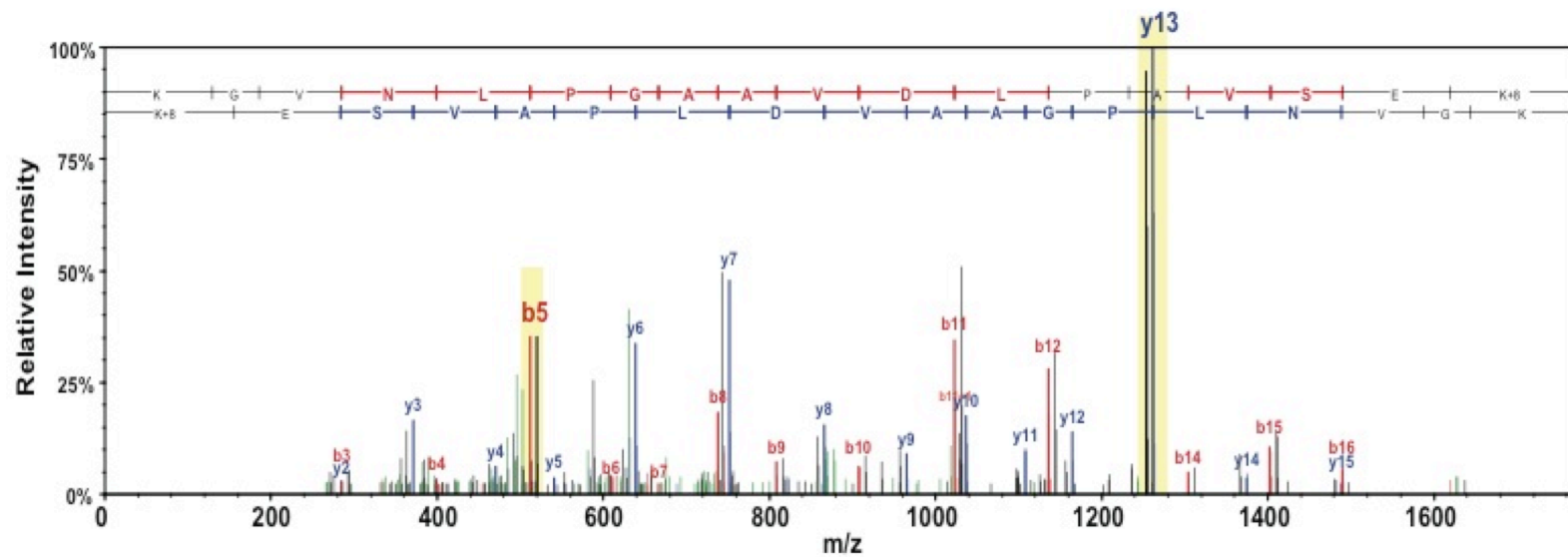
Figure 30. MS/MS Spectrum Showing Incomplete Labeling. MS/MS spectrum for the tryptic peptide KGVNLPGAAVDLPAVSEK showing a pattern for incomplete labeling. Lower case lysine is heavy.

3.3. Ubiquitin Proteome of Mouse Skeletal Muscle using Quantitative diGly Proteomics

Since identification of ubiquitinated proteins by SILAC in MEFs was not achievable, we used mouse skeletal muscle instead, utilizing a similar diGly proteomics approach. Around 800 mg of frozen mouse skeletal muscle from 6 month-old wild type male mice was used. Around 150 mg of protein was obtained, which was digested overnight by trypsin after reduction and alkylation of the cysteines. The diGly peptides generated after trypsin digestion were immunoprecipitated using anti-diGly antibody and then analyzed by mass spectrometry (Figure 31), which resulted in identification of ubiquitinated peptides. Technical replicates of the sample were analyzed and the data were pooled together for the analysis. In total, 244 non-redundant ubiquitination sites were detected in 182 proteins following combination of all MudPIT-LC/MS analyses. The 25 most abundant proteins identified based on the peptide spectral match (PSM) are shown in Table 3. A PSM is a match between an observed peptide spectrum and the theoretical peptide spectrum in the database. In our experiments, we record the total number of PSMs by which a particular peptide is identified over a course of a MudPIT by the mass spectrometer and matched with the database. For example, in Table 3, Myh4 was detected 26093 times (PSM 26093) as compared to Ube2n, which was detected 24 times (PSM 24).

**Mouse skeletal muscle
tissue lysate**

Trypsinolysis

GG

GG
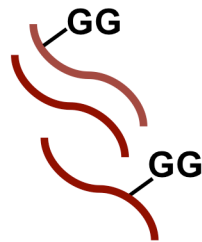
Tryptic peptides

**IP α-diGly
remnant**

m/z
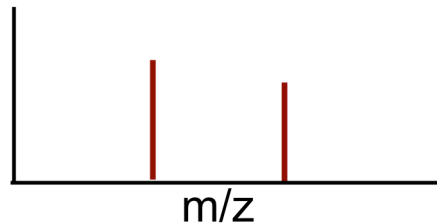
Figure 31. Approach for diGly Proteomics in Mouse Skeletal Muscle. Tissue lysate prepared from mouse skeletal muscle was digested by trypsin to yield peptides that contain diGly remnant. These peptides were immunoprecipitated using anti-diGly antibody and analyzed by mass spectrometry.

Table 3. **Mouse Ubiquitylome using diGly Proteomics Approach.** 25 most abundant proteins from mouse skeletal muscle identified with ubiquitinated peptides following diGly immunoaffinity purification and MudPIT-LC/MS analysis.

Accession	Description	Coverage	#PSMs	MW
Q5SX39	Myosin heavy chain 4	66.99	26093	222.7
Q5SX40	Myosin heavy chain 1	60.30	17222	223.2
P13542	Myosin heavy chain 8	47.81	12666	222.6
G3UW82	Myosin heavy chain 2	59.53	12580	223.1
P68134	Alpha-actin 1	58.09	9126	42
P62737	Alpha-actin 2	57.82	8976	42
P13541	Myosin heavy chain 3	26.19	7401	223.7
Q91Z83	Myosin heavy chain 7	37.31	6629	222.7
Q02566	Myosin heavy chain 6	31.68	6311	223.4
P07310	Creatine kinase M-type	49.08	5697	39.3
B1AR69	Myosin heavy chain 13	23.07	4949	223.4
P97457	Myosin regulatory light chain 2	92.31	2120	18.9
P60710	Actin 2	41.67	2602	11.4
P05977	Myosin light chain 1	63.83	2094	20.6
P05064	Fructose-bisphosphate aldolase A	47.53	1916	39.3
A6Z147	Fructose-bisphosphate aldolase	22.80	1158	39.3
P20801	Troponin C	22.50	619	18.1
P11404	Fatty acid-binding protein, heart	39.10	186	14.8
F8WIX8	Histone H2A	28.80	90	13.6
D3YYZ2	Uncharacterized protein	46.72	58	14.1
E9Q6Z0	Cullin 5	3.38	28	75.9
Q497M3	Putative C->-U-editing enzyme APOBEC-4	4.01	24	42.7

Accession	Description	Coverage	#PSMs	MW
P70295	Ancient ubiquitous protein 1	3.66	21	46.1
Q02053	Ubiquitin-activating enzyme 1	5.10	17	117.7
P61089	Ubiquitin-conjugating enzyme E2 N	36.18	24	17.1

Accession: The unique accession number for protein in UniProtKB
Coverage: The percentage of amino acid sequence identified by matching tryptic peptides
PSMs: The number of peptide spectral matches
#Peptides: The number of peptides that were detected
MW: The molecular weight of protein in kilodaltons

Histone H2A is one of the five histones involved in the structure of chromatin in cells (176). H2A has been shown to be monoubquitinated at lysine 119 (K119) to regulate target genes (177) As a validation of the approach, H2A was identified with a diGly remnant present at lysine 119 (K119). Figure 32 represents the MS/MS spectrum of the ubiquitinated tryptic peptide VTIAQGGVLPNIQAVLLPKK identified in our studies for Histone H2A.

A (K)VTIAQGGVLPNIQAVLLPkK(T)
k=GlyGly

B
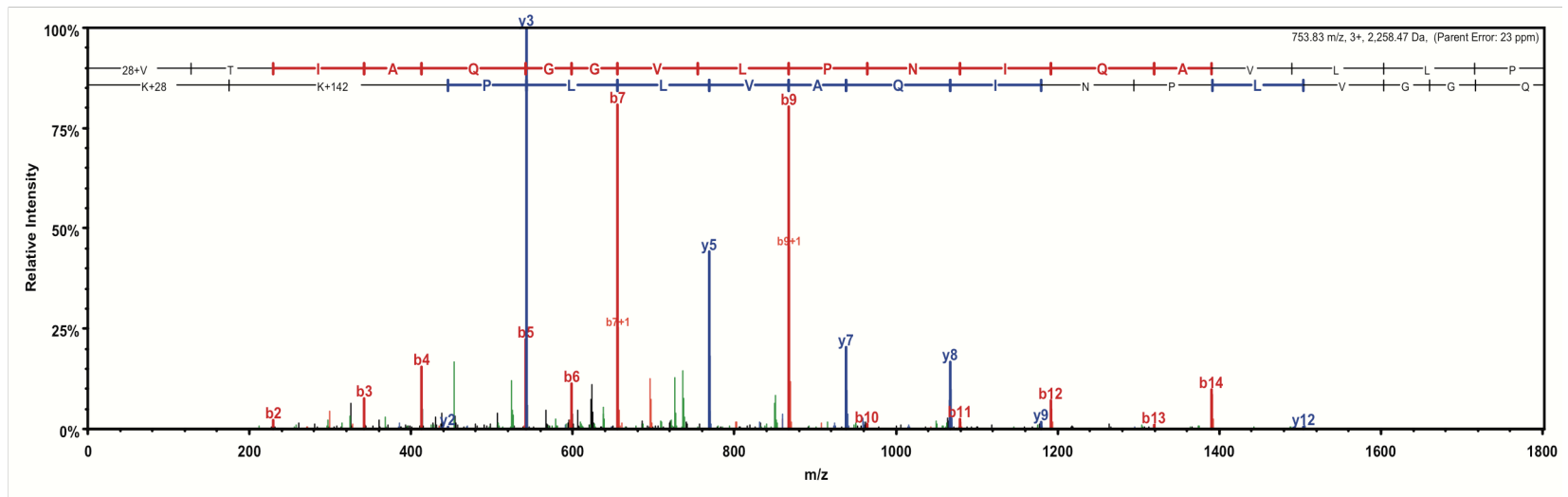
Figure 32. MS/MS Spectrum of Histone H2A. *A)* Sequence of tryptic peptide containing the site of ubiquitintation (GlyGly). *B)* MS/MS spectrum obtained from the tryptic peptide VTIAQGGVLPNIQAVLLPKK. The y-ion series is shown in blue while the b-ion series is shown in red.

Myosin-4, the top hit from the analysis, had nine distinct ubiquitination sites. Figure 33 shows the sequence coverage for myosin-4. With an overall coverage of 46% (894 amino acids out of 1939), we detected a total of 4715 spectra, 27 exclusive unique peptides and 65 exclusive unique spectra for myosin-4. Figure 34 (A-I) shows the MS/MS spectra for myosin-4 for all the nine ubiquitination sites identified after diGly immunoaffinity purification. Out of the nine, four modified sites were identified in redundant peptides found in other myosin family members. In brief, the potential sites that could be ubiquitinated in other myosin isoforms include: lysine 1902 (exact peptide also found in myosin-1), lysine 1809 (exact peptide also found in myosin 1, 2, 3, 6, 7, 8 and 13), lysine 1922 (exact peptide also found in myosin 1, 3, 6, 7, 8 and 13) and lysine 453 (exact peptide also found in myosin 1, 2, 8 and 13).

```
MSSDAEMAVF   GEAAPYLRKS   EKERIEAQNK   PFDAKSSVFV   VDAKESYVKA   TVQSREGGKV
TAKTEGGATV   TVKDDQVFSM   NPPKYDKIED   MAMMTHLHEP   AVLYNLKERY   AAWMIYTYSG
LFCVTVNPYK   WLPVYNPEVV   AAYRGKKRQE   APPHIFSISD   NAYQFMLTDR   ENQSILITGE
SGAGKTVNTK   RVIQYFATIA   VTGDKKKEEA   TSGKMQGTLE   DQIISANPLL   EAFGNAKTVR
NDNSSRFGKF   IRIHFGATGK   LASADIETYL   LEKSRVTFQL   KAERSYHIFY   QIMSNKKPEL
IEMLLITTNP   YDFAYVSQGE   ITVPSIDDQE   ELMATDTAVD   ILGFSADEKV   AIYKLTGAVM
HYGNMKFKQK   QREEQAEPDG   TEVADKAAYL   TSLNSADLLK   ALCYPRVKVG   NEYVTKGQTV
QQVYNSVGAL   AKSMYEKMFL   WMVTRINQQL   DTKQPRQYFI   GVLDIAGFEI   FDFNTLEQLC
INFTNEKLQQ   FFNHHMFVLE   QEEYKKEGID   WEFIDFGMDL   AACIELIEKP   MGIFSILEEE
CMFPKATDTS   FKNKLYEQHL   GKSNNFQKPK   PAKGKAEAHF   SLVHYAGTVD   YNIIGWLDKN
KDPLNETVVG   LYQKSGLKTL   AFLFSGGQAA   EAEGGGGKKG   GKKKGSSFQT   VSALFRENLN
KLMTNLKSTH   PHFVRCLIPN   ETKTPGAMEH   ELVLHQLRCN   GVLEGIRICR   KGFPSRILYA
DFKQRYKVLN   ASAIPEGQFI   DSKKASEKLL   GSIDIDHTQY   KFGHTKVFFK   AGLLGTLEEM
RDEKLAQLIT   RTQAVCRGYL   MRVEFKKMME   RRESIFCIQY   NVRAFMNVKH   WPWMKLYFKI
KPLLKSAETE   KEMANMKEDF   EKAKEDLAKS   EAKRKELEEK   MVALMQEKND   LQLQVQAEAD
GLADAEERCD   QLIKTKIQLE   AKIKELTERA   EDEEEINAEL   TAKKRKLEDE   CSELKKDIDD
LELTLAKVEK   EKHATENKVK   NLTEEMAGLD   ENIAKLTKEK   KALQEAHQQT   LDDLQAEEDK
VNTLTKAKTK   LEQQVDDLEG   SLEQEKKLRM   DLERAKRKLE   GDLKLAQEST   MDIENDKQQL
DEKLKKKEFE   MSNLQSKIED   EQALGMQLQK   KIKELQARIE   ELEEIEAER    ASRAKAEKQR
SDLSRELEEI   SERLEEAGGA   TSAQIEMNKK   REAEFQKMRR   TVSKAKGNLE   ATAAALRKKH
ADSVAELGEQ   IDNLQRVKQK   LEKEKSELKM   EIDDLASNME   MVSQLSRGKQ   KMCRTLEDQL
SEVKTKEEEQ   QRLINELSTQ   KARLHTESGE   FSRQLDEKDA   LQRAMSKANS   EVAQWRTKYE
RQLEEESKAK   NALAHALQSA   RHDCDLLREQ   YEEEQEAKAE   TKQRLQNEVE   DLMIDVERSN
TDAIQRTEEL   EEAKKKLAQR   LQDAEEHVEA   VNSKCASLEK   KSELQASLEE   AYEESLDQLE
AACAALDKKQ   RNFDKVLAEW   KQKYEETQAE   LEASQKESRS   LSTELFKVKN   AEASLEHEEG
TLKRENKNLQ   QEISDLTEQI   AEGGKHIHEL   EKIKKQIDQE   MQSTLDAEIR   SRNDALRIKK
KILRIQLELN   QVKSEIDRKI   AEKDEEIDQL   KRNHLRVVES   LDDALRGQDD   LKEQLAMVER
KMEGDLNEME   IQLNHANRQA   AEAIRNLRNT   QGMLKDTQLH   HTQNTSLINT   KKKLETDISQ
RANLMQAEIE   ELRASLEQTE   RSRRVAEQEL   LDASERVQLL   AHLERMKKNM   EQTVKDLQHR
IQGEMEDIVQ   EARNAEEKAK   KAITDAAMMA   EELKKEQDTS   VKGLRKHERR   VKELTYQTEE
LDEAEQLALK   GGKKQIQKLE   ARVRELENEV   ENEQKRNIEA   RKIQHELEEA   EERADIAESQ
DRKNVLRLQD   LVDKLQTKVK   AYKRQAEEAE   EQSNVNLAKF
VNKLRVKSRE   VHTKVISEE
```

Figure 33. Myosin-4 Sequence Coverage. Schematic representation of myosin-4 with sequence coverage indicated in yellow; the modified residues (including methylation labeling, methionine oxidation and diGly) are indicated in green. A total of 4715 total spectra were detected with 46% coverage, 27 exclusive unique peptides and 65 exclusive unique spectra.

A Myosin 4, lysine 1476 (K)yEETQAELEASQkESR(S)
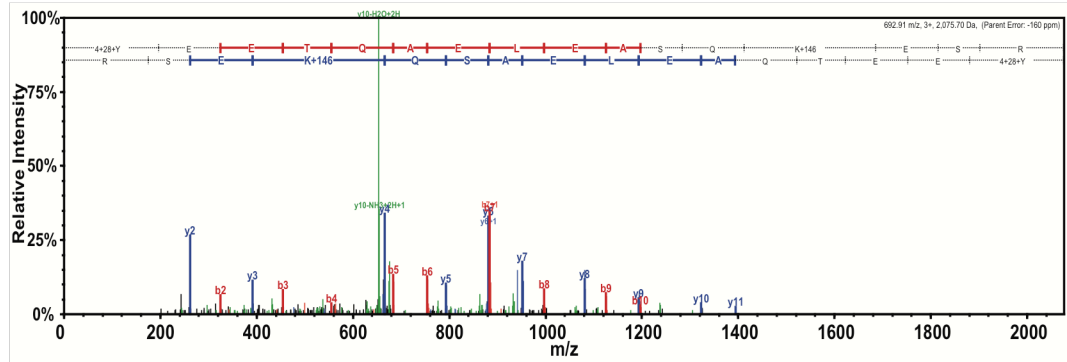
B Myosin 4, lysine 1448 (R)SNAACAALDkK(Q)
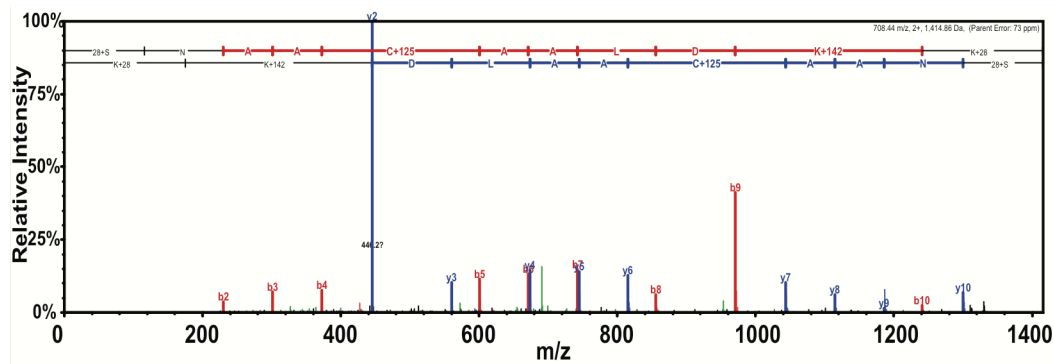
C Myosin 4, lysine 44 (K)sSVFVVDAkESYVk(A)
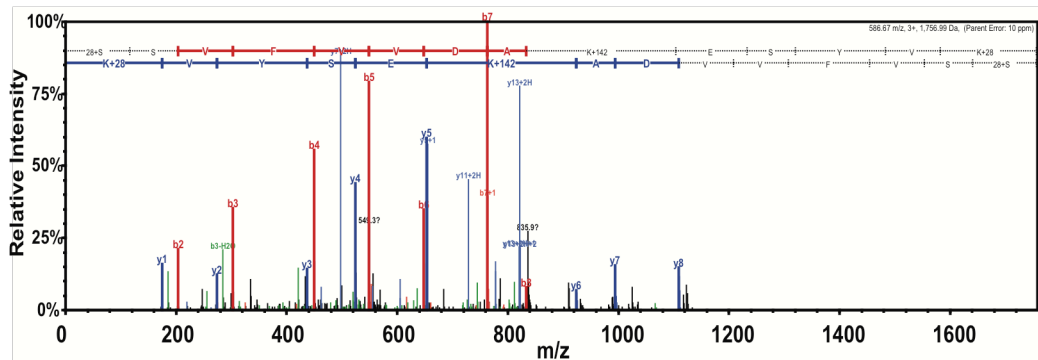
D   Myosin 4, lysine 73 (K)tEGGATVTVkDDQVFSmNPPk(Y)
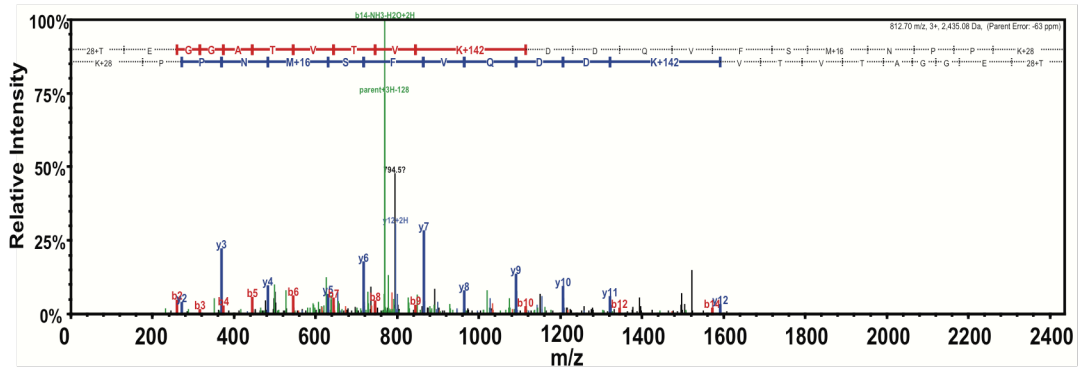
E   Myosin 4, lysine 64 (k)VTAkTEGGATCTCk(D)
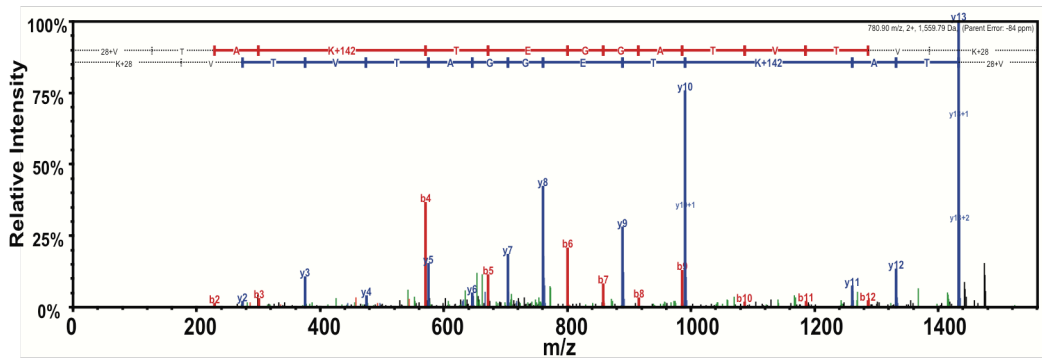
F   Myosin 4, lysine 1902 (also conserved in myosin 1)
(R)qAEEAEEQSNVNLAkFR(K)

G Myosin 4 - lysine 1809 (also conserved in myosin 1, 3, 6, 7, 8, B1AR69, and G3UW82)
(R)IDEAEQLALkGGk(K)

H Myosin 4 - lysine 1922 (also conserved in myosin 1, 3, 6, 7, 8, and B1AR69)
(R)aDIAESQVNkLR(V)

I Myosin 4 - lysine 453 (also conserved in myosin 1, 8, B1AR69, and G3UW82)
(R)iNQQLDTkQPR(Q)
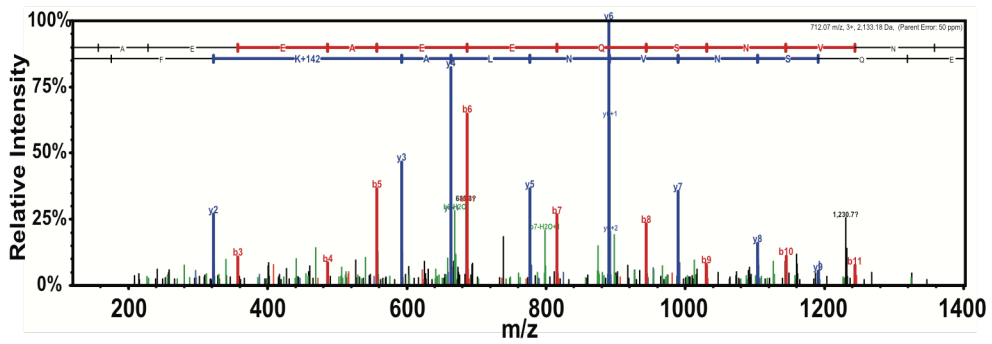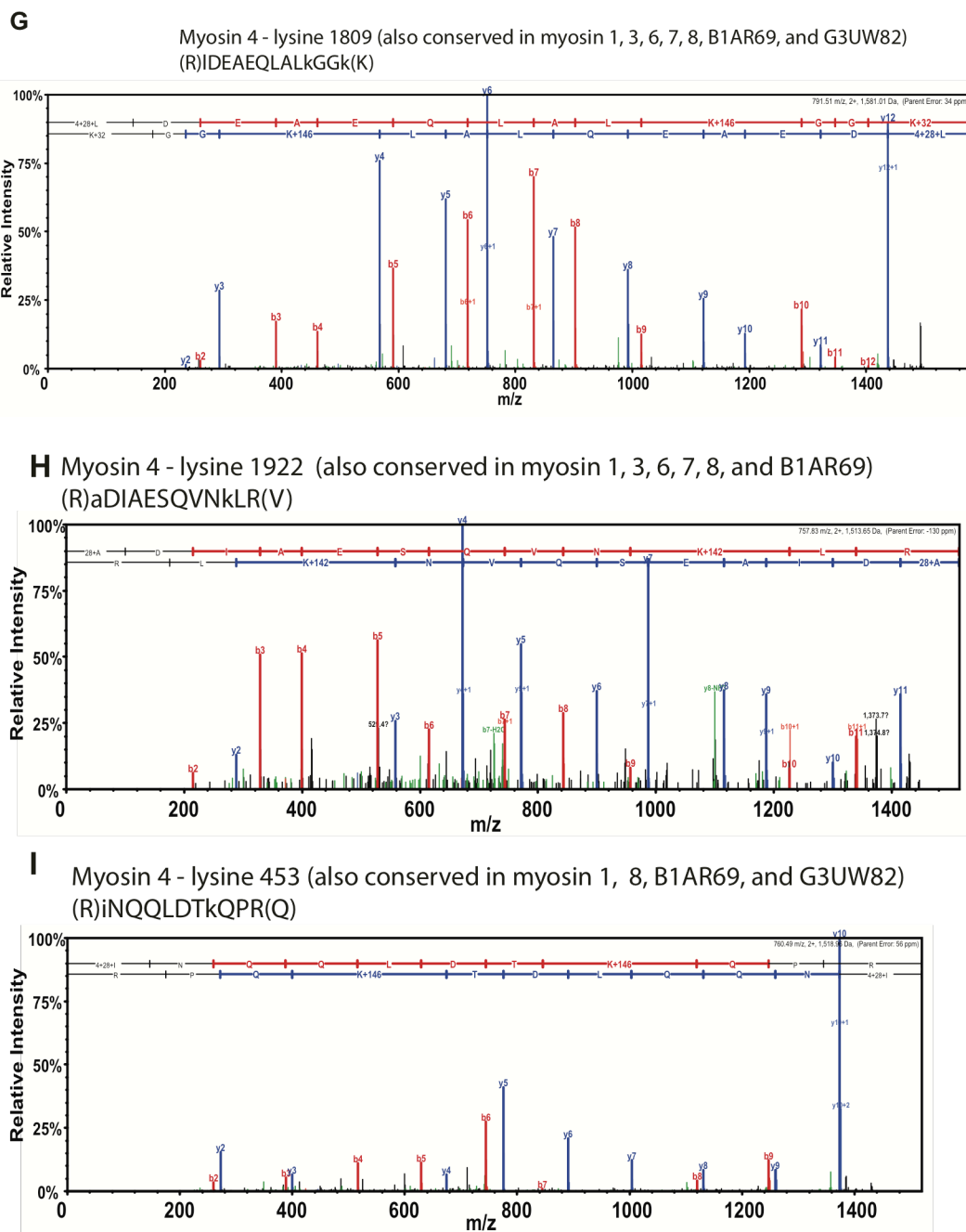
Figure 34. MS/MS Spectra for Myosin-4. MS/MS spectra obtained after diGly immunoaffinity purification from tryptic peptides of modified lysine in myosin-4 *A)* Lysine 1476; *B)* Lysine 1448; *C)* Lysine 44; *D)* Lysine 73; *E)* Lysine 64; *F)* Lysine 1902; *G)* Lysine 1809; *H)* Lysine 1922 and *I)* Lysine 453. The modified residues are represented in lower case. The y-ion series is shown in blue while the b-ion series is shown in red.

Technical replicates of the sample were analyzed on a LTQ Velos Pro ion trap or a Q-Exactive mass spectrometer. Data were collected for MS/MS analysis following collision-induced dissociation (CID) or higher-energy collision-induced dissociation (HCD) fragmentation. Figure 35 and Figure 36 show a comparison between the CID and HCD fragmentation pattern of peptides. There is much lower b ion fragmentation coverage in HCD in comparison to CID. Compared to CID, HCD fragmentation has high resolution precursor ion detection set at resolution of 70,000 for these experiments (178) and therefore we used it to confirm the sites of diGly modification obtained from CID fragmentation.

Myosin 4
SSVFVVDAkESYVK (k=GlyGly)
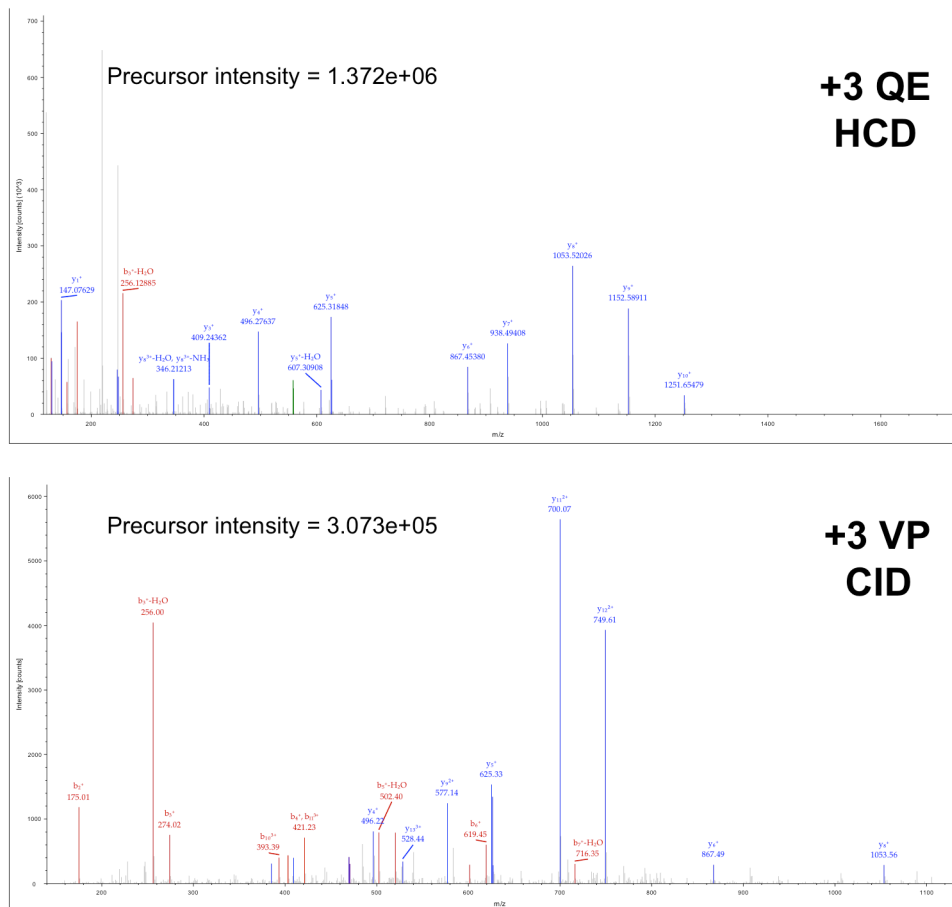
Figure 35. MS/MS Spectra for Myosin-4: HCD vs. CID. Comparison of MS/MS spectra after HCD and CID fragmentation for peptide SSVFVVDAkESYVK obtained from myosin 4 after diGly immunoaffinity purification. The y-ion series is shown in blue while the b-ion series is shown in red. QE; Q-Exactive, VP; Velos Pro.

Histone H2A
VTIAQGGVLPNIQAVLLPkK (k=GlyGly)
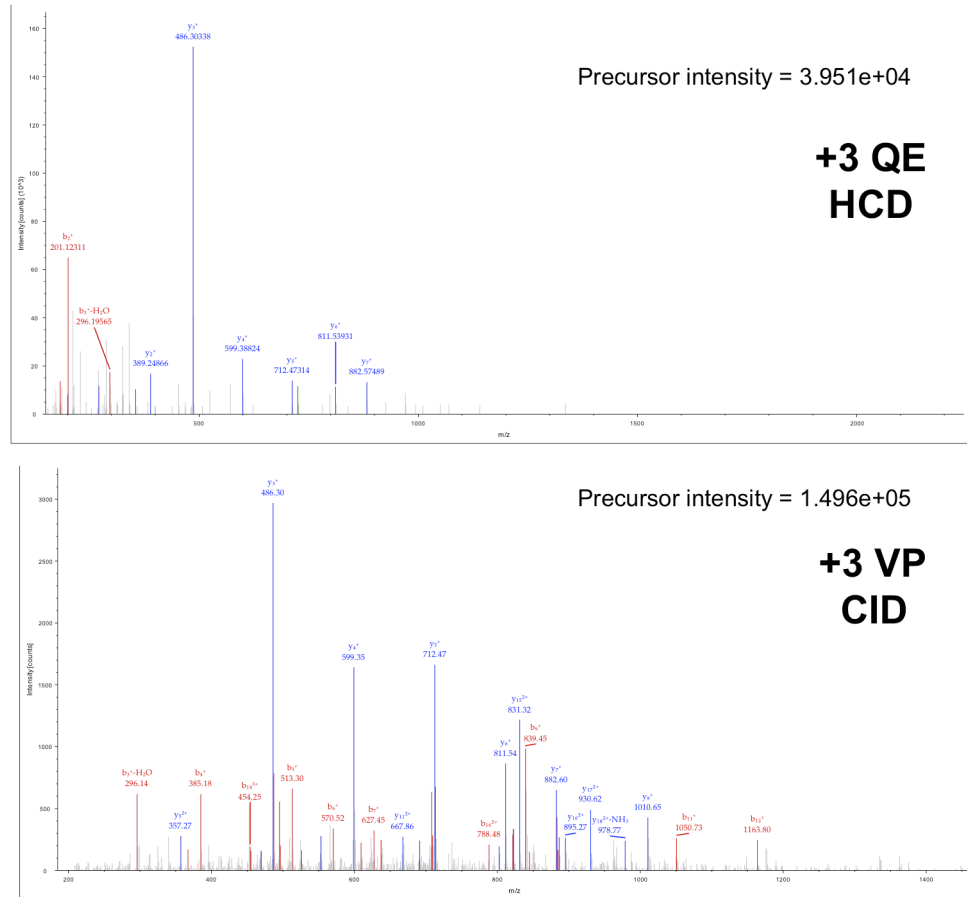
Figure 36. MS/MS Spectra for Histone H2A: HCD vs. CID. Comparison of MS/MS spectra after HCD and CID fragmentation for peptide VTIAQGGVLPNIQAVLLPkK obtained from histone H2A after diGly immunoaffinity purification. The y-ion series is shown in blue while the b-ion series is shown in red. QE; Q-Exactive, VP; Velos Pro.

An unbiased approach was used for functional annotation by using the database for annotation, visualization and integrated discovery (DAVID), which was developed by Huang et al. (179). The DAVID bioinformatics database was queried using the 25 most abundant proteins that were obtained from MudPIT LC/MS analysis in Table 3. The top 25 proteins' dataset organized into biofunctional categories can be seen in Figure 37. Biofunctions with (-log p-values) from this analysis (Table 4) are represented in Figure 38. The ubiquitinated proteins could either be substrates that undergo ubiquitination as a post-translational modification for regulation of function or substrates of the quality control process and protein turnover. Data analysis by DAVID (Figure 37) highlights that the majority of the ubiquitinated proteins are cytoskeletal or motor proteins primarily involved in muscle function. Small groups of proteins were predicted to be involved in development of muscle and cellular or catabolic processes.
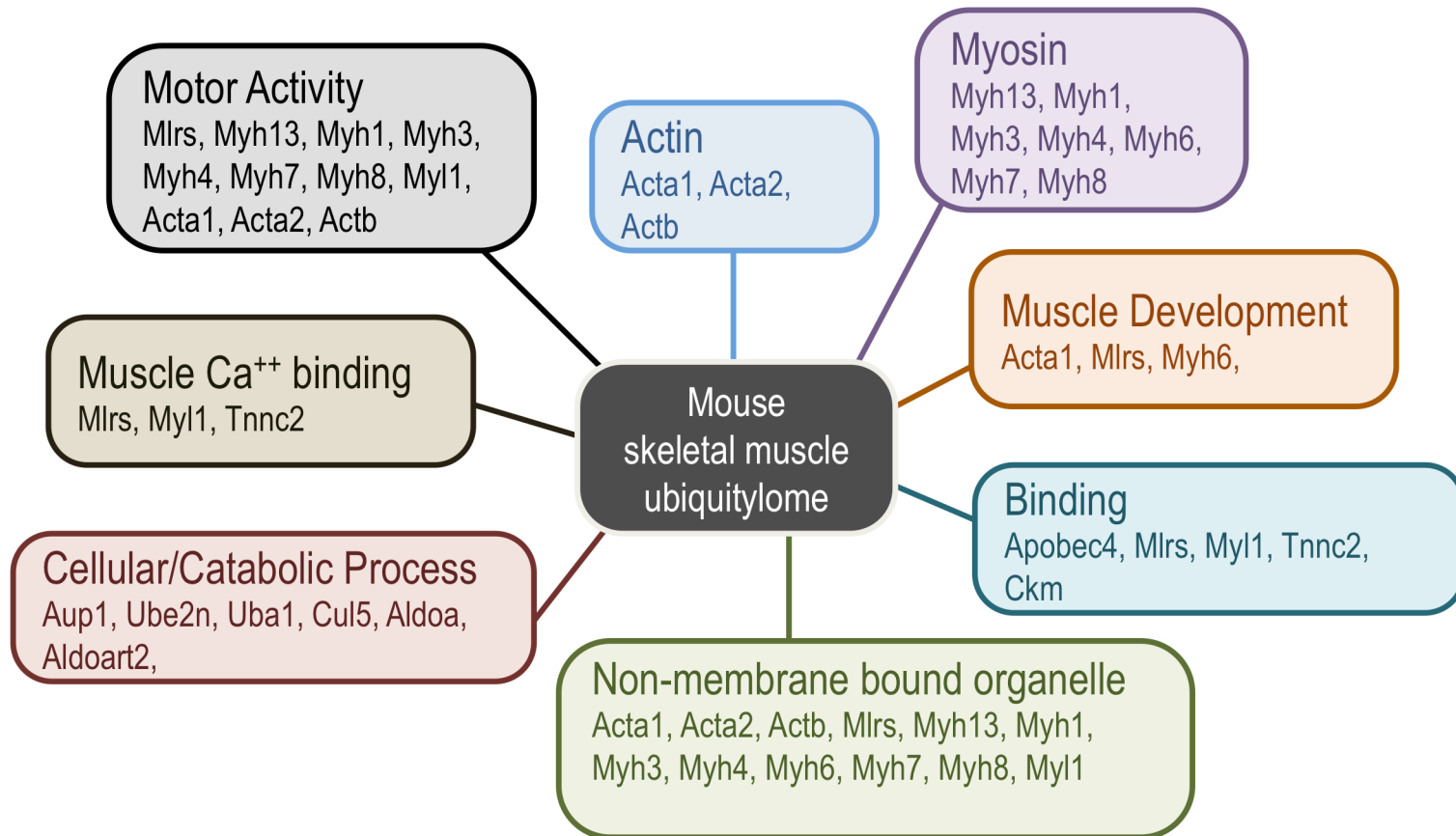
Figure 37. Biofunctional Categories in Mouse Ubiquitylome. Using DAVID, biofunctional categorization was performed for 25 most abundant proteins from mouse skeletal muscle identified with ubiquitination peptides following diGly immunoaffinity purification and MudPIT LC/MS analysis.

Table 4. Functional Annotation for Mouse Ubiquitylome. Using DAVID, functional annotation was performed for 25 most abundant proteins from mouse skeletal muscle identified with ubiquitination peptides following diGly immunoaffinity purification and MudPIT LC/MS analysis.

Annotation Cluster 1	p-value	-log(p-value)
Enrichment Score: 13.63		
Motor Activity	7.6E-12	11.12
Annotation Cluster 2	**p-value**	**-log(p-value)**
Enrichment Score: 10.42		
Heavy chain of Myosin	2.5E-17	16.60
Myosin filament	2.8E-15	14.55
Myosin tail	2.7E-15	14.57
Myosin head, motor region	2.4E-12	11.62
Annotation Cluster 3	**p-value**	**-log(p-value)**
Enrichment Score: 9.28		
Actin-binding	4.1E-11	10.39
Actin filament binding	6.2E-9	8.21
Annotation Cluster 4	**p-value**	**-log(p-value)**
Enrichment Score: 7.43		
Non-membrane-bounded organelle	2.5E-7	6.60
Intracellular non-membrane-bounded organelle	2.5E-7	6.60
Annotation Cluster 5	**p-value**	**-log(p-value)**
Enrichment Score: 6.81		
ATP-binding	1.4E-9	8.85
Nucleotide-binding	2.0E-8	7.70
Nucleoside-binding	1.5E-7	6.82
Annotation Cluster 6	**p-value**	**-log(p-value)**
Enrichment Score: 3.29		
Striated muscle development	9.5E-3	2.02
Muscle tissue development	1.1E-2	1.96

Muscle organ development	1.8E-2	1.74
Annotation Cluster 7	**p-value**	**-log(p-value)**
Enrichment Score:1.7		
Domain: EF hand 3	3.8E-3	2.42
Calcium-binding EF-hand	1.0E-2	2.00
Annotation Cluster 8	**p-value**	**-log(p-value)**
Enrichment Score:0.83		
Ubl conjugation pathway	1.0E-1	1.00
Modification-dependent protein catabolic process	1.2E-1	0.92
Protein catabolic process	1.4E-1	0.85
Proteolysis	3.5E-1	0.46

Annotation cluster: A group of terms having similar biological meaning due to sharing similar gene members.

Enrichment score: The overall enrichment score for the group based on the EASE scores of each term members; the higher, the more enriched.

p-value: Modified Fisher Exact p-value or the EASE score; the smaller, the more enriched.

-log(p-value): Calculated negative logarithm of the p-value
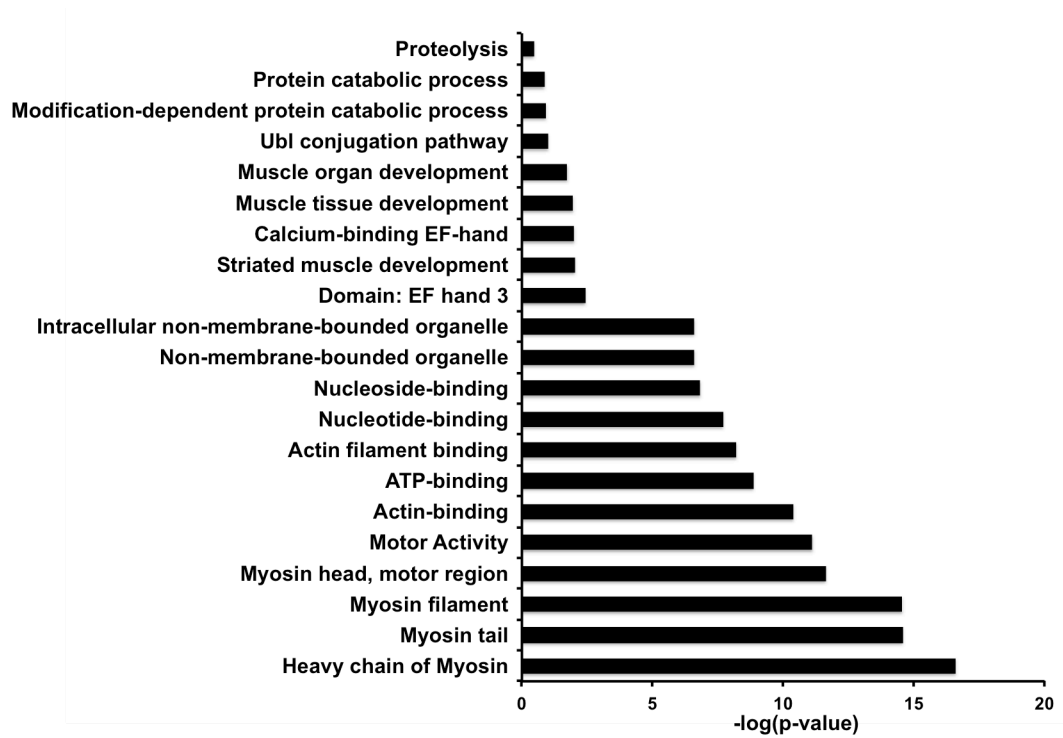
Figure 38. Functional Annotation for Mouse Ubiquitylome.
Using DAVID, functional annotation was performed for 25 most
abundant proteins from mouse skeletal muscle identified with
ubiquitination peptides following diGly immunoaffinity purification
and MudPIT LC/MS analysis.

3.4. Differential Labeling of Mouse Skeletal Muscle by Stable Isotope Dimethyl Labeling

In order to perform a comparative and quantitative ubiquitin-proteomic study, a differential isotopic labeling approach was developed using stable isotope dimethyl labeling. Dimethyl labeling, first described by Hsu et al. (180), is based on a reaction between primary amines of a peptide (the N-terminus or an ε-amino group of a lysine residue) and formaldehyde to form a Schiff base that is reduced by sodium cyanoborohydride to form a dimethylamino group. Use of regular formaldehyde and sodium cyanoborohydride generates a mass increase of 28 Da per primary amine on the peptide (light), while deuterated formaldehyde and sodium cyanoborohydride generates a mass increase of 32 Da per primary amine (heavy) (Figure 39). Differential labeling of the proteins enables simultaneous quantitative LC-MS analysis of different samples. Labeling of the tryptic peptides with the aforementioned method generates peptides with a mass difference of either 4 Da (cleaved after an arginine residue) or 8 Da (when cleaved after a lysine residue) between the light and heavy label. If this peptide is also ubiquitinated at an internal lysine residue, an additional mass difference of 4 Da will be observed due to labeling of the N-terminus of the diGly remnant. Boersema et al. (148) have described a method for performing on-column (C18 Sep-Pak®) dimethylation of peptide samples. This method was employed with small modifications as described in section 14.7 of Experimental Procedures. Tissue lysates were prepared from 40 mg of mouse skeletal muscle as described in section 14.2 of Experimental Procedures. Proteolysis was done by overnight

digestion with trypsin after reduction and alkylation of the cysteines. The tryptic peptides were then labeled using the stable isotope dimethyl labeling approach described above. The efficiency of labeling as analyzed by mass spectrometry was 99.7 and 99.9% for both light and heavy peptides, respectively.
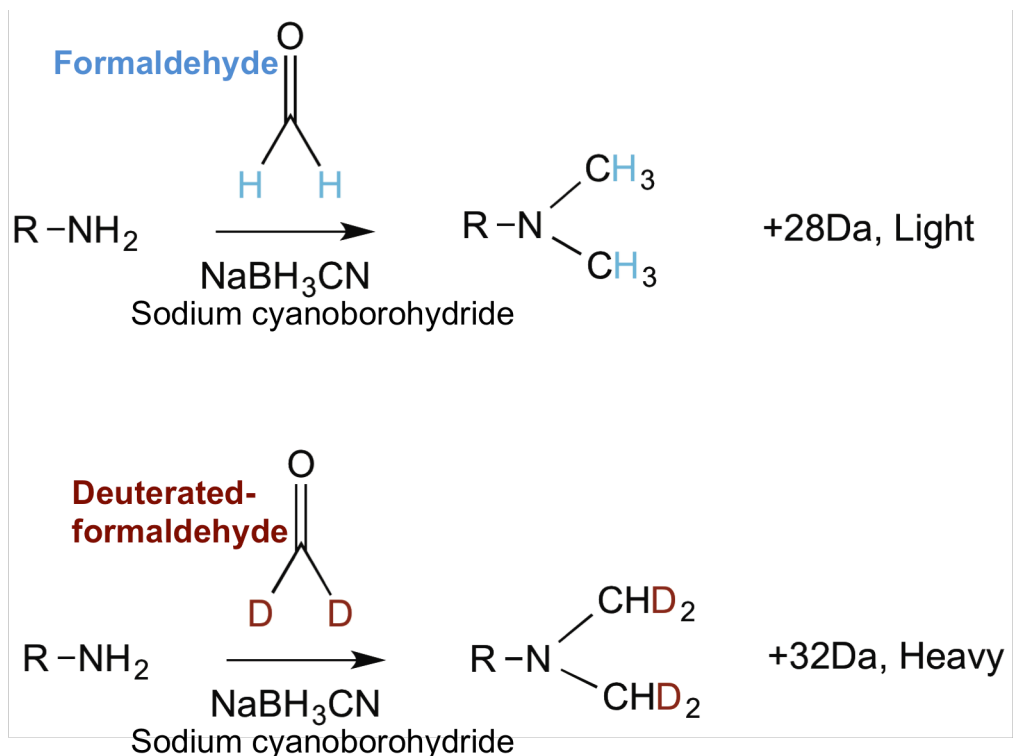
Figure 39. Stable Isotope Dimethyl Labeling. Labeling schemes for differential stable isotopic dimethyl labeling. Combination of regular formaldehyde and cyanoborohydride generates a mass difference of 28Da. Use of deuterated formaldehyde generates a mass difference of 32Da. R-remainder of the peptide.

3.5. Dimethyl Labeling and diGly Immunoaffinity Purification

To allow for quantification of ubiquitination of proteins, stable isotope dimethyl labeling was incorporated into the diGly immunoaffinity purification workflow. Figure 40 A is a diagrammatic representation of the approach. The tryptic peptides from mouse skeletal muscle were purified using a Sep-Pak® column and on-column labeling was performed during the same purification step. This was advantageous as sample clean-up and labeling steps were combined and a quenching step was avoided. The labeled tryptic peptides were then purified by diGly immunoaffinity purification and analyzed by mass spectrometry. The MudPIT-LC/MS analysis failed to detect any diGly peptides although numerous unmodified peptides were identified, thus suggesting that dimethylation of peptides prior to diGly immunoaffinity purification interfered with antibody recognition of the diGly peptides.

To circumvent this problem, the protocol was modified and the on-column labeling was performed after the diGly immunoaffinity purification. The labeled peptides were lyophilized and resuspended in buffer for analysis by mass spectrometry. Figure 40 B shows the modified approach for dimethyl labeling of peptides and diGly immunoaffinity purification in which peptides from the different genotypes are mixed after the labeling procedure.
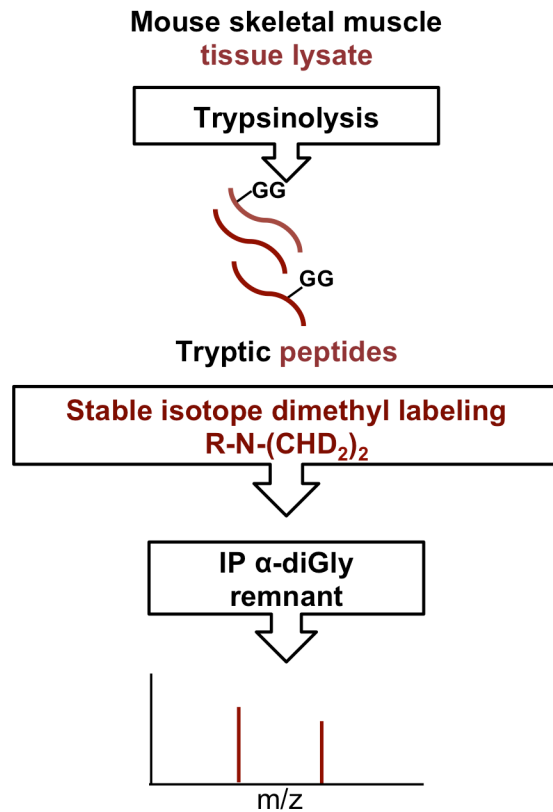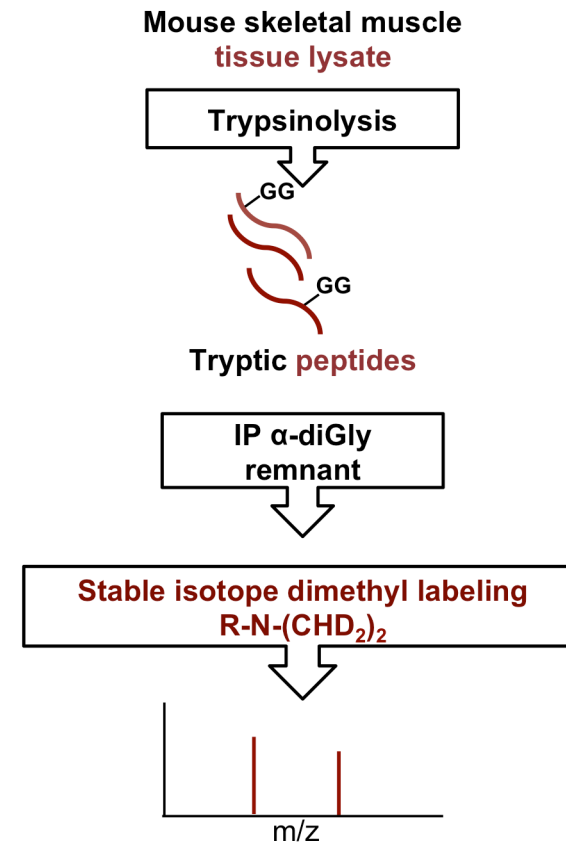
Figure 40. Approach for Differential Labeling and diGly Immunoaffinity Purification in Mouse Tissue. Approach for *A)* Dimethyl labeling of tryptic peptides before immunoaffinity purification and *B)* Dimethyl labeling of peptides after immunoaffinity purification.

Figure 41 depicts the MS/MS spectra of heavy and light labeled versions of the tryptic peptide, VTIAQGGVLPNIQAVLLPKK, derived from histone H2A. The peptide has two labeled sites at the N- and C-termini. There was a mass difference of 4 Da between the heavy and the light b ions, which had only one labeled site at the N-terminus of the peptide. A mass difference of 8 Da was observed between heavy and light y ions because of the presence of two labeled sites, the N-terminus of the diGly remnant and the lysine at the C-terminus (Table 5 and 6). As expected, the peptide ion signals from the heavy and light labeled peptides were similar, thus confirming that stable isotope labeling did not alter the ubiquitination states of the peptide or interfere with the detection by mass spectrometry.

Table 5. Mass Difference between Heavy and Light Labeled b-ions. Calculated mass difference between light and heavy dimethyl labeled peptide derived from histone H2A. (Peptide sequence VTIAQGGVLPNIQAVLLPKK).

Seq. No.	Light b ion	Heavy b ion	Mass Difference
b3	342.29	346.25	3.96
b4	413.28	417.38	4.10
b6	598.34	602.46	4.12
b7	655.44	659.40	3.96
b9	867.54	871.56	4.02
b12	1191.84	1195.74	3.90

Table 6. Mass Difference between Heavy and Light Labeled y-ions. Calculated mass difference between light and heavy dimethyl labeled peptide derived from histone H2A. (Peptide sequence VTIAQGGVLPNIQAVLLPKK).

Seq. No.	Light y ion	Heavy y ion	Mass Difference
y3	542.35	550.42	8.07
y5	768.55	776.54	7.99
y7	938.79	946.69	7.9
y8	1066.88	1074.77	7.89
y11	1390.86	1398.87	8.01
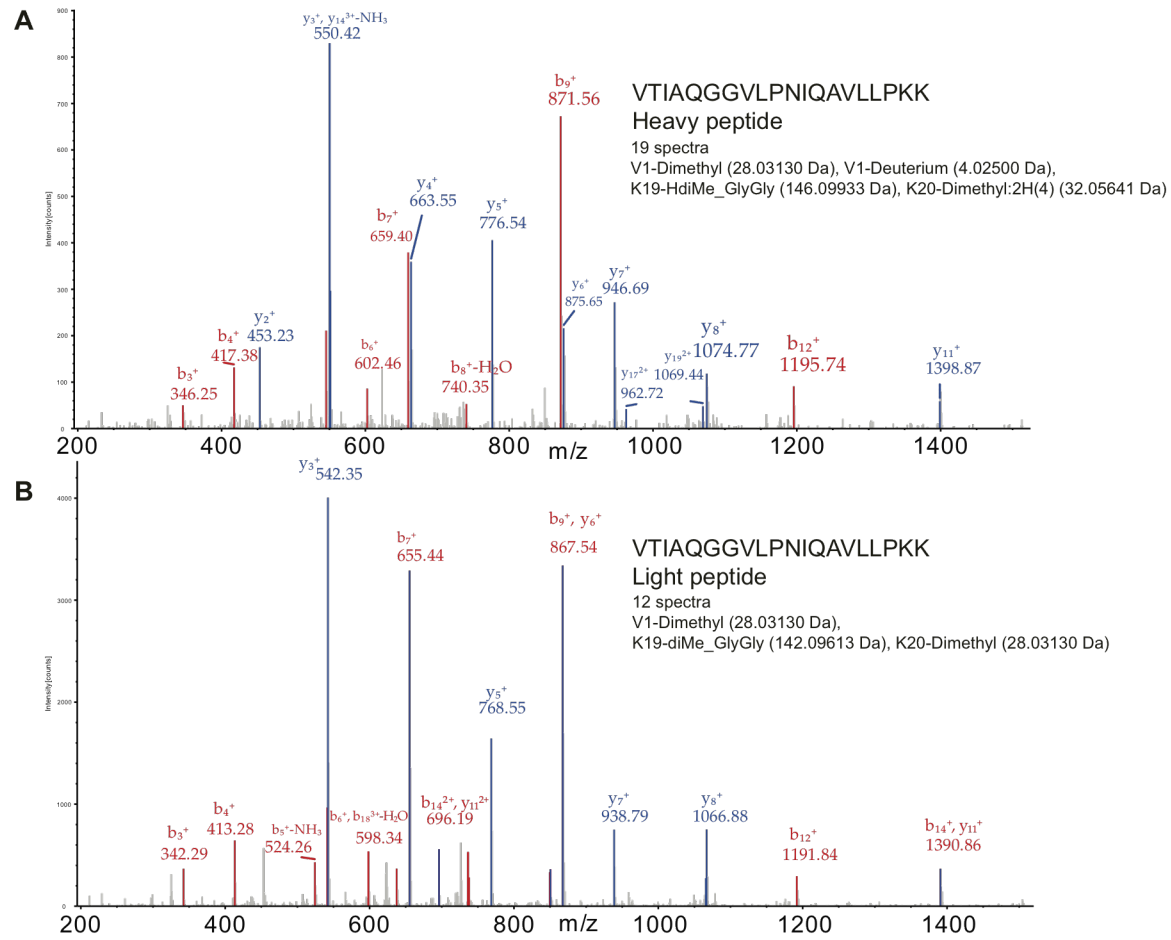
Figure 41. MS/MS Spectra Showing Dimethyl Labeling. Selected MS/MS spectra of *A)* heavy and *B)* light labeled tryptic peptide, VTIAQGGVLPNIQAVLLPKK, derived from histone H2A. The y-ion series is shown in blue while the b-ion series is shown in red.

3.6. Identification of Malin Substrates

3.6.1. Approach

Tissue lysates were prepared from skeletal muscle of wild type and *Epm2b*-/- mice. Trypsinolysis of the proteins resulted in the generation of diGly remnants on the ubiquitinated peptides, which were immunoaffinity purified with anti-diGly antibody. The wild type and *Epm2b*-/- eluate were differentially labeled by stable isotope dimethyl labeling, mixed, lyophilized and analyzed by mass spectrometry. In the absence of malin in *Epm2b*-/- tissue, potential substrates should not be ubiquitinated and therefore would lack the diGly remnant (Figure 42).

Around 800 mg of frozen mouse skeletal muscle from 6-month-old male wild type and *Epm2b*-/- mice was homogenized as described in section 14.2 of Experimental Procedures. The protein yield from tissue of each genotype was around 150 mg of protein. Equal amounts of protein were taken for each genotype. After reduction and alkylation of cysteines, proteolysis by trypsin was done overnight. The diGly peptides generated after trypsinolysis were purified on a C18 Sep-Pak® column and immunoaffinity purified using anti-diGly antibody. The purified diGly peptides were differentially labeled by dimethylation. The peptides from wild type tissue were labeled with heavy and those from *Epm2b*-/- tissue were labeled with light reagents. The differentially labeled peptides were mixed and analyzed by mass spectrometry.
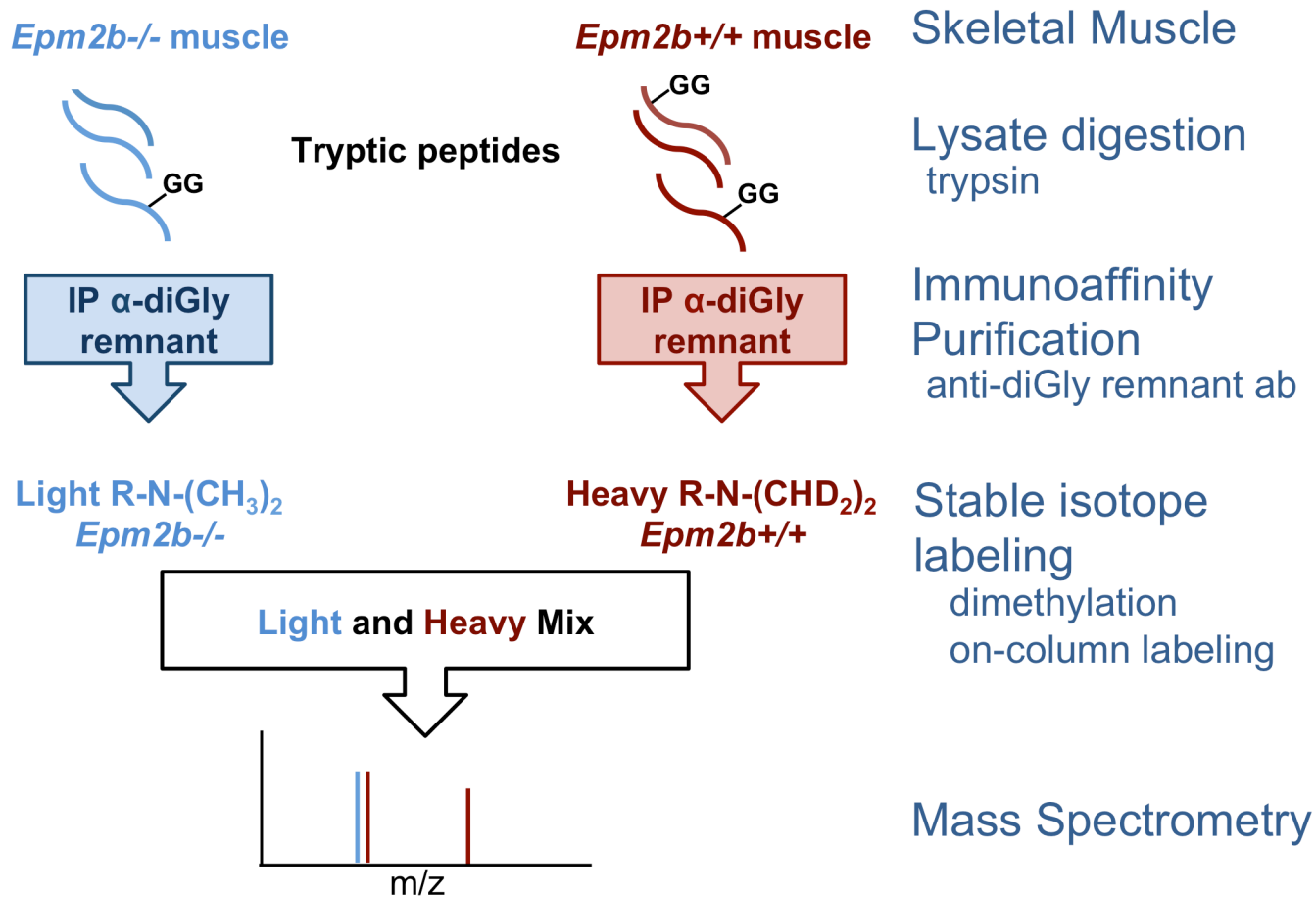
Figure 42. Quantitative diGly Proteomics using Dimethyl Labeling in Mouse Skeletal Muscle. Tissue lysates from skeletal muscle of wild type and *Epm2b*-/- mice was digested by trypsin yielding diGly remnant on peptides. These peptides were immunoaffinity purified using anti-diGly antibody, differentially labeled by dimethylation, mixed and analyzed by mass spectrometry.

In our analysis of the data, we observed that tryptic peptide NYDIGAALDTIQYSKHPPPL, derived from sequestosome-1 or p62 was present in the *Epm2b-/-* light sample but was absent from the wild type heavy sample. Figure 43 shows the heat map showing the relative abundance of diGly peptides from different proteins. p62 is a known autophagy substrate and the levels of p62 are increased upon inhibition of autophagy (44). We observed in section 2.3 of Results that autophagy is impaired in MEFs from *Epm2b-/-* mice. We speculate that in the wild type skeletal muscle p62 would be ubiquitinated and degraded, however in the *Epm2b-/-* skeletal muscle, with impairment of autophagy p62 would accumulate and was therefore detected on mass spectrometry analysis. This result corroborates our earlier result that autophagy is impaired in *Epm2b-/-* mice.

3.6.2. Potential Malin Substrates

As described above, in the absence of malin in the *Epm2b-/-* tissue, potential substrates of malin might not be ubiquitinated and therefore, will lack the diGly remnant. Therefore, the absence of the light diGly peptide would indicate that the protein is a potential substrate of malin. The proteins identified as potential substrates of malin are presented in Tables 7 and 8. Table 7 lists malin substrates with at least 2 PSMs and Table 8 contains proteins with only 1 PSM. In all, 70 proteins were detected that might be substrates of malin. Out of these 70 proteins, only 14 proteins had at least 2 PSMs.

Table 7. Potential Substrates of Malin E3 Ubiquitin Ligase.
Proteins with diGly peptides present in wild type but not in *Epm2b-/-*
tissue. Peptides with at least 2 PSMs are included.

Accession	Description	Coverage	#PSMs	MW
A2RTH5	Leucine carboxyl methyltransferase 1	3.01	65	38.2
Q8R429	Sarcoplasmic/endoplasmic reticulum calcium ATPase 1	46.18	13	109.4
Q6P4T1	Sorting nexin 19	1.30	6	109.7
Q9CX83	Armadillo repeat-containing X-linked protein	3.73	4	50.6
D3YYZ2	C-type lectin domain family 9	46.72	4	14.1
Q3ULF4	Paraplegin 4	13.45	4	87.01
E9Q8K5	Titin	28.59	3	3713.7
Q80U58	Pumilio homolog 2	1.59	3	114.2
Q02053	Ubiquitin-like modifier-activating enzyme 1	5.10	3	117.7
P05064	Fructose-bisphosphate aldolase A	47.53	3	39.3
Q14B15	Myomesin 2	38.14	3	164.6
Q9CS72	Filamin-A-interacting protein 1	1.16	2	137.5
Q60932	Voltage-dependent anion-selective channel protein 1	67.23	2	32.3
Q9JMH7	Sialidase 3	32.14	2	48

Accession: The unique accession number for protein in UniProtKB
Coverage: The percentage of amino acid sequence identified by matching tryptic peptides
PSMs: The number of peptide spectral matches
MW: The molecular weight of protein in kilodaltons

Table 8. "One Hit Wonder" Substrates of Malin. Proteins with diGly peptides present in wild type but not in *Epm2b*-/- tissue. Peptides with only one PSM are included.

Accession	Description	Coverage	MW
Q3TYA6	M-phase phosphoprotein 8	1.40	97.4
E9PWP1	Protein Zfp599	1.82	63.3
Q91V83	TELO2-interacting protein 1 homolog	2.67	120.7
Q62073	Mitogen-activated protein kinase kinase kinase 7	2.07	64.2
Q9D6R2	Isocitrate dehydrogenase subunit alpha	28.14	39.6
Q3UQ97	Predicted gene EG432838	5.12	27.2
Q9D5U5	Protein FAM115E	1.53	102.2
Q91VJ4	Serine/threonine-protein kinase 38	2.58	54.1
Q6ZQB6	Inositol hexakisphosphate and diphosphoinositol-pentakisphosphate kinase 2	1.15	128.3
Q99KP6	Pre-mRNA-processing factor 19	1.98	55.2
F6SRT8	Neuron navigator 3	0.73	175.1
P15975	Inactive ubiquitin carboxyl-terminal hydrolase 53	0.94	119.2
P0DM40	Fer-1-like protein 5	0.44	235.7
P09411	Phosphoglycerate kinase 1	59.23	44.5
Q99KI0	Aconitate hydratase, mitochondrial	34.74	85.4
J3QMT0	Heterogeneous nuclear ribonucleoprotein F	8.13	23.4
P18761	Carbonic anhydrase 6	6.31	36.5
O35098	Dihydropyrimidinase-related protein 4	1.75	61.9
P62631	Elongation factor 1-alpha 2	25.92	50.4
P56391	Cytochrome C oxidase subunit 6B1	39.53	10.1
F8WIU3	Zinc finger protein 618	1.16	95.4
E9Q6A7	Protein Bptf	0.89	321.4

Accession	Description	Coverage	MW
D3Z007	Interleukin-1 receptor-associated kinase 3	3.48	58.3
A0AUV4	Sperm motility kinase Y	2.36	57.0
F6YTC4	Zinc transporter ZIP10	1.54	73.4
Q5XKE0	Myosin-binding protein C, fast type	44.45	127.3
Q6P5B0	RRP12-like protein	0.62	143.0
P21550	Beta-enolase	58.99	47.0
O54724	Polymerase I and transcript release factor	17.09	43.9
F6UGV8	Major facilitator superfamily domain-containing protein 4	28.36	7.4
Q9ESB3	Histidine-rich glycoprotein	3.43	59.1
E9Q2K4	Actin-related protein 2/3 complex subunit 5	6.67	16.1
O35594	Intraflagellar transport protein 81 homolog	1.92	79.2
O54799	Neuromedin-B receptor	5.90	43.6
Q9JKX3	Transferrin receptor protein 2	1.25	88.3
E9QQ10	A-kinase anchor protein 9	0.32	433.9
Q6PHB0	Interleukin-20 receptor subunit alpha	4.21	61.9
Q504P4	Heat shock cognate 71	23.44	68.7
B1ASN7	EF-hand calcium-binding domain-containing protein 3	4.18	40.8
P59240	Nephrocystin-4	0.98	157.2
Q9R1E6	Ectonucleotide pyrophosphatase/phosphodiesterase	1.86	98.8
Q3TIV5	Zinc finger CCCH domain-containing protein	3.99	48.3
D3YV40	Protein kinase C-binding protein NELL1	3.69	42.3

Accession	Description	Coverage	MW
Q8K224	N-acetyltransferase 10	1.07	115.3
J3KMJ8	Axonemal dynein light chain domain-containing protein 1	0.80	102.2
Q3TCV3	Gamma-secretase-activating protein	0.93	98.6
Q07113	Cation-independent mannose-6-phosphate receptor	0.52	273.6
P26262	Plasma kallikrein	1.25	71.3
F7AIZ1	Protein 1700011I03Rik	3.54	28.3
E9QPI5	Sister chromatid cohesion protein PDS5 homolog A	0.75	150.1
Q9D0F9	Phosphoglucomutase 1	44.54	62.0
Q000896	Alpha-1-antitrypsin 1-3	25.21	44.32
Q80VM8	PNMA-like protein 1	13.28	48.16

Accession: The unique accession number for protein in UniProtKB
Coverage: The percentage of amino acid sequence identified by matching tryptic peptides
PSMs: The number of peptide spectral matches
MW: The molecular weight of protein in kilodaltons

Leucine carboxyl methyltransferase 1 or Lcmt1 was present in the wild type but not in the malin knockout muscle. Out of all the potential substrates identified following diGly immunoaffinity purification and MudPIT-LC/MS analysis, Lcmt1 had the highest PSMs at 65. Figure 43 shows the heat map for the number of PSMs detected. Figure 44 represents the MS/MS spectrum for the tryptic peptide: DLSELEEKLK from Lcmt1.

Voltage-dependent anion-selective channel protein 1 or Vdac1 is another example of a potential malin substrate. Figure 43 shows the heat map for number of PSMs for Vdac1. Our analysis showed that two peptides of Vdac1; NVNAGGHkLGLGLEFQA and DVFTkGYGFGLIK were ubiquitinated in the wild type skeletal muscle but not in the knockout muscle. The MS/MS spectra for the two peptides are represented in Figure 45 (NVNAGGHkLGLGLEFQA) and Figure 46 (DVFTkGYGFGLIK).
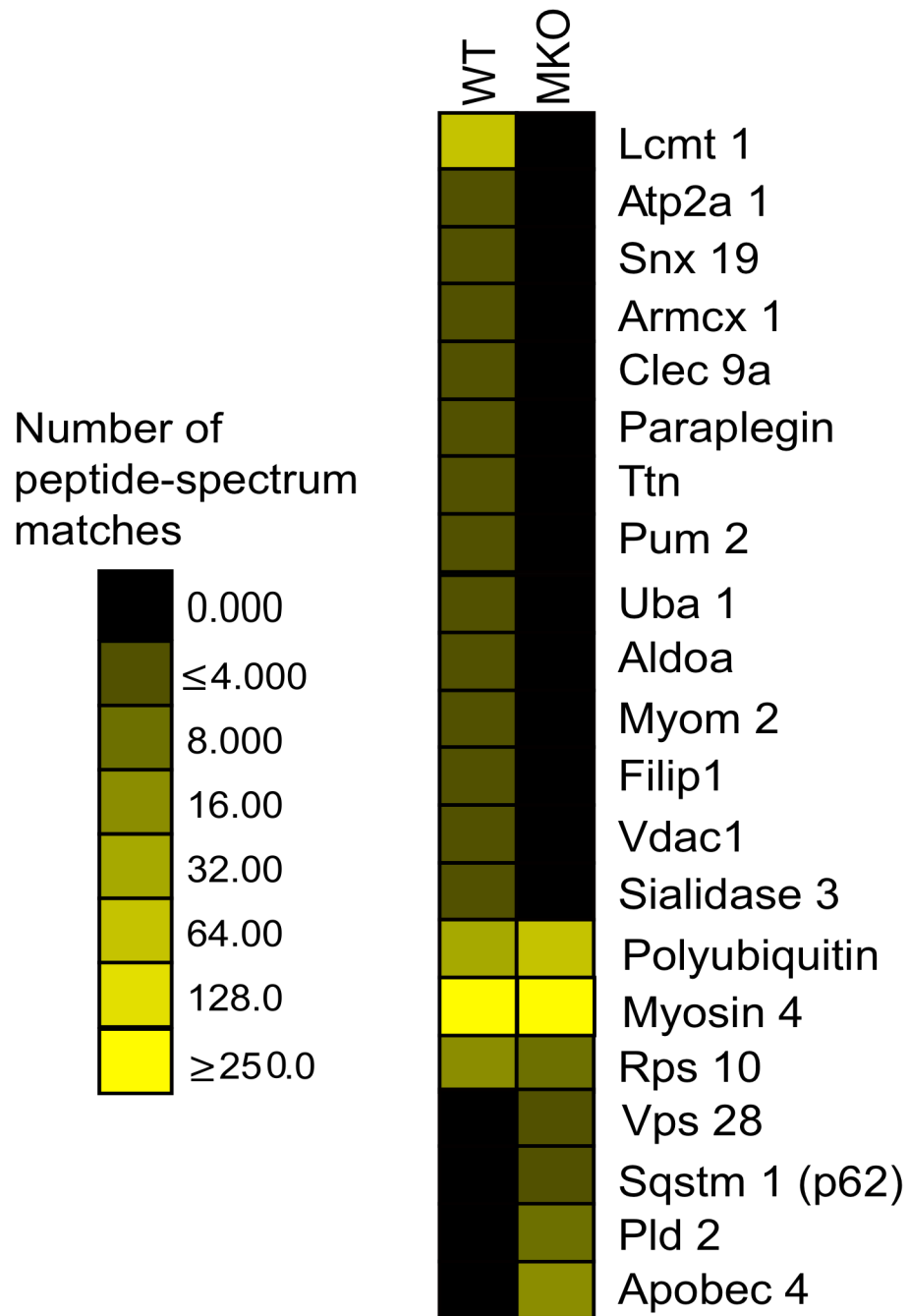
Figure 43. Heat Map showing Relative Abundance of diGly Peptides. Heat map showing number of peptide spectrum matches for differnet proteins identified after diGly immunoaffinity purification and MudPIT-LC/MS analysis.

Lcmt 1
DLSELEEkLk
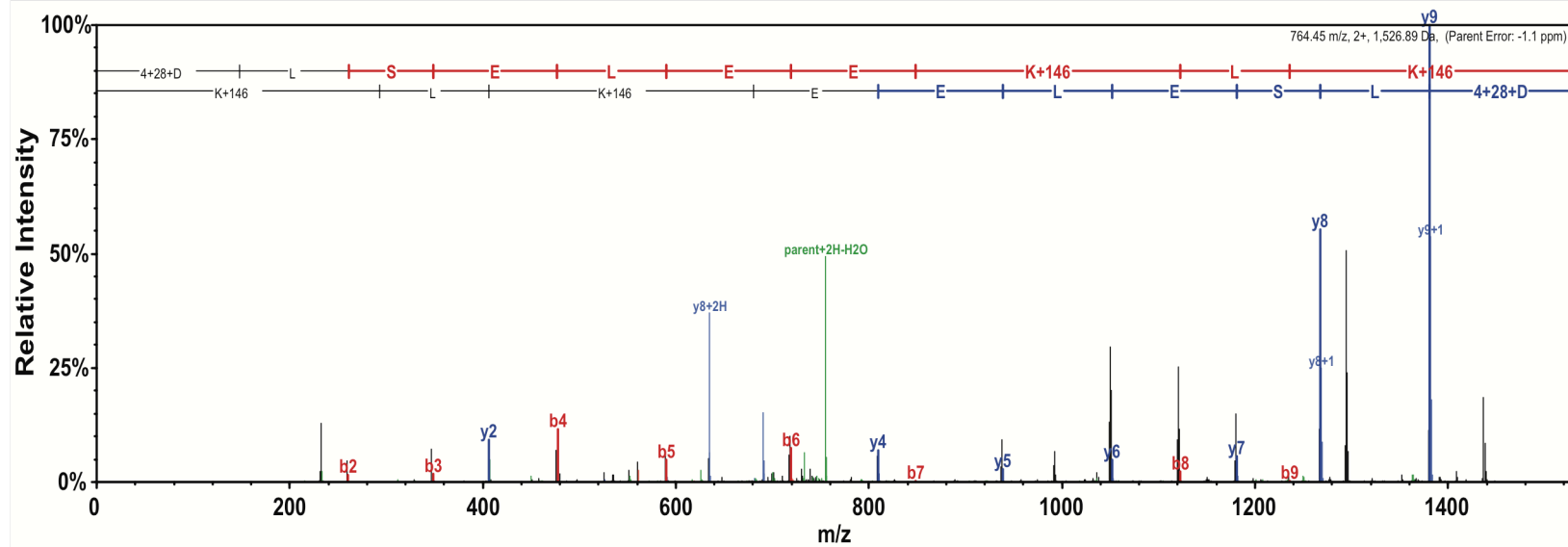
Figure 44. MS/MS Spectrum for Lcmt1. MS/MS spectra obtained after diGly immunoaffinity purification and MudPIT-LC/MS analysis of tryptic peptide DLSELEEkLk derived from Lcmt1. Lower case lysine in blue is ubiquitinated. The fragments for the b-ion series are shown in red while the fragments for the y-ion series are shown in blue.

Sequence: NVNAGGH**k**LGLGLEFQA,
N1-Label:2H(4) (4.02500 Da), N1-Dimethyl (28.03130 Da), K8-GlyGly_diMe_H2 (146.09933 Da)

Charge: +3, Monoisotopic m/z: 635.35443 Da (-25.12 mmu/-39.54 ppm), MH+: 1904.04874 Da, RT: 89.20 min,
Identified with: Sequest HT (v1.3); XCorr:3.31, Ions matched by search engine: 0/0
Fragment match tolerance used for search: 0.8 Da
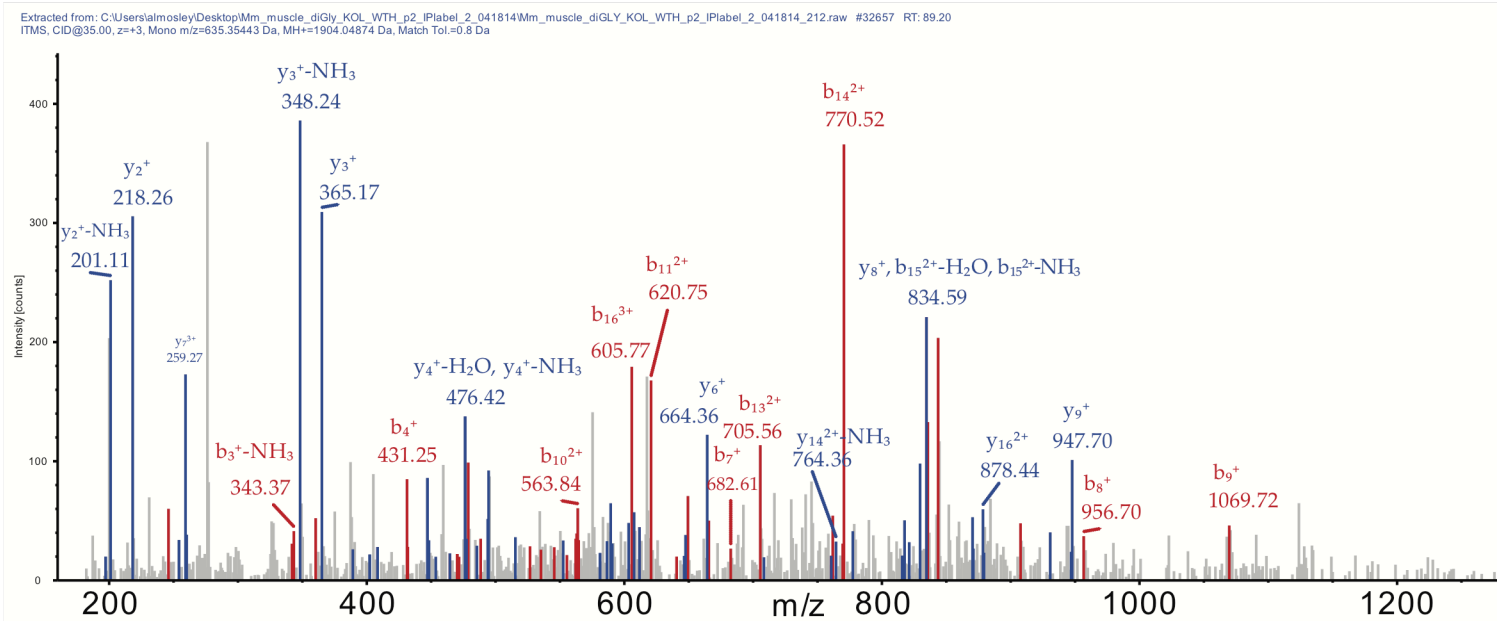
Figure 45. MS/MS Spectrum for Vdac1: 1. MS/MS spectra obtained after diGly immunoaffinity purification and MudPIT-LC/MS analysis of tryptic peptide NVNAGGHkLGLGLEFQA derived from Vdac1. Lower case lysine in blue is ubiquitinated. The fragments for the b-ion series are shown in red while the fragments for the y-ion series are shown in blue.

Sequence: DVFT**k**GYGFGLIK,
D1-Dimethyl (28.03130 Da), D1-Label:2H(4) (4.02500 Da),
K5-GlyGly_diMe_H2 (146.09933 Da), K13-Dimethyl:2H(4) (32.05641 Da)

Charge: +3, Monoisotopic m/z: 553.09283 Da (+435.47 mmu/+787.34 ppm), MH+: 1657.26395 Da, RT: 98.22 min,
Identified with: Sequest HT (v1.3); XCorr:2.28, Ions matched by search engine: 0/0
Fragment match tolerance used for search: 0.8 Da

Extracted from: C:\Users\almosley\Desktop\Mm_muscle_diGly_KOL_WTH_p2_IPlabel_2_041814\Mm_muscle_diGLY_KOL_WTH_p2_IPlabel_2_041814_212.raw #35553 RT: 98.22
ITMS, CID@35.00, z=+3, Mono m/z=553.09283 Da, MH+=1657.26395 Da, Match Tol.=0.8 Da
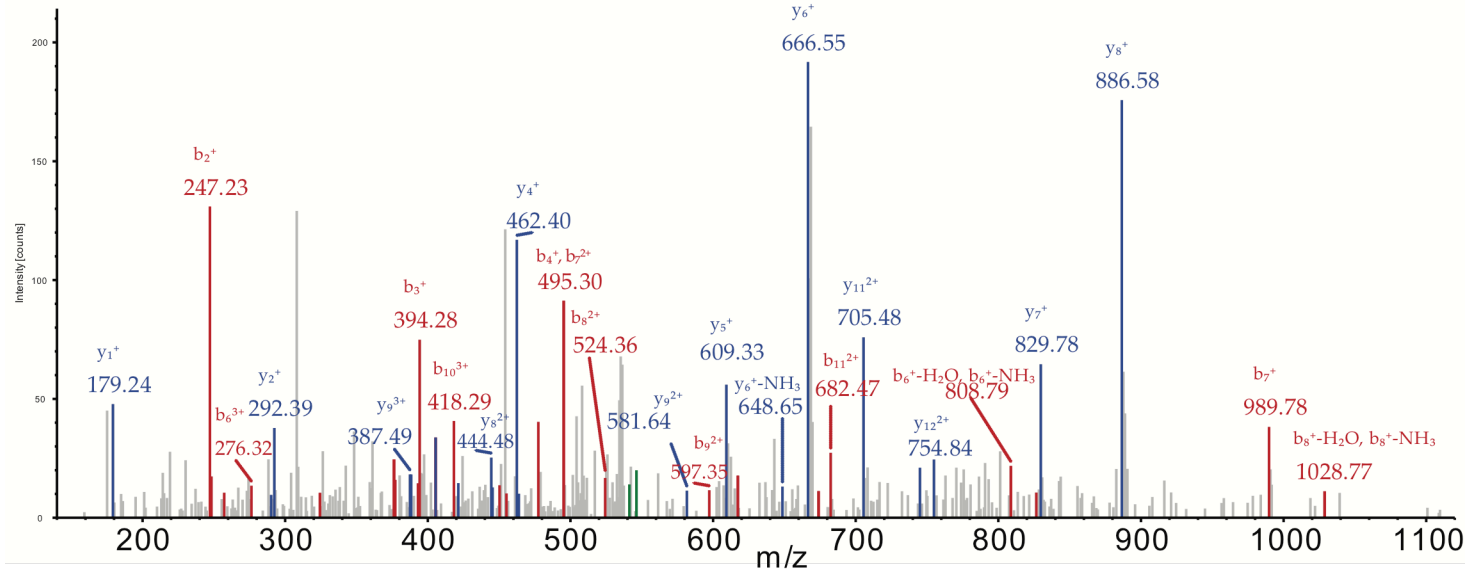
Figure 46. MS/MS Spectrum for Vdac1: 2. MS/MS spectra obtained after diGly immunoaffinity purification and MudPIT-LC/MS analysis of tryptic peptide DVFTkGYGFGLIK derived from Vdac1. Lower case lysine in blue is ubiquitinated. The fragments for the b-ion series are shown in red while the fragments for the y-ion series are shown in blue.

3.6.3. Bioinformatics Analysis of Potential Malin Substrates

The proteins that had at least 2 PSMs after diGly immunoaffinity purification and MudPIT-LC/MS analysis were subjected to bioinformatics analysis by querying the DAVID bioinformatics database. The dataset was organized into biofunctional categories and is shown in Figure 47. The results of functional annotation clustering by DAVID are presented in Table 9. These proteins could be ubiquitinated by malin either as a part of protein degradation process or for regulation of activity. The substrates fall into four clusters; nucleotide-, metal- and ion-binding, transmembrane proteins and non-membrane bound organelles. The nucleotide-binding cluster has the highest enrichment score among all the clusters.
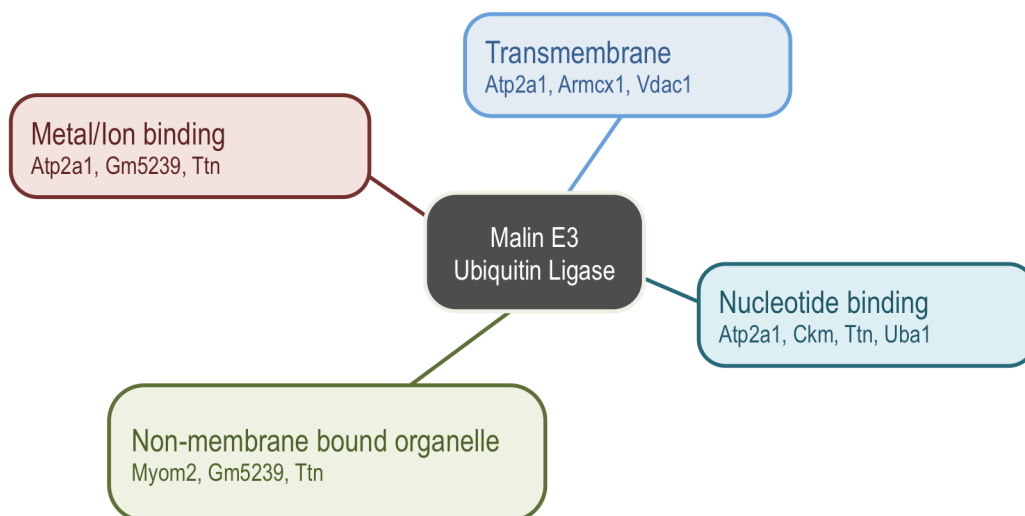
Figure 47. Biofunctional Categorization of Malin Substrates.
Using DAVID, biofunctional categorization was performed for potential malin substrates identified following diGly immunoaffinity purification and MudPIT LC/MS analysis.

Table 9. Functional Annotation for Malin Substrates. Using DAVID, functional annotation was performed for potential malin substrates identified following diGly immunoaffinity purification and MudPIT LC/MS analysis.

Annotation Cluster 1	p-value
Enrichment Score: 0.9	
ATP-binding	5.0E-2
Adenyl ribonucleotide binding	1.1E-1
Purine Nucleoside binding	1.3E-1
Ribonucleotide binding	1.8E-1
Annotation Cluster 2	**p-value**
Enrichment Score: 0.78	
Structural molecule activity	5.1E-2
Non-membrane-bounded organelle	2.9E-1
Intracellular non-membrane-bounded organelle	2.9E-1
Annotation Cluster 3	**p-value**
Enrichment Score: 0.11	
Metal-binding	5.6E-1
Metal ion binding	8.7E-1
Cation binding	8.8E-1
Ion binding	8.8E-1
Annotation Cluster 4	**p-value**
Enrichment Score: 0.05	
Transmembrane region	7.7E-1
Integral to membrane	9.0E-1
Transmembrane	9.1E-1
Membrane	9.2E-1

Annotation cluster: A group of terms having similar biological meaning due to sharing similar gene members.

Enrichment score: The overall enrichment score for the group based on the EASE scores of each term members; the higher, the more enriched.

p-value: Modified Fisher Exact p-value or the EASE score; the smaller, the more enriched.

Maere et al. (181) developed an open-source Java tool, the Biological Networks Gene Ontology tool or BiNGO, to determine the Gene Ontology (GO) terms that are significantly overrepresented in a set of genes. We used BiNGO to assess the functional themes present in our set of genes from Table 7. Biofunctions with (-log p-values) from this analysis with the GO term is represented in Figure 48. The substrates were categorized in nucleotide-, metal- or ion-transport, cellular or metabolic processes and muscle function.

Montojo et al. (182) designed a tool, GeneMANIA, for gene function predictions. GeneMANIA is available as a Cytoscape plugin and it identifies the most related genes to a query gene set using a guilt-by-association approach. Using the GeneMANIA plugin for Cytoscape, we looked for predicted physical interactions (Figure 49) and predicted pathways involved (Figure 50) from our set of potential malin substrates. *Vdac1* directly interacts with apoptotic gene *Bax,* which interacts with other apoptotic genes, *Bid*, *Bcl2l1* and *Moap1*. *Vdac1* also interacts indirectly with *Aldoa* via *Vdac1* interaction with *Snca*. Similarly, *Dlg4* mediates *Vdac1's* interaction with *Uba1*. GeneMANIA predicted no interacting genes for *Filip1*, *Myom2*, *Armcx1*, *Lcmt1*, *Gm5239*, *Gm3839* and *Pum2* (Figure 49). GeneMANIA predicted pathways involved multiple pathways for groups of genes; for example *Vdac1, Ttn* and *Myom2* were in the pathway with predicted genes *Trim63* and *Tcap* (Figure 50).
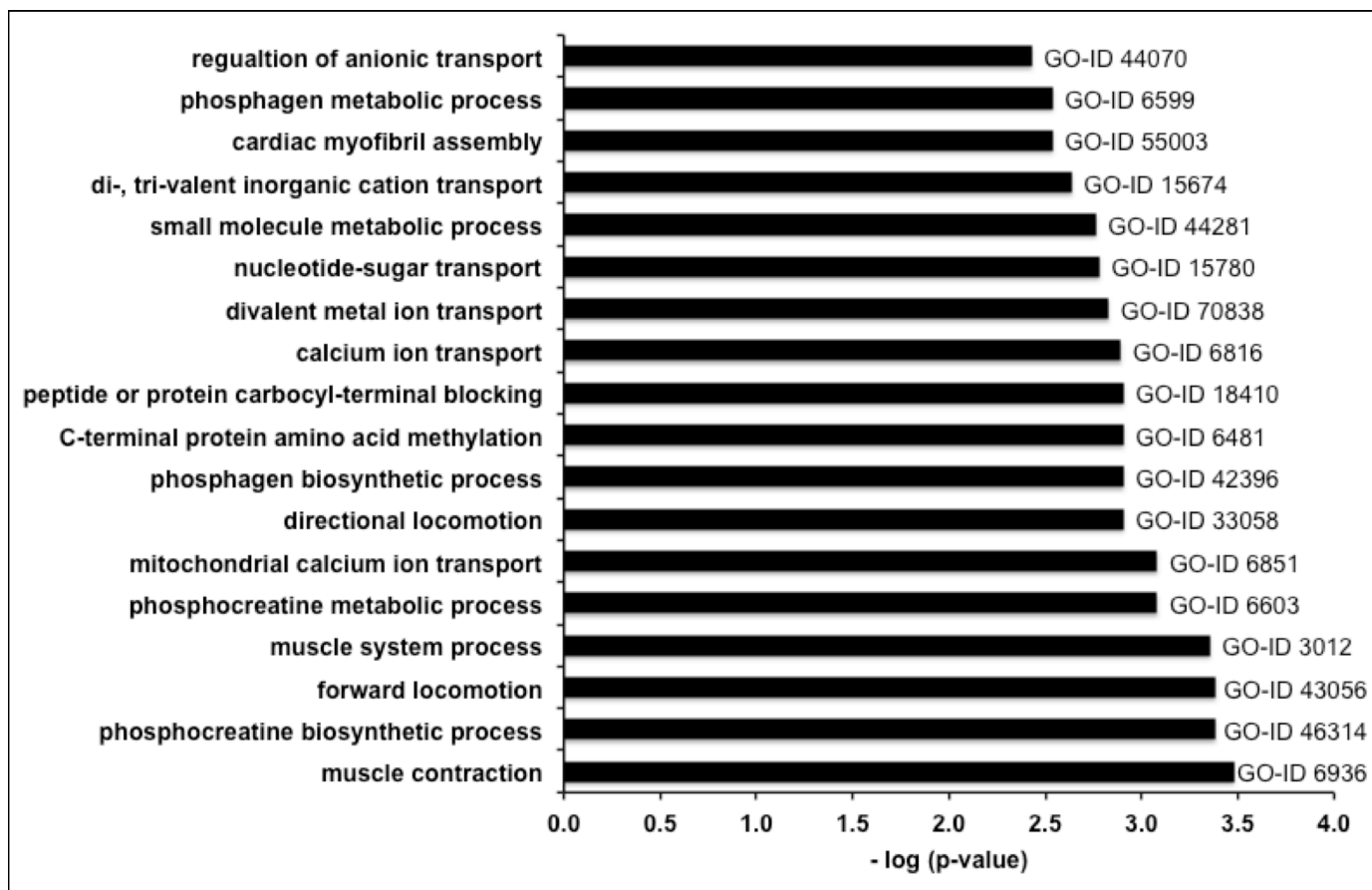
Figure 48. Gene Ontology. Using BiNGO, assessment of functional themes was performed for potential malin substrates identified following diGly immunoaffinity purification and MudPIT LC/MS analysis.
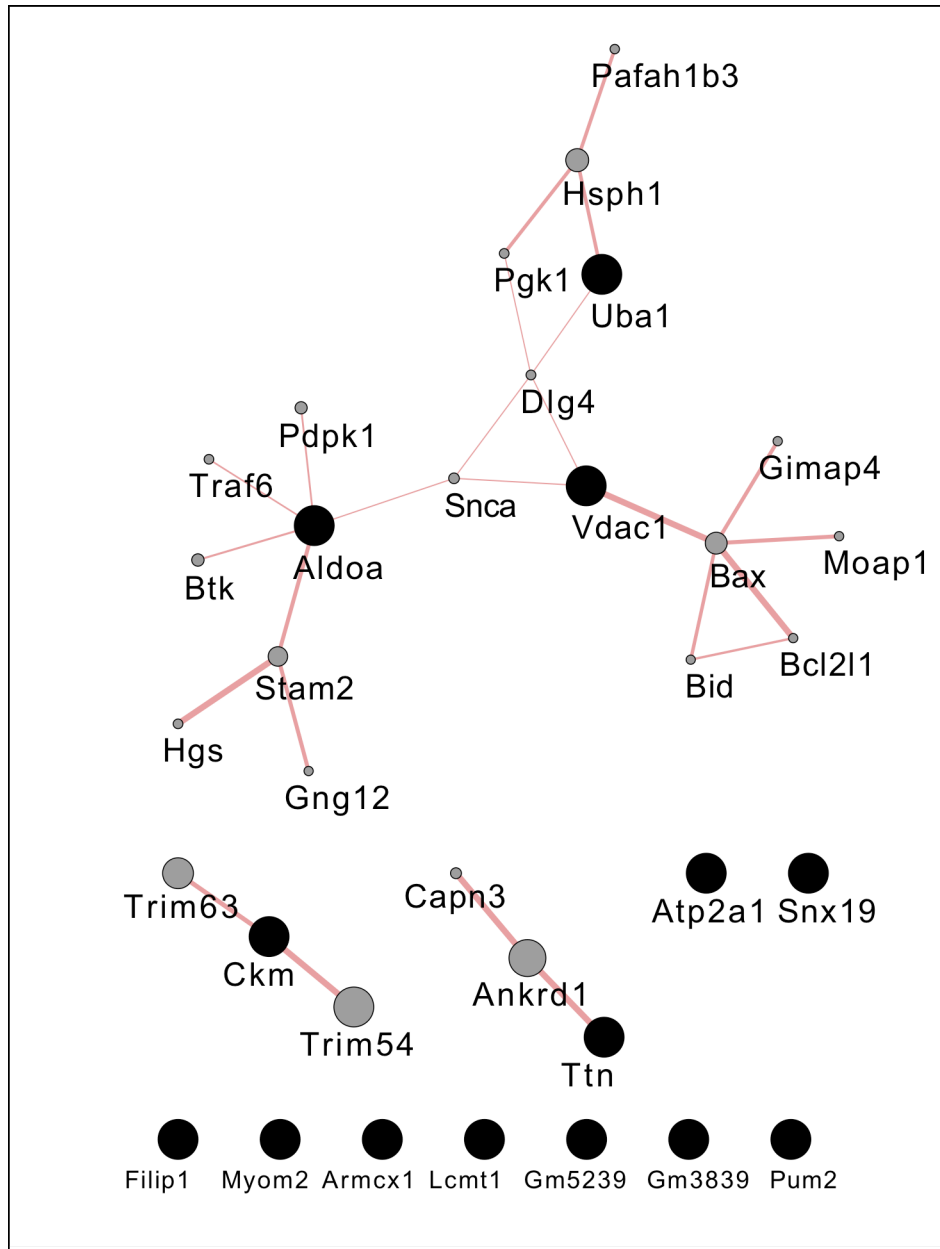
Figure 49. Predicted Physical Interactions by GeneMANIA. Using GeneMANIA, physical interactions were predicted for potential malin substrates identified following diGly immunoaffinity purification and MudPIT LC/MS analysis. Black dots are query genes, grey dots are predicted genes, thickness of line represents interactions' score, thicker the line, higher the interaction score.
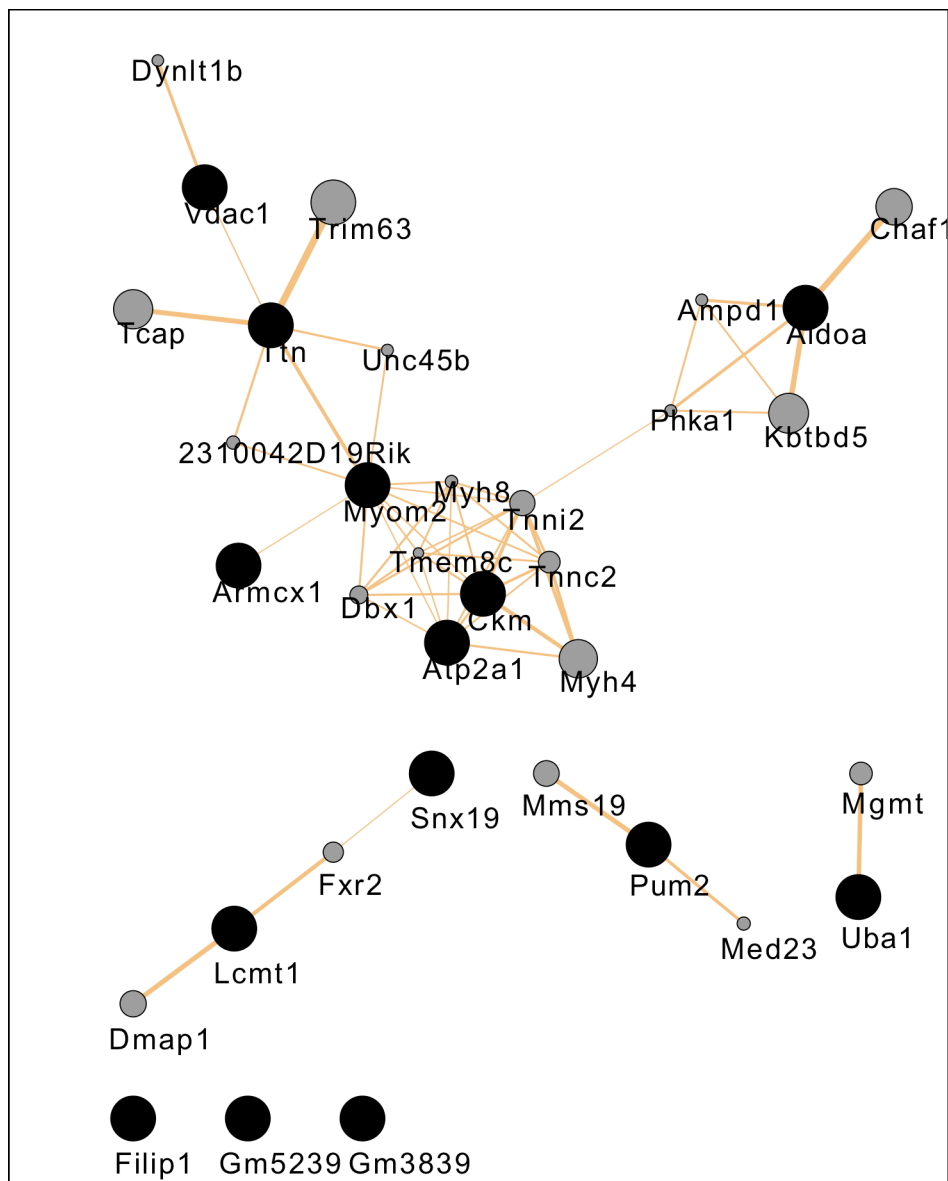
Figure 50. Predicted Pathways by GeneMANIA. Using GeneMANIA, pathways involved were predicted for potential malin substrates identified following diGly immunoaffinity purification and MudPIT LC/MS analysis. Black dots are query genes, grey dots are predicted genes, thickness of line represents score for interactions, thicker the line, higher the score for involvement in the pathway.

DISCUSSION

Lafora disease was first described by Dr. Gonzalo Lafora and is an autosomal recessive neurodegenerative epileptic disorder with onset during early adolescence, gradual progression to neurological symptoms and eventually death due to cardio-respiratory arrest. Lafora disease is usually a diagnosis of exclusion and is confirmed by the presence of characteristic polyglucosan Lafora bodies present in many tissues such as skin, neurons, muscle and heart (183). So far there is no cure or effective treatment available for Lafora disease. Ninety five percent of the patients with Lafora disease have mutations in either of the two genes, *EPM2A* (32) encoding a phosphatase, laforin or *EPM2B* (81) encoding an E3 ubiquitin ligase, malin with clinically indistinguishable symptoms. Since the identification of the two genes, Lafora research has been focused on defining the physiological functions of laforin and malin and how mutations in either gene lead to similar clinical symptoms. Lafora disease is a non-classical type of glycogen storage disease and therefore, glycogen metabolism has been an obvious area of investigation.

1.   Laforin as a Glycogen Phosphatase

Laforin, a dual specificity phosphatase, contains a carbohydrate-binding domain and has been shown to interact more strongly with poorly branched polysaccharides such as amylopectin (90,184,185). The first reported substrate of laforin was the protein kinase GSK-3 (115,118) that, among other functions, regulates glycogen synthase activity. Dephosphorylation of the N-terminal site in

GSK-3 would activate the enzyme and in turn decrease glycogen synthase activity. In the absence of laforin, glycogen synthase would be activated because of the lack of the inhibitory effect of GSK-3. However, other independent studies have observed no change in glycogen synthase activity or the phosphorylation state of GSK3 in *Epm2a-/-* mice (9,116,119). Earlier work in our laboratory by Tagliabracci et al. demonstrated that laforin functions as a glycogen phosphatase *in vivo* (8,9). Analysis of 9- to 12-month-old *Epm2a-/-* mice revealed a three-fold increase in total glycogen levels and a six-fold increase in glycogen phosphorylation (8). Laforin is a glycogen metabolic enzyme that dephosphorylates glycogen possibly as part of a "repair" or "damage control" mechanism similar to the repair mechanism for DNA (10). Normal glycogen contains low amounts of phosphate, which are maintained at structurally tolerated levels by laforin. In the absence of laforin in Lafora disease, the cycles of glycogen synthesis and degradation proceed relatively normally, but the patients gradually start accumulating structurally defective glycogen eventually developing polyglucosan Lafora bodies. This also explains the fact that the patients are symptom-free with a normal growth curve till early adolescence when the cells reach the threshold for glycogen phosphorylation beyond which the structurally abnormal glycogen becomes insoluble causing the disease pathology.

Besides functioning as a glycogen phosphatase, laforin could have additional functions. Ongoing Lafora research has identified several proteins that interact with laforin and most of these proteins are known glycogen-binding

proteins. In most cases, laforin has been reported to regulate the activity of these interacting proteins with the aid of the E3 ubiquitin ligase malin, (described below), which also has been reported to interact with laforin.

2.   Malin as an E3 Ubiquitin Ligase

Defects in malin cause the formation of Lafora bodies and it is interesting how mutations in either of the genes lead to the same disease. This could be because the two proteins are involved in the same pathway or alternatively, the two proteins function independent of each other but converge to the same common end point, causing the same phenotype. Malin has been shown to biochemically function as an E3 ubiquitin ligase (101). Gentry et al. (101) reported that laforin was a substrate of malin. Malin was shown to ubiquitinate and degrade laforin via the proteasome. This hypothesis does not explain how in the absence of malin, increased levels of laforin could still cause symptoms of Lafora disease. Various studies have identified multiple proteins as targets for malin, including glycogen synthase (115), debranching enzyme (125), PTG (94,117,126,127), laforin (101), neuronatin (128) and AMPK (186). Except for AMPK, which is ubiquitinated at K63, all other substrates are modified by K48-linked polyubiquitination and are targeted to the proteasome for degradation. Vilchez et al. (126) proposed that a laforin-malin complex ubiquitinates and degrades PTG and in neurons, also glycogen synthase. Worby et al. (127) reported that malin degrades PTG in a laforin-dependent manner. Impaired degradation of either glycogen synthase or PTG would result in increased

141

glycogen levels by increasing glycogen synthase levels or by increased targeting of PP1 leading to dephosphorylation and activation of glycogen synthase. Debranching enzyme, AGL, has been shown to be ubiquitinated and degraded by malin and in Lafora disease increased AGL levels would lead to abnormal branching in glycogen (125). Thus, all these studies focused on the idea that in the absence of malin in Lafora disease, there would be elevated levels of the substrates that eventually lead to either downstream increase in glycogen levels or production of defective glycogen. The studies described so far have been performed either *in vitro* or with overexpression in cultured cells. If the laforin-malin complex targets these proteins for degradation, one would expect an increase in the levels of these proteins in animals lacking malin or laforin. However, our analysis of the 3-month-old *Epm2b*-/- mice (108) revealed no differences in the activity of glycogen synthase or protein levels of PTG or AGL in skeletal muscle.

Several studies have also shown that laforin protein level follows glycogen accumulation independently of whether *Epm2b* is deleted or not suggesting that, contrary to previous proposals, laforin too is not a malin substrate (108,142,185). In the *Epm2b*-/- mice, we observed increased levels of laforin but only in the insoluble fraction, which suggests that malin may prevent the sequestration of laforin in the insoluble fraction rather than playing a role in the proteasomal-dependent degradation of laforin. Turnbull et al. (110) reported that the phosphate content of glycogen in *Epm2b*-/- mice was elevated, but to slightly lower levels than *Epm2a*-/- mice. In *Epm2b*-/- mice, we showed that laforin was

depleted from the soluble fraction (108,110), where it would function to dephosphorylate glycogen. This could explain how a loss of function mutation in *EPM2B* would also cause loss of function of laforin and therefore, elevated levels of phosphate in the glycogen.

3.   Laforin-malin Complex in Protein Quality Control

Besides malin's role in proteasomal degradation of proteins involved in glycogen metabolism, the laforin-malin complex has been shown to participate in protein quality control to maintain cellular homeostasis. For the most part, these studies have been done using an overexpression cell culture model. Mittal et al. (187) first reported the formation of aggresomes upon proteasomal inhibition in neuronal and non-neuronal cells expressing both laforin and malin. Both proteins co-localized to the aggresomes leading to the speculation that laforin and malin might be involved in the proteasomal degradation of misfolded proteins and laforin might be a novel component of signaling circuits involved with protein clearance. Using cellular models for misfolded protein disorders such as expanded polyglutamine proteins (Huntingtin disease), polyalanine proteins (Ocular-myopathy) and α-synuclein (Parkinson's disease), the laforin-malin complex was shown to form a functional complex with the cellular chaperone, Hsp70 and suppressed the cellular toxicity of the aforementioned misfolded proteins by promoting their degradation via the ubiquitin-proteasomal and the autophago-lysosomal pathway. This was supported by evidence that laforin and

malin colocalize with huntingtin aggregates in the neurons of transgenic mice model (R6/2) for Huntington disease (129).

Aguado et al. (121) observed decreased LC3-II and increased p62 in human fibroblasts from Lafora disease patients and MEFs from *Epm2a*-/- mice. The impairment of autophagy in the absence of laforin was mTOR-dependent. Criado et al. (112) reported that impairment in autophagy in the absence of malin, however, was independent of mTOR. Puri et al. (136) speculated that defects in the autophagy and endosomal-lysosomal pathways were a cause for Lafora disease, but they were unable to report differences in LC3-II in the brain of *Epm2a*-/- mice. These studies argue that defects in protein clearance to be the primary cause of the disease phenotype, involving disposal of proteins beyond the malin targets involved in glycogen metabolism.

In an effort to further understand the physiological roles of laforin and malin, we analyzed the protein degradation and quality control systems in MEFs derived from *Epm2a-/-*, *Epm2b-/-* and double *Epm2a-/- Epm2b-/-* mice. Lack of laforin and/or malin impairs autophagy in an mTOR-dependent manner. While there was an overall decrease in LC3-II, indicating reduced formation of autophagosomes, in all the knockout MEFs, induction of autophagy upon starvation or rapamycin treatment was still observed, although to a much lower extent than in the wild type cells. This could be because the capacity of the knockout MEFs to form new autophagosomes is limited. Criado et al. (112) reported that malin regulates autophagy in an mTOR-independent manner, which is inconsistent with the conclusion that laforin and malin regulate autophagy as a

144

complex. However, in our studies, both laforin and malin are mTOR-dependent in their regulation of autophagy.

In contrast to previous studies (112,136), we found that in MEFs there was proteasomal dysfunction in the absence of either laforin or malin. Deletion of both genes in double *Epm2a-/- Epm2b-/-* MEFs did not cause a further decrease in the proteasomal activity. The proteasomal activity was, however, not completely absent in the knockout MEFs. Under basal conditions, the levels of ubiquitinated proteins were not altered in the knockout MEFs as compared to the wild type cells. Upon starvation, ubiquitinated proteins in the wild-type cells were degraded either via the proteasome or the lysosome because blocking either of the two pathways prevented the degradation of the proteins. However, the starvation-induced degradation of the ubiquitinated proteins was absent in all the knockout MEFs suggesting impairment of the protein clearance pathways. These results, therefore, suggest either an overlap in malin and laforin functions or an effect secondary to a common phenotype such as generalized cell stress caused by abnormal glycogen accumulation (Figure 51). An uncompromised ER stress response points towards a secondary effect that becomes enhanced under stress.

4.   Glycogen Accumulation: Cause or Consequence

Independent studies by Turnbull et al. (140,188) and Pederson et al. (141) have linked the overaccumulation of abnormal glycogen to the causation of Lafora disease since genetic reduction of the glycogen levels either by

145

eliminating glycogen synthase or PTG rescues not only Lafora body formation but also the neurological symptoms associated with the disease. Recent work by Duran et al. (142) showed a reversal of autophagy impairment in *Epm2b-/-* mice with impaired glycogen synthesis. We have observed that decreased glycogen accumulation in *Epm2b-/-* mice restored autophagy markers and proteasomal activity in the brain (Unpublished results, A.A. DePaoli-Roach, D.M. Segvich, C. J. Contreras, P. Garyali and P.J. Roach). Thus, the defect in protein clearance in Lafora disease may be secondary to the accumulation of abnormal glycogen and sequestration of cellular proteins in the Lafora bodies.

5.   Role of Malin Independent of Laforin

Interestingly, we found that in *Epm2a-/-* MEFs levels of GABARAPL1 and LAMP1 were similar to wild type but much lower in *Epm2b-/-* and double *Epm2a-/- Epm2b-/-* MEFs, suggesting a function of malin independent of laforin. We have shown earlier that Starch-binding domain protein 1 (Stbd1) preferentially binds to abnormal and hyperphosphorylated glycogen (33). It has been proposed that Stbd1 may participate in the lysosomal trafficking of glycogen by anchoring glycogen to intracellular membranes. Stbd1 interacts with GABARAPL1, which may function as a novel cargo binding protein that delivers glycogen to lysosomes (60). In knockout MEFs, the protein level of Stbd1 is not altered, although GABARAPL1, an interacting partner of Stbd1, and LAMP1 are decreased in *Epm2b-/-* and double *Epm2a-/- Epm2b-/-* MEFs suggesting a

146

possible role of malin in glycogen trafficking to lysosomes and/or lysosome
biogenesis.
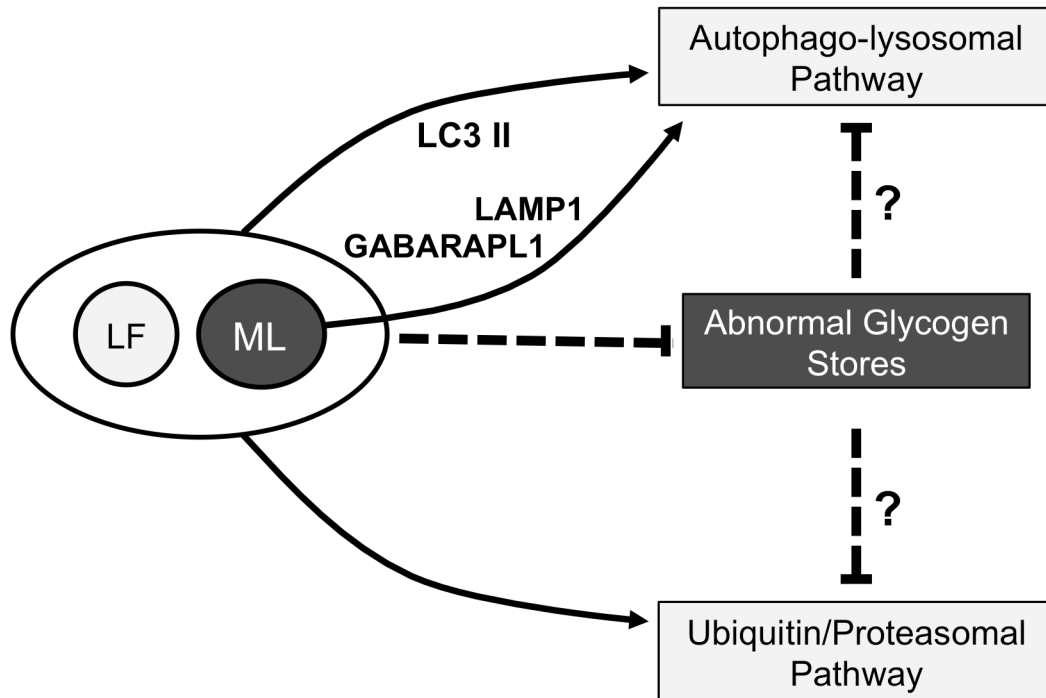
**Figure 51. Model of Possible Roles for Laforin and Malin in
Protein Degradation and Quality Control.** Genetic depletion of
malin and/or laforin resulted in impaired macroautophagy, as
indexed by LC3 II formation, as well as reduced proteasomal
degradation of proteins, consistent with laforin and malin either
acting together or at least in the same pathway. Only loss of malin,
however, caused decreases in LAMP1 and GABARAPL1, raising
the possibility of a pathway specific to malin function. The model
also suggests that effects on autophagy and the
ubiquitin/proteasomal pathways might be due to generalized cell
stress secondary to abnormal glycogen metabolism. LF, laforin;
ML, malin.

6.   Quantitative diGly Proteomics

The precise physiological role of malin is still not clear. The targets proposed, so far, have not been validated in studies of *Epm2b-/-* mice. In this study, an unbiased quantitative proteomics approach was developed with the goal of identifying the physiological substrates of malin. SILAC is a widely used proteomics approach to compare two or more conditions or genotypes. Metabolic labeling helps obtain the most precise quantification because the different samples can be combined before lysis of the cells (189). For this reason, our initial attempts were focused on developing a method based on SILAC in primary MEFs from wild type and malin knockout mice. Since the cells were not immortalized by transformation, they could still represent the cellular picture of the corresponding mouse. One of the major difficulties that we faced during these experiments was the presence of contaminating serum proteins, mainly albumin. The levels of albumin were four orders of magnitude higher than the most abundant mouse protein, which considerably interfered with the detection of mouse peptides by mass spectrometry (data not shown). Cross-contamination by albumin is difficult to avoid because of inherent adherence of albumin to not only the cells but also to the culture plates or flasks. A final concentration of 10% serum in the medium equates to around 5-6 mg protein/ml from serum (174). Extensive washes prior to cell harvesting failed to completely remove albumin to levels below detection by mass spectrometry (174). We tried modifying the washing techniques by using serum-free medium instead of buffered saline or

washing cells in suspension but we were unable to completely eliminate the contaminating proteins.

There are serum-free media commercially available that contain the required growth factors and other essential ingredients. We tried sequentially adapting the cells to the serum-free medium by gradually changing the ratio of full medium: serum-free medium from 100:0 to 0:100. The cells started showing altered morphology at 20:80 ratio of full medium: serum-free medium and failed to grow at 10:90 ratio. We continued to grow MEFs at low serum concentration of 2%, which was well tolerated by the cells. There was no change in the morphology of the cells, although they grew much more slowly. Serum contains factors that bind to the antibiotics added to the medium, thus reducing the concentration of antibiotics available. With a 5-fold decrease in the serum concentration, the factors would no longer be available at the same ratio to bind with the antibiotics. We, therefore, scaled down the concentration of antibiotics to prevent cell death because of antibiotics toxicity.

SILAC ultimately depends on the efficiency of labeling in cells growing in heavy or light medium. Incomplete labeling, especially in cells growing in the heavy medium, affects the results since it fails to provide the necessary guide as to which proteins are from growth in heavy medium. We observed that in our primary MEFs efficient labeling was not achieved even after culturing cells in heavy medium for 8 weeks. It could be because of issues with amino acid uptake specific to primary cells like MEFs. We were unable to resolve these problems.

We then established a method for studying the murine skeletal muscle ubiquitylome using the quantitative diGly approach. In this study, we identified about 244 non-redundant ubiquitinated sites in 142 proteins. We found known ubiquitination sites such as lysine 119 in histone H2A (177) and validated our approach. Among the 25 most abundant proteins from our study were myosin subunits, actin, histones and E3 ubiquitin ligases. There are likely ubiquitinated proteins in muscle that we have not been able to identify in our study because of inherent stochastic low abundance of certain proteins or loss of the ubiquitin moiety during sample preparation despite use of inhibitors. The MS/MS spectra were isolated and subjected to detection by high resolution HCD fragmentation in addition to CID, thus enabling us to identify the exact ubiquitination site in the proteins, but our approach lacks the ability to identity if a protein is mono- or poly-ubiquitinated. Nine ubiquitination sites were identified in myosin-4, the most abundant protein in the mouse muscle ubiquitylome. Five of these ubiquitination sites were present only in myosin-4, while four peptides were present in other myosin heavy chains as well. So far, there is no experimental evidence in the literature for ubiquitination of myosin-4 in mouse muscle. Myosin heavy chains could be polyubiquitinated and degraded by the ubiquitin-proteasomal or the autophagolysosomal pathway as a part of protein turnover/quality control process. The other possibility is that ubiquitination could be a post-translational modification for regulation of myosin activity. Since our approach cannot identify the type of ubiquitination chain formed, further studies will be required to understand the exact role of ubiquitination in myosin and muscle function.

To establish a comparative approach to study two different genotypes, we optimized immunoaffinity purification using the diGly antibody combined with stable isotope dimethyl labeling. The advantage of dimethyl labeling is that it can easily be applied to tissues and human samples, which is impossible to perform with SILAC. The starting material for the diGly immunoprecipitations or immunoprecipitation for other modifications such as phosphorylation is typically several milligrams of proteins, which makes the use of labeling with iTRAQ cost-prohibitive. On the other hand, dimethyl labeling can be performed with inexpensive generic reagents without posing financial restrictions to the amount of sample to be labeled (148,190). Boersema et al. described the method to perform on-column dimethyl labeling of tryptic peptides (148). In this study, we further explored and optimized the dimethyl labeling coupled with diGly immunoaffinity purification. Our initial approach was to perform chemical labeling before immunoprecipitation so that the differentially labeled peptides can be immunoprecipitated together, thereby neutralizing the potentially biggest source of variation. However, labeling followed by immunoaffinity purification resulted in complete failure to detect any diGly peptides. The N-terminus of the diGly remnant would be modified by dimethylation and methyl, being a bulky group, likely interferes with the interaction of the diGly remnant with the antibody. In our final approach, we performed the immunoaffinity purification separately on samples derived from the two genotypes followed by the dimethyl labeling. The chemical labeling is performed after cell lysis and proteolysis, which makes the method more generically applicable to any biological sample including human

tissue. Since quantification was done at the peptide rather than protein levels, different ubiquitylation events in the same protein can be monitored.

We used the dimethyl-coupled diGly proteomics approach to search for physiological substrates of malin E3 ubiquitin ligase. In the absence of malin in *Epm2b*-/- mice, malin substrates might not be ubiquitinated. After diGly immunoaffinity purification and MudPIT-LC/MS analysis, we identified 70 proteins which were present in the wild type but not in the *Emp2b*-/- tissue. Out of these proteins, 56 proteins had only 1 peptide spectral match and thus, are not reliable as positives in our screen. The remaining proteins had more than 2 peptide spectral matches and therefore were more likely to be potential malin substrates. Out of these potential malin substrates Leucine carboxyl methyltransferase 1 or Lcmt1 had the highest PSM score of 65. In other words, the ubiquitinated tryptic peptide of Lcmt1 protein was not detected in skeletal muscle proteome of malin knockout mice, but it was detected 65 times in the wild type tissue, which makes Lcmt1 very likely to be a substrate of malin. Second in the list was sarcoplasmic/endoplasmic reticulum calcium ATPase 1 or Atp2a1 with a PSM score of 13. All other potential substrates had a PSM score of less than 10. Since the PSM score of Lcmt1 is significantly higher than the other proteins, it makes it the most likely substrate of malin that we identified.

Lcmt1 has been reported to methylate the carboxyl group of the C-terminal leucine residue of protein phosphatase 2A catalytic subunit, which is required for assembly of the holoenzyme containing the B subunit (191,192). Lcmt1 is localized to the cytoplasm, Golgi region and the late endosomes (193),

is required for normal progression through mitosis and cell survival and is essential for embryonic development in mice (194). Recently Sontag et al. reported that LCMT1-dependent methylation of PP2A catalytic subunit leads to distinct compartmentalization of PP2A and PP2A regulatory enzymes in plasma membrane microdomains/rafts of neuroblastoma cells (195). Carboxyl methylation of PP2A catalytic subunit is required to regulate the microtubule cytoskeleton and tau. Analysis in patients with Alzheimer disease (AD) revealed that LCMT1 protein expression and methylation of catalytic subunit of PP2A were decreased in AD-affected brain regions (196). Jackson et al. (197) reported an increased phosphorylation of Akt T308 upon Lcmt 1 knockdown in HEKTERASB56γ cells suggesting that Akt phosphorylation might be regulated directly or indirectly by methylation-sensitive PP2A B-subunits. Lcmt 1 knockdown was also reported to activate p70/p85 S6K and rpS6, so that Lcmt 1-dependent activation of the S6K pathway might be a consequence of Akt and mTOR pathway activation. While further experiments need to be performed to validate Lcmt1 as a malin substrate and to understand the role, if any, of Lcmt1 in Lafora disease, from our analysis by mass spectrometry, Lcmt1 is currently our most promising candidate to be a malin substrate.

In conclusion, we observed that in MEFs from mouse models of Lafora disease autophagy is impaired in an mTOR-dependent manner, there is impairment of the proteasomal activity while the ER stress response is not compromised. We propose that this defect in protein clearance might be secondary to generalized cellular stress because of glycogen overaccumulation.

Laforin and malin do not always function as a complex and malin may play a role, independent of laforin, in lysosomal biogenesis or lysosomal trafficking of glycogen. We developed an unbiased comparative quantitative diGly proteomics approach to study the mouse muscle ubiquitylome and identified 14 proteins as potential malin substrates. We consider Lcmt1 to be a promising candidate substrate of the malin E3 ubiquitin ligase. Future experiments will need to focus on validation of the potential substrates, Lcmt1 in particular, to understand better the precise physiological role of malin in Lafora disease.

REFERENCES

1. Roach, P. J. (2002) Glycogen and its metabolism. *Curr Mol Med* **2**, 101-120
2. Melendez, R., Melendez-Hevia, E., and Cascante, M. (1997) How did glycogen structure evolve to satisfy the requirement for rapid mobilization of glucose? A problem of physical constraints in structure building. *J Mol Evol* **45**, 446-455
3. Melendez-Hevia, E., Waddell, T. G., and Shelton, E. D. (1993) Optimization of molecular design in the evolution of metabolism: the glycogen molecule. *Biochem J* **295 (Pt 2)**, 477-483
4. Drochmans, P. (1962) [Morphology of glycogen. Electron microscopic study of the negative stains of particulate glycogen]. *J Ultrastruct Res* **6**, 141-163
5. Kirkman, B. R., and Whelan, W. J. (1986) Glucosamine is a normal component of liver glycogen. *FEBS Lett* **194**, 6-11
6. Kirkman, B. R., Whelan, W. J., and Bailey, J. M. (1989) The distribution of glucosamine in mammalian glycogen from different species, organs and tissues. *Biofactors* **2**, 123-126
7. Fontana, J. D. (1980) The presence of phosphate in glycogen. *FEBS Lett* **109**, 85-92
8. Tagliabracci, V. S., Girard, J. M., Segvich, D., Meyer, C., Turnbull, J., Zhao, X., Minassian, B. A., Depaoli-Roach, A. A., and Roach, P. J. (2008) Abnormal metabolism of glycogen phosphate as a cause for Lafora disease. *J Biol Chem* **283**, 33816-33825
9. Tagliabracci, V. S., Turnbull, J., Wang, W., Girard, J. M., Zhao, X., Skurat, A. V., Delgado-Escueta, A. V., Minassian, B. A., Depaoli-Roach, A. A., and Roach, P. J. (2007) Laforin is a glycogen phosphatase, deficiency of which leads to elevated phosphorylation of glycogen in vivo. *Proc Natl Acad Sci U S A* **104**, 19262-19266
10. Tagliabracci, V. S., Heiss, C., Karthik, C., Contreras, C. J., Glushka, J., Ishihara, M., Azadi, P., Hurley, T. D., DePaoli-Roach, A. A., and Roach, P. J. (2011) Phosphate incorporation during glycogen synthesis and Lafora disease. *Cell Metab* **13**, 274-282
11. Nitschke, F., Wang, P., Schmieder, P., Girard, J. M., Awrey, D. E., Wang, T., Israelian, J., Zhao, X., Turnbull, J., Heydenreich, M., Kleinpeter, E., Steup, M., and Minassian, B. A. (2013) Hyperphosphorylation of glucosyl C6 carbons and altered structure of glycogen in the neurodegenerative epilepsy Lafora disease. *Cell Metab* **17**, 756-767
12. Chikwana, V. M., Khanna, M., Baskaran, S., Tagliabracci, V. S., Contreras, C. J., DePaoli-Roach, A., Roach, P. J., and Hurley, T. D. (2013) Structural basis for 2'-phosphate incorporation into glycogen by glycogen synthase. *Proc Natl Acad Sci U S A* **110**, 20976-20981
13. Blennow, A., Nielsen, T. H., Baunsgaard, L., Mikkelsen, R., and Engelsen, S. B. (2002) Starch phosphorylation: a new front line in starch research. *Trends Plant Sci* **7**, 445-450

14. Ritte, G., Heydenreich, M., Mahlow, S., Haebel, S., Kotting, O., and Steup, M. (2006) Phosphorylation of C6- and C3-positions of glucosyl residues in starch is catalysed by distinct dikinases. *FEBS Lett* **580**, 4872-4876

15. Kotting, O., Santelia, D., Edner, C., Eicke, S., Marthaler, T., Gentry, M. S., Comparot-Moss, S., Chen, J., Smith, A. M., Steup, M., Ritte, G., and Zeeman, S. C. (2009) STARCH-EXCESS4 is a laforin-like Phosphoglucan phosphatase required for starch degradation in Arabidopsis thaliana. *Plant Cell* **21**, 334-346

16. Cavanagh, J. B. (1999) Corpora-amylacea and the family of polyglucosan diseases. *Brain Res Brain Res Rev* **29**, 265-295

17. Rosai, J., and Lascano, E. F. (1970) Basophilic (mucoid) degeneration of myocardium: a disorder of glycogen metabolism. *Am J Pathol* **61**, 99-116

18. Lomako, J., Lomako, W. M., Kirkman, B. R., and Whelan, W. J. (1994) The role of phosphate in muscle glycogen. *Biofactors* **4**, 167-171

19. Roach, P. J., Cheng, C., Huang, D., Lin, A., Mu, J., Skurat, A. V., Wilson, W., and Zhai, L. (1998) Novel aspects of the regulation of glycogen storage. *J Basic Clin Physiol Pharmacol* **9**, 139-151

20. Shearer, J., and Graham, T. E. (2004) Novel aspects of skeletal muscle glycogen and its regulation during rest and exercise. *Exerc Sport Sci Rev* **32**, 120-126

21. Graham, T. E. (2009) Glycogen: an overview of possible regulatory roles of the proteins associated with the granule. *Appl Physiol Nutr Metab* **34**, 488-492

22. Rybicka, K. K. (1996) Glycosomes--the organelles of glycogen metabolism. *Tissue Cell* **28**, 253-265

23. Stapleton, D., Nelson, C., Parsawar, K., McClain, D., Gilbert-Wilson, R., Barker, E., Rudd, B., Brown, K., Hendrix, W., O'Donnell, P., and Parker, G. (2010) Analysis of hepatic glycogen-associated proteins. *Proteomics* **10**, 2320-2329

24. Haschke, R. H., Heilmeyer, L. M., Jr., Meyer, F., and Fischer, E. H. (1970) Control of phosphorylase activity in a muscle glycogen particle. 3. Regulation of phosphorylase phosphatase. *J Biol Chem* **245**, 6657-6663

25. Meyer, F., Heilmeyer, L. M., Jr., Haschke, R. H., and Fischer, E. H. (1970) Control of phosphorylase activity in a muscle glycogen particle. I. Isolation and characterization of the protein-glycogen complex. *J Biol Chem* **245**, 6642-6648

26. Roach, P. J., Depaoli-Roach, A. A., Hurley, T. D., and Tagliabracci, V. S. (2012) Glycogen and its metabolism: some new developments and old themes. *Biochem J* **441**, 763-787

27. Hudson, E. R., Pan, D. A., James, J., Lucocq, J. M., Hawley, S. A., Green, K. A., Baba, O., Terashima, T., and Hardie, D. G. (2003) A novel domain in AMP-activated protein kinase causes glycogen storage bodies similar to those seen in hereditary cardiac arrhythmias. *Curr Biol* **13**, 861-866

28. Polekhina, G., Gupta, A., Michell, B. J., van Denderen, B., Murthy, S., Feil, S. C., Jennings, I. G., Campbell, D. J., Witters, L. A., Parker, M. W.,

Kemp, B. E., and Stapleton, D. (2003) AMPK beta subunit targets metabolic stress sensing to glycogen. *Curr Biol* **13**, 867-871

29. Christiansen, C., Abou Hachem, M., Janecek, S., Vikso-Nielsen, A., Blennow, A., and Svensson, B. (2009) The carbohydrate-binding module family 20--diversity, structure, and function. *FEBS J* **276**, 5006-5029

30. Machovic, M., and Janecek, S. (2006) The evolution of putative starch-binding domains. *FEBS Lett* **580**, 6349-6356

31. Ganesh, S., Amano, K., Delgado-Escueta, A. V., and Yamakawa, K. (1999) Isolation and characterization of mouse homologue for the human epilepsy gene, EPM2A. *Biochem Biophys Res Commun* **257**, 24-28

32. Minassian, B. A., Lee, J. R., Herbrick, J. A., Huizenga, J., Soder, S., Mungall, A. J., Dunham, I., Gardner, R., Fong, C. Y., Carpenter, S., Jardim, L., Satishchandra, P., Andermann, E., Snead, O. C., 3rd, Lopes-Cendes, I., Tsui, L. C., Delgado-Escueta, A. V., Rouleau, G. A., and Scherer, S. W. (1998) Mutations in a gene encoding a novel protein tyrosine phosphatase cause progressive myoclonus epilepsy. *Nat Genet* **20**, 171-174

33. Jiang, S., Heller, B., Tagliabracci, V. S., Zhai, L., Irimia, J. M., DePaoli-Roach, A. A., Wells, C. D., Skurat, A. V., and Roach, P. J. (2010) Starch binding domain-containing protein 1/genethonin 1 is a novel participant in glycogen metabolism. *J Biol Chem* **285**, 34960-34971

34. Caudwell, F. B., and Cohen, P. (1980) Purification and subunit structure of glycogen-branching enzyme from rabbit skeletal muscle. *Eur J Biochem* **109**, 391-394

35. McGarry, J. D., Kuwajima, M., Newgard, C. B., Foster, D. W., and Katz, J. (1987) From dietary glucose to liver glycogen: the full circle round. *Annu Rev Nutr* **7**, 51-73

36. Thorens, B., and Mueckler, M. (2010) Glucose transporters in the 21st Century. *Am J Physiol Endocrinol Metab* **298**, E141-145

37. Krisman, C. R., and Barengo, R. (1975) A precursor of glycogen biosynthesis: alpha-1,4-glucan-protein. *Eur J Biochem* **52**, 117-123

38. Lomako, J., Lomako, W. M., and Whelan, W. J. (1988) A self-glucosylating protein is the primer for rabbit muscle glycogen biosynthesis. *FASEB J* **2**, 3097-3103

39. Pitcher, J., Smythe, C., Campbell, D. G., and Cohen, P. (1987) Identification of the 38-kDa subunit of rabbit skeletal muscle glycogen synthase as glycogenin. *Eur J Biochem* **169**, 497-502

40. Taniguchi, C. M., Emanuelli, B., and Kahn, C. R. (2006) Critical nodes in signalling pathways: insights into insulin action. *Nat Rev Mol Cell Biol* **7**, 85-96

41. Cross, D. A., Alessi, D. R., Cohen, P., Andjelkovich, M., and Hemmings, B. A. (1995) Inhibition of glycogen synthase kinase-3 by insulin mediated by protein kinase B. *Nature* **378**, 785-789

42. Rosenfeld, E. L. (1975) Alpha-glucosidases (gamma-amylases) in human and animal organisms. *Pathol Biol (Paris)* **23**, 71-84

43. Raben, N., Plotz, P., and Byrne, B. J. (2002) Acid alpha-glucosidase deficiency (glycogenosis type II, Pompe disease). *Curr Mol Med* **2**, 145-166

44. Yang, Z., and Klionsky, D. J. (2009) An overview of the molecular mechanism of autophagy. *Curr Top Microbiol Immunol* **335**, 1-32

45. Yang, Z., and Klionsky, D. J. (2010) Mammalian autophagy: core molecular machinery and signaling regulation. *Curr Opin Cell Biol* **22**, 124-131

46. Nakatogawa, H., Suzuki, K., Kamada, Y., and Ohsumi, Y. (2009) Dynamics and diversity in autophagy mechanisms: lessons from yeast. *Nat Rev Mol Cell Biol* **10**, 458-467

47. Klionsky, D. J., Cregg, J. M., Dunn, W. A., Jr., Emr, S. D., Sakai, Y., Sandoval, I. V., Sibirny, A., Subramani, S., Thumm, M., Veenhuis, M., and Ohsumi, Y. (2003) A unified nomenclature for yeast autophagy-related genes. *Dev Cell* **5**, 539-545

48. Johansen, T., and Lamark, T. (2011) Selective autophagy mediated by autophagic adapter proteins. *Autophagy* **7**, 279-296

49. Komatsu, M., and Ichimura, Y. (2010) Selective autophagy regulates various cellular functions. *Genes Cells* **15**, 923-933

50. Kotoulas, O. B., Kalamidas, S. A., and Kondomerkos, D. J. (2004) Glycogen autophagy. *Microsc Res Tech* **64**, 10-20

51. Dawes, G. S. (1968) Sudden death in babies: physiology of the fetus and newborn. *Am J Cardiol* **22**, 469-478

52. Raben, N., Roberts, A., and Plotz, P. H. (2007) Role of autophagy in the pathogenesis of Pompe disease. *Acta Myol* **26**, 45-48

53. Raben, N., Hill, V., Shea, L., Takikita, S., Baum, R., Mizushima, N., Ralston, E., and Plotz, P. (2008) Suppression of autophagy in skeletal muscle uncovers the accumulation of ubiquitinated proteins and their potential role in muscle damage in Pompe disease. *Hum Mol Genet* **17**, 3897-3908

54. Raben, N., Schreiner, C., Baum, R., Takikita, S., Xu, S., Xie, T., Myerowitz, R., Komatsu, M., Van der Meulen, J. H., Nagaraju, K., Ralston, E., and Plotz, P. H. (2010) Suppression of autophagy permits successful enzyme replacement therapy in a lysosomal storage disorder--murine Pompe disease. *Autophagy* **6**, 1078-1089

55. Wang, Z., Wilson, W. A., Fujino, M. A., and Roach, P. J. (2001) Antagonistic controls of autophagy and glycogen accumulation by Snf1p, the yeast homolog of AMP-activated protein kinase, and the cyclin-dependent kinase Pho85p. *Mol Cell Biol* **21**, 5742-5752

56. Wilson, W. A., Wang, Z., and Roach, P. J. (2002) Systematic identification of the genes affecting glycogen storage in the yeast Saccharomyces cerevisiae: implication of the vacuole as a determinant of glycogen level. *Mol Cell Proteomics* **1**, 232-242

57. Cardell, R. R., Jr., Michaels, J. E., Hung, J. T., and Cardell, E. L. (1985) SERGE, the subcellular site of initial hepatic glycogen deposition in the rat: a radioautographic and cytochemical study. *J Cell Biol* **101**, 201-206

58. Bouju, S., Lignon, M. F., Pietu, G., Le Cunff, M., Leger, J. J., Auffray, C., and Dechesne, C. A. (1998) Molecular cloning and functional expression of a novel human gene encoding two 41-43 kDa skeletal muscle internal membrane proteins. *Biochem J* **335 (Pt 3)**, 549-556

59. Janecek, S. (2002) A motif of a microbial starch-binding domain found in human genethonin. *Bioinformatics* **18**, 1534-1537

60. Jiang, S., Wells, C. D., and Roach, P. J. (2011) Starch-binding domain-containing protein 1 (Stbd1) and glycogen metabolism: Identification of the Atg8 family interacting motif (AIM) in Stbd1 required for interaction with GABARAPL1. *Biochem Biophys Res Commun* **413**, 420-425

61. Orho, M., Bosshard, N. U., Buist, N. R., Gitzelmann, R., Aynsley-Green, A., Blumel, P., Gannon, M. C., Nuttall, F. Q., and Groop, L. C. (1998) Mutations in the liver glycogen synthase gene in children with hypoglycemia due to glycogen storage disease type 0. *J Clin Invest* **102**, 507-515

62. Chou, J. Y., Matern, D., Mansfield, B. C., and Chen, Y. T. (2002) Type I glycogen storage diseases: disorders of the glucose-6-phosphatase complex. *Curr Mol Med* **2**, 121-143

63. Koeberl, D. D., Kishnani, P. S., Bali, D., and Chen, Y. T. (2009) Emerging therapies for glycogen storage disease type I. *Trends Endocrinol Metab* **20**, 252-258

64. Koster, J. F., Busch, H. F., Slee, R. G., and Van Weerden, T. W. (1978) Glycogenosis type II: the infantile- and late-onset acid maltase deficiency observed in one family. *Clin Chim Acta* **87**, 451-453

65. Raben, N., Nagaraju, K., Lee, E., Kessler, P., Byrne, B., Lee, L., LaMarca, M., King, C., Ward, J., Sauer, B., and Plotz, P. (1998) Targeted disruption of the acid alpha-glucosidase gene in mice causes an illness with critical features of both infantile and adult human glycogen storage disease type II. *J Biol Chem* **273**, 19086-19092

66. Douillard-Guilloux, G., Raben, N., Takikita, S., Ferry, A., Vignaud, A., Guillet-Deniau, I., Favier, M., Thurberg, B. L., Roach, P. J., Caillaud, C., and Richard, E. (2010) Restoration of muscle functionality by genetic suppression of glycogen synthesis in a murine model of Pompe disease. *Hum Mol Genet* **19**, 684-696

67. Shen, J. J., and Chen, Y. T. (2002) Molecular characterization of glycogen storage disease type III. *Curr Mol Med* **2**, 167-175

68. Wolfsdorf, J. I., and Weinstein, D. A. (2003) Glycogen storage diseases. *Rev Endocr Metab Disord* **4**, 95-102

69. Raju, G. P., Li, H. C., Bali, D. S., Chen, Y. T., Urion, D. K., Lidov, H. G., and Kang, P. B. (2008) A case of congenital glycogen storage disease type IV with a novel GBE1 mutation. *J Child Neurol* **23**, 349-352

70. Dimaur, S., Andreu, A. L., Bruno, C., and Hadjigeorgiou, G. M. (2002) Myophosphorylase deficiency (glycogenosis type V; McArdle disease). *Curr Mol Med* **2**, 189-196

71. Ozen, H. (2007) Glycogen storage diseases: new perspectives. *World J Gastroenterol* **13**, 2541-2553

72. Nakajima, H., Raben, N., Hamaguchi, T., and Yamasaki, T. (2002) Phosphofructokinase deficiency; past, present and future. *Curr Mol Med* **2**, 197-212

73. Berkovic, S. F., Andermann, F., Carpenter, S., and Wolfe, L. S. (1986) Progressive myoclonus epilepsies: specific causes and diagnosis. *N Engl J Med* **315**, 296-305

74. Harriman, D. G., Millar, J. H., and Stevenson, A. C. (1955) Progressive familial myoclonic epilepsy in three families: its clinical features and pathological basis. *Brain* **78**, 325-349

75. Lafora, G. R. (1911) Contribution on Histopathology of the Spinal Coprd in Dementia Arteriosclerotica. *Monatsschrift Fur Psychiatrie Und Neurologie* **29**, 1-32

76. Minassian, B. A. (2001) Lafora's disease: towards a clinical, pathologic, and molecular synthesis. *Pediatr Neurol* **25**, 21-29

77. Yokoi, S., Austin, J., Witmer, F., and Sakai, M. (1968) Studies in myoclonus epilepsy (Lafora body form). I. Isolation and preliminary characterization of Lafora bodies in two cases. *Arch Neurol* **19**, 15-33

78. Delgado-Escueta, A. V. (2007) Advances in lafora progressive myoclonus epilepsy. *Curr Neurol Neurosci Rep* **7**, 428-433

79. Ganesh, S., Puri, R., Singh, S., Mittal, S., and Dubey, D. (2006) Recent advances in the molecular basis of Lafora's progressive myoclonus epilepsy. *J Hum Genet* **51**, 1-8

80. Robitaille, Y., Carpenter, S., Karpati, G., and DiMauro, S. D. (1980) A distinct form of adult polyglucosan body disease with massive involvement of central and peripheral neuronal processes and astrocytes: a report of four cases and a review of the occurrence of polyglucosan bodies in other conditions such as Lafora's disease and normal ageing. *Brain* **103**, 315-336

81. Chan, E. M., Young, E. J., Ianzano, L., Munteanu, I., Zhao, X., Christopoulos, C. C., Avanzini, G., Elia, M., Ackerley, C. A., Jovic, N. J., Bohlega, S., Andermann, E., Rouleau, G. A., Delgado-Escueta, A. V., Minassian, B. A., and Scherer, S. W. (2003) Mutations in NHLRC1 cause progressive myoclonus epilepsy. *Nat Genet* **35**, 125-127

82. Serratosa, J. M., Gomez-Garre, P., Gallardo, M. E., Anta, B., de Bernabe, D. B., Lindhout, D., Augustijn, P. B., Tassinari, C. A., Malafosse, R. M., Topcu, M., Grid, D., Dravet, C., Berkovic, S. F., and de Cordoba, S. R. (1999) A novel protein tyrosine phosphatase gene is mutated in progressive myoclonus epilepsy of the Lafora type (EPM2). *Hum Mol Genet* **8**, 345-352

83. Chan, E. M., Omer, S., Ahmed, M., Bridges, L. R., Bennett, C., Scherer, S. W., and Minassian, B. A. (2004) Progressive myoclonus epilepsy with polyglucosans (Lafora disease): evidence for a third locus. *Neurology* **63**, 565-567

84. Singh, S., and Ganesh, S. (2009) Lafora progressive myoclonus epilepsy: a meta-analysis of reported mutations in the first decade following the discovery of the EPM2A and NHLRC1 genes. *Hum Mutat* **30**, 715-723

85. Baykan, B., Striano, P., Gianotti, S., Bebek, N., Gennaro, E., Gurses, C., and Zara, F. (2005) Late-onset and slow-progressing Lafora disease in four siblings with EPM2B mutation. *Epilepsia* **46**, 1695-1697

86. Gomez-Abad, C., Gomez-Garre, P., Gutierrez-Delicado, E., Saygi, S., Michelucci, R., Tassinari, C. A., Rodriguez de Cordoba, S., and Serratosa, J. M. (2005) Lafora disease due to EPM2B mutations: a clinical and genetic study. *Neurology* **64**, 982-986

87. Singh, S., Suzuki, T., Uchiyama, A., Kumada, S., Moriyama, N., Hirose, S., Takahashi, Y., Sugie, H., Mizoguchi, K., Inoue, Y., Kimura, K., Sawaishi, Y., Yamakawa, K., and Ganesh, S. (2005) Mutations in the NHLRC1 gene are the common cause for Lafora disease in the Japanese population. *J Hum Genet* **50**, 347-352

88. Franceschetti, S., Gambardella, A., Canafoglia, L., Striano, P., Lohi, H., Gennaro, E., Ianzano, L., Veggiotti, P., Sofia, V., Biondi, R., Striano, S., Gellera, C., Annesi, G., Madia, F., Civitelli, D., Rocca, F. E., Quattrone, A., Avanzini, G., Minassian, B., and Zara, F. (2006) Clinical and genetic findings in 26 Italian patients with Lafora disease. *Epilepsia* **47**, 640-643

89. Serratosa, J. M., Delgado-Escueta, A. V., Posada, I., Shih, S., Drury, I., Berciano, J., Zabala, J. A., Antunez, M. C., and Sparkes, R. S. (1995) The gene for progressive myoclonus epilepsy of the Lafora type maps to chromosome 6q. *Hum Mol Genet* **4**, 1657-1663

90. Chan, E. M., Ackerley, C. A., Lohi, H., Ianzano, L., Cortez, M. A., Shannon, P., Scherer, S. W., and Minassian, B. A. (2004) Laforin preferentially binds the neurotoxic starch-like polyglucosans, which form in its absence in progressive myoclonus epilepsy. *Hum Mol Genet* **13**, 1117-1129

91. Wang, J., Stuckey, J. A., Wishart, M. J., and Dixon, J. E. (2002) A unique carbohydrate binding domain targets the lafora disease phosphatase to glycogen. *J Biol Chem* **277**, 2377-2380

92. Ganesh, S., Agarwala, K. L., Ueda, K., Akagi, T., Shoda, K., Usui, T., Hashikawa, T., Osada, H., Delgado-Escueta, A. V., and Yamakawa, K. (2000) Laforin, defective in the progressive myoclonus epilepsy of Lafora type, is a dual-specificity phosphatase associated with polyribosomes. *Hum Mol Genet* **9**, 2251-2261

93. Ganesh, S., Agarwala, K. L., Amano, K., Suzuki, T., Delgado-Escueta, A. V., and Yamakawa, K. (2001) Regional and developmental expression of Epm2a gene and its evolutionary conservation. *Biochem Biophys Res Commun* **283**, 1046-1053

94. Fernandez-Sanchez, M. E., Criado-Garcia, O., Heath, K. E., Garcia-Fojeda, B., Medrano-Fernandez, I., Gomez-Garre, P., Sanz, P., Serratosa, J. M., and Rodriguez de Cordoba, S. (2003) Laforin, the dual-phosphatase responsible for Lafora disease, interacts with R5 (PTG), a regulatory subunit of protein phosphatase-1 that enhances glycogen accumulation. *Hum Mol Genet* **12**, 3161-3171

95. Gomez-Garre, P., Sanz, Y., Rodriguez De Cordoba, S. R., and Serratosa, J. M. (2000) Mutational spectrum of the EPM2A gene in progressive

myoclonus epilepsy of Lafora: high degree of allelic heterogeneity and prevalence of deletions. *Eur J Hum Genet* **8**, 946-954

96. Ganesh, S., Delgado-Escueta, A. V., Suzuki, T., Francheschetti, S., Riggio, C., Avanzini, G., Rabinowicz, A., Bohlega, S., Bailey, J., Alonso, M. E., Rasmussen, A., Thomson, A. E., Ochoa, A., Prado, A. J., Medina, M. T., and Yamakawa, K. (2002) Genotype-phenotype correlations for EPM2A mutations in Lafora's progressive myoclonus epilepsy: exon 1 mutations associate with an early-onset cognitive deficit subphenotype. *Hum Mol Genet* **11**, 1263-1271

97. Chan, E. M., Bulman, D. E., Paterson, A. D., Turnbull, J., Andermann, E., Andermann, F., Rouleau, G. A., Delgado-Escueta, A. V., Scherer, S. W., and Minassian, B. A. (2003) Genetic mapping of a new Lafora progressive myoclonus epilepsy locus (EPM2B) on 6p22. *J Med Genet* **40**, 671-675

98. Freemont, P. S. (2000) RING for destruction? *Curr Biol* **10**, R84-87

99. Pickart, C. M. (2001) Mechanisms underlying ubiquitination. *Annu Rev Biochem* **70**, 503-533

100. Edwards, T. A., Wilkinson, B. D., Wharton, R. P., and Aggarwal, A. K. (2003) Model of the brain tumor-Pumilio translation repressor complex. *Genes Dev* **17**, 2508-2513

101. Gentry, M. S., Worby, C. A., and Dixon, J. E. (2005) Insights into Lafora disease: malin is an E3 ubiquitin ligase that ubiquitinates and promotes the degradation of laforin. *Proc Natl Acad Sci U S A* **102**, 8501-8506

102. Gentry, M. S., Dixon, J. E., and Worby, C. A. (2009) Lafora disease: insights into neurodegeneration from plant metabolism. *Trends Biochem Sci* **34**, 628-639

103. Gentry, M. S., Dowen, R. H., 3rd, Worby, C. A., Mattoo, S., Ecker, J. R., and Dixon, J. E. (2007) The phosphatase laforin crosses evolutionary boundaries and links carbohydrate metabolism to neuronal disease. *J Cell Biol* **178**, 477-488

104. Gentry, M. S., and Pace, R. M. (2009) Conservation of the glucan phosphatase laforin is linked to rates of molecular evolution and the glucan metabolism of the organism. *BMC Evol Biol* **9**, 138

105. Gentry, M. S., Roma-Mateo, C., and Sanz, P. (2013) Laforin, a protein with many faces: glucan phosphatase, adapter protein, et alii. *FEBS J* **280**, 525-537

106. Niittyla, T., Comparot-Moss, S., Lue, W. L., Messerli, G., Trevisan, M., Seymour, M. D., Gatehouse, J. A., Villadsen, D., Smith, S. M., Chen, J., Zeeman, S. C., and Smith, A. M. (2006) Similar protein phosphatases control starch metabolism in plants and glycogen metabolism in mammals. *J Biol Chem* **281**, 11815-11818

107. Roma-Mateo, C., Moreno, D., Vernia, S., Rubio, T., Bridges, T. M., Gentry, M. S., and Sanz, P. (2011) Lafora disease E3-ubiquitin ligase malin is related to TRIM32 at both the phylogenetic and functional level. *BMC Evol Biol* **11**, 225

108. DePaoli-Roach, A. A., Tagliabracci, V. S., Segvich, D. M., Meyer, C. M., Irimia, J. M., and Roach, P. J. (2010) Genetic depletion of the malin E3

ubiquitin ligase in mice leads to lafora bodies and the accumulation of insoluble laforin. *J Biol Chem* **285**, 25372-25381

109. Ganesh, S., Delgado-Escueta, A. V., Sakamoto, T., Avila, M. R., Machado-Salas, J., Hoshii, Y., Akagi, T., Gomi, H., Suzuki, T., Amano, K., Agarwala, K. L., Hasegawa, Y., Bai, D. S., Ishihara, T., Hashikawa, T., Itohara, S., Cornford, E. M., Niki, H., and Yamakawa, K. (2002) Targeted disruption of the Epm2a gene causes formation of Lafora inclusion bodies, neurodegeneration, ataxia, myoclonus epilepsy and impaired behavioral response in mice. *Hum Mol Genet* **11**, 1251-1262

110. Turnbull, J., Wang, P., Girard, J. M., Ruggieri, A., Wang, T. J., Draginov, A. G., Kameka, A. P., Pencea, N., Zhao, X., Ackerley, C. A., and Minassian, B. A. (2010) Glycogen hyperphosphorylation underlies lafora body formation. *Ann Neurol* **68**, 925-933

111. Machado-Salas, J., Avila-Costa, M. R., Guevara, P., Guevara, J., Duron, R. M., Bai, D., Tanaka, M., Yamakawa, K., and Delgado-Escueta, A. V. (2012) Ontogeny of Lafora bodies and neurocytoskeleton changes in Laforin-deficient mice. *Exp Neurol* **236**, 131-140

112. Criado, O., Aguado, C., Gayarre, J., Duran-Trio, L., Garcia-Cabrero, A. M., Vernia, S., San Millan, B., Heredia, M., Roma-Mateo, C., Mouron, S., Juana-Lopez, L., Dominguez, M., Navarro, C., Serratosa, J. M., Sanchez, M., Sanz, P., Bovolenta, P., Knecht, E., and Rodriguez de Cordoba, S. (2012) Lafora bodies and neurological defects in malin-deficient mice correlate with impaired autophagy. *Hum Mol Genet* **21**, 1521-1533

113. Valles-Ortega, J., Duran, J., Garcia-Rocha, M., Bosch, C., Saez, I., Pujadas, L., Serafin, A., Canas, X., Soriano, E., Delgado-Garcia, J. M., Gruart, A., and Guinovart, J. J. (2011) Neurodegeneration and functional impairments associated with glycogen synthase accumulation in a mouse model of Lafora disease. *EMBO Mol Med* **3**, 667-681

114. Garcia-Cabrero, A. M., Marinas, A., Guerrero, R., de Cordoba, S. R., Serratosa, J. M., and Sanchez, M. P. (2012) Laforin and malin deletions in mice produce similar neurologic impairments. *J Neuropathol Exp Neurol* **71**, 413-421

115. Lohi, H., Ianzano, L., Zhao, X. C., Chan, E. M., Turnbull, J., Scherer, S. W., Ackerley, C. A., and Minassian, B. A. (2005) Novel glycogen synthase kinase 3 and ubiquitination pathways in progressive myoclonus epilepsy. *Hum Mol Genet* **14**, 2727-2736

116. Worby, C. A., Gentry, M. S., and Dixon, J. E. (2006) Laforin, a dual specificity phosphatase that dephosphorylates complex carbohydrates. *J Biol Chem* **281**, 30412-30418

117. Solaz-Fuster, M. C., Gimeno-Alcaniz, J. V., Ros, S., Fernandez-Sanchez, M. E., Garcia-Fojeda, B., Criado Garcia, O., Vilchez, D., Dominguez, J., Garcia-Rocha, M., Sanchez-Piris, M., Aguado, C., Knecht, E., Serratosa, J., Guinovart, J. J., Sanz, P., and Rodriguez de Cordoba, S. (2008) Regulation of glycogen synthesis by the laforin-malin complex is modulated by the AMP-activated protein kinase pathway. *Hum Mol Genet* **17**, 667-678

118. Wang, Y., Liu, Y., Wu, C., Zhang, H., Zheng, X., Zheng, Z., Geiger, T. L., Nuovo, G. J., Liu, Y., and Zheng, P. (2006) Epm2a suppresses tumor growth in an immunocompromised host by inhibiting Wnt signaling. *Cancer Cell* **10**, 179-190

119. Wang, W., Lohi, H., Skurat, A. V., DePaoli-Roach, A. A., Minassian, B. A., and Roach, P. J. (2007) Glycogen metabolism in tissues from a mouse model of Lafora disease. *Arch Biochem Biophys* **457**, 264-269

120. Komatsu, M., Waguri, S., Chiba, T., Murata, S., Iwata, J., Tanida, I., Ueno, T., Koike, M., Uchiyama, Y., Kominami, E., and Tanaka, K. (2006) Loss of autophagy in the central nervous system causes neurodegeneration in mice. *Nature* **441**, 880-884

121. Aguado, C., Sarkar, S., Korolchuk, V. I., Criado, O., Vernia, S., Boya, P., Sanz, P., de Cordoba, S. R., Knecht, E., and Rubinsztein, D. C. (2010) Laforin, the most common protein mutated in Lafora disease, regulates autophagy. *Hum Mol Genet* **19**, 2867-2876

122. Deshaies, R. J., and Joazeiro, C. A. (2009) RING domain E3 ubiquitin ligases. *Annu Rev Biochem* **78**, 399-434

123. Ye, Y., and Rape, M. (2009) Building ubiquitin chains: E2 enzymes at work. *Nat Rev Mol Cell Biol* **10**, 755-764

124. Haglund, K., and Dikic, I. (2005) Ubiquitylation and cell signaling. *EMBO J* **24**, 3353-3359

125. Cheng, A., Zhang, M., Gentry, M. S., Worby, C. A., Dixon, J. E., and Saltiel, A. R. (2007) A role for AGL ubiquitination in the glycogen storage disorders of Lafora and Cori's disease. *Genes Dev* **21**, 2399-2409

126. Vilchez, D., Ros, S., Cifuentes, D., Pujadas, L., Valles, J., Garcia-Fojeda, B., Criado-Garcia, O., Fernandez-Sanchez, E., Medrano-Fernandez, I., Dominguez, J., Garcia-Rocha, M., Soriano, E., Rodriguez de Cordoba, S., and Guinovart, J. J. (2007) Mechanism suppressing glycogen synthesis in neurons and its demise in progressive myoclonus epilepsy. *Nat Neurosci* **10**, 1407-1413

127. Worby, C. A., Gentry, M. S., and Dixon, J. E. (2008) Malin decreases glycogen accumulation by promoting the degradation of protein targeting to glycogen (PTG). *J Biol Chem* **283**, 4069-4076

128. Sharma, J., Rao, S. N., Shankar, S. K., Satishchandra, P., and Jana, N. R. (2011) Lafora disease ubiquitin ligase malin promotes proteasomal degradation of neuronatin and regulates glycogen synthesis. *Neurobiol Dis* **44**, 133-141

129. Garyali, P., Siwach, P., Singh, P. K., Puri, R., Mittal, S., Sengupta, S., Parihar, R., and Ganesh, S. (2009) The malin-laforin complex suppresses the cellular toxicity of misfolded proteins by promoting their degradation through the ubiquitin-proteasome system. *Hum Mol Genet* **18**, 688-700

130. Tsai, Y. C., Fishman, P. S., Thakor, N. V., and Oyler, G. A. (2003) Parkin facilitates the elimination of expanded polyglutamine proteins and leads to preservation of proteasome function. *J Biol Chem* **278**, 22044-22055

131. Jana, N. R., Dikshit, P., Goswami, A., Kotliarova, S., Murata, S., Tanaka, K., and Nukina, N. (2005) Co-chaperone CHIP associates with expanded

polyglutamine protein and promotes their degradation by proteasomes. *J Biol Chem* **280**, 11635-11640

132. Ishigaki, S., Niwa, J., Yamada, S., Takahashi, M., Ito, T., Sone, J., Doyu, M., Urano, F., and Sobue, G. (2007) Dorfin-CHIP chimeric proteins potently ubiquitylate and degrade familial ALS-related mutant SOD1 proteins and reduce their cellular toxicity. *Neurobiol Dis* **25**, 331-341

133. Mishra, A., Dikshit, P., Purkayastha, S., Sharma, J., Nukina, N., and Jana, N. R. (2008) E6-AP promotes misfolded polyglutamine proteins for proteasomal degradation and suppresses polyglutamine protein aggregation and toxicity. *J Biol Chem* **283**, 7648-7656

134. Polajnar, M., and Zerovnik, E. (2011) Impaired autophagy: a link between neurodegenerative diseases and progressive myoclonus epilepsies. *Trends Mol Med* **17**, 293-300

135. Vernia, S., Rubio, T., Heredia, M., Rodriguez de Cordoba, S., and Sanz, P. (2009) Increased endoplasmic reticulum stress and decreased proteasomal function in lafora disease models lacking the phosphatase laforin. *PLoS One* **4**, e5907

136. Puri, R., Suzuki, T., Yamakawa, K., and Ganesh, S. (2012) Dysfunctions in endosomal-lysosomal and autophagy pathways underlie neuropathology in a mouse model for Lafora disease. *Hum Mol Genet* **21**, 175-184

137. Rao, S. N., Sharma, J., Maity, R., and Jana, N. R. (2010) Co-chaperone CHIP stabilizes aggregate-prone malin, a ubiquitin ligase mutated in Lafora disease. *J Biol Chem* **285**, 1404-1413

138. Sengupta, S., Badhwar, I., Upadhyay, M., Singh, S., and Ganesh, S. (2011) Malin and laforin are essential components of a protein complex that protects cells from thermal stress. *J Cell Sci* **124**, 2277-2286

139. Sharma, J., Mulherkar, S., Mukherjee, D., and Jana, N. R. (2012) Malin regulates Wnt signaling pathway through degradation of dishevelled2. *J Biol Chem* **287**, 6830-6839

140. Turnbull, J., DePaoli-Roach, A. A., Zhao, X., Cortez, M. A., Pencea, N., Tiberia, E., Piliguian, M., Roach, P. J., Wang, P., Ackerley, C. A., and Minassian, B. A. (2011) PTG depletion removes Lafora bodies and rescues the fatal epilepsy of Lafora disease. *PLoS Genet* **7**, e1002037

141. Pederson, B. A., Turnbull, J., Epp, J. R., Weaver, S. A., Zhao, X., Pencea, N., Roach, P. J., Frankland, P., Ackerley, C. A., and Minassian, B. A. (2013) Inhibiting glycogen synthesis prevents lafora disease in a mouse model. *Ann Neurol*

142. Duran, J., Gruart, A., Garcia-Rocha, M., Delgado-Garcia, J. M., and Guinovart, J. J. (2014) Glycogen accumulation underlies neurodegeneration and autophagy impairment in Lafora disease. *Hum Mol Genet*

143. DePaoli-Roach, A. A., Segvich, D. M., Meyer, C. M., Rahimi, Y., Worby, C. A., Gentry, M. S., and Roach, P. J. (2012) Laforin and malin knockout mice have normal glucose disposal and insulin sensitivity. *Hum Mol Genet* **21**, 1604-1610

144. Bradford, M. M. (1976) A rapid and sensitive method for the quantitation of microgram quantities of protein utilizing the principle of protein-dye binding. *Anal Biochem* **72**, 248-254

145. Akopian, T. N., Kisselev, A. F., and Goldberg, A. L. (1997) Processive degradation of proteins and other catalytic properties of the proteasome from Thermoplasma acidophilum. *J Biol Chem* **272**, 1791-1798

146. Suzuki, Y., Lanner, C., Kim, J. H., Vilardo, P. G., Zhang, H., Yang, J., Cooper, L. D., Steele, M., Kennedy, A., Bock, C. B., Scrimgeour, A., Lawrence, J. C., Jr., and DePaoli-Roach, A. A. (2001) Insulin control of glycogen metabolism in knockout mice lacking the muscle-specific protein phosphatase PP1G/RGL. *Mol Cell Biol* **21**, 2683-2694

147. Bergmeyer, H. U. (1974) *Methods of Enzymatic Analysis*, 2nd English ed., Academic Press, New York

148. Boersema, P. J., Raijmakers, R., Lemeer, S., Mohammed, S., and Heck, A. J. (2009) Multiplex peptide stable isotope dimethyl labeling for quantitative proteomics. *Nat Protoc* **4**, 484-494

149. Wolters, D. A., Washburn, M. P., and Yates, J. R., 3rd. (2001) An automated multidimensional protein identification technology for shotgun proteomics. *Anal Chem* **73**, 5683-5690

150. Giddings, J. C. (1984) Two-dimensional separations: concept and promise. *Anal Chem* **56**, 1258A-1260A, 1262A, 1264A passim

151. Mosley, A. L., Hunter, G. O., Sardiu, M. E., Smolle, M., Workman, J. L., Florens, L., and Washburn, M. P. (2013) Quantitative proteomics demonstrates that the RNA polymerase II subunits Rpb4 and Rpb7 dissociate during transcriptional elongation. *Mol Cell Proteomics* **12**, 1530-1538

152. Yates, J. R., 3rd. (2004) Mass spectral analysis in proteomics. *Annu Rev Biophys Biomol Struct* **33**, 297-316

153. Makarov, A., Denisov, E., Lange, O., and Horning, S. (2006) Dynamic range of mass accuracy in LTQ Orbitrap hybrid mass spectrometer. *J Am Soc Mass Spectrom* **17**, 977-982

154. Michalski, A., Damoc, E., Hauschild, J. P., Lange, O., Wieghaus, A., Makarov, A., Nagaraj, N., Cox, J., Mann, M., and Horning, S. (2011) Mass spectrometry-based proteomics using Q Exactive, a high-performance benchtop quadrupole Orbitrap mass spectrometer. *Mol Cell Proteomics* **10**, M111 011015

155. Paradela, A., and Albar, J. P. (2008) Advances in the analysis of protein phosphorylation. *J Proteome Res* **7**, 1809-1818

156. Smith-Kinnaman, W. R., Berna, M. J., Hunter, G. O., True, J. D., Hsu, P., Cabello, G. I., Fox, M. J., Varani, G., and Mosley, A. L. (2014) The interactome of the atypical phosphatase Rtr1 in Saccharomyces cerevisiae. *Mol Biosyst* **10**, 1730-1741

157. Frank, A. M. (2009) A ranking-based scoring function for peptide-spectrum matches. *J Proteome Res* **8**, 2241-2252

158. Kim, W., Bennett, E. J., Huttlin, E. L., Guo, A., Li, J., Possemato, A., Sowa, M. E., Rad, R., Rush, J., Comb, M. J., Harper, J. W., and Gygi, S.

P. (2011) Systematic and quantitative assessment of the ubiquitin-modified proteome. *Mol Cell* **44**, 325-340

159. Sarraf, S. A., Raman, M., Guarani-Pereira, V., Sowa, M. E., Huttlin, E. L., Gygi, S. P., and Harper, J. W. (2013) Landscape of the PARKIN-dependent ubiquitylome in response to mitochondrial depolarization. *Nature* **496**, 372-376

160. Pederson, B. A., Chen, H., Schroeder, J. M., Shou, W., DePaoli-Roach, A. A., and Roach, P. J. (2004) Abnormal cardiac development in the absence of heart glycogen. *Mol Cell Biol* **24**, 7179-7187

161. Pederson, B. A., Cope, C. R., Irimia, J. M., Schroeder, J. M., Thurberg, B. L., Depaoli-Roach, A. A., and Roach, P. J. (2005) Mice with elevated muscle glycogen stores do not have improved exercise performance. *Biochem Biophys Res Commun* **331**, 491-496

162. Pederson, B. A., Schroeder, J. M., Parker, G. E., Smith, M. W., DePaoli-Roach, A. A., and Roach, P. J. (2005) Glucose metabolism in mice lacking muscle glycogen synthase. *Diabetes* **54**, 3466-3473

163. Rubinsztein, D. C. (2006) The roles of intracellular protein-degradation pathways in neurodegeneration. *Nature* **443**, 780-786

164. Ardley, H. C., Hung, C. C., and Robinson, P. A. (2005) The aggravating role of the ubiquitin-proteasome system in neurodegeneration. *FEBS Lett* **579**, 571-576

165. Hershko, A. (1983) Ubiquitin: roles in protein modification and breakdown. *Cell* **34**, 11-12

166. Ravikumar, B., Duden, R., and Rubinsztein, D. C. (2002) Aggregate-prone proteins with polyglutamine and polyalanine expansions are degraded by autophagy. *Hum Mol Genet* **11**, 1107-1117

167. Kopito, R. R. (2000) Aggresomes, inclusion bodies and protein aggregation. *Trends Cell Biol* **10**, 524-530

168. Seki, T., Takahashi, H., Adachi, N., Abe, N., Shimahara, T., Saito, N., and Sakai, N. (2007) Aggregate formation of mutant protein kinase C gamma found in spinocerebellar ataxia type 14 impairs ubiquitin-proteasome system and induces endoplasmic reticulum stress. *Eur J Neurosci* **26**, 3126-3140

169. Tanida, I., Minematsu-Ikeguchi, N., Ueno, T., and Kominami, E. (2005) Lysosomal turnover, but not a cellular level, of endogenous LC3 is a marker for autophagy. *Autophagy* **1**, 84-91

170. Ravikumar, B., Futter, M., Jahreiss, L., Korolchuk, V. I., Lichtenberg, M., Luo, S., Massey, D. C., Menzies, F. M., Narayanan, U., Renna, M., Jimenez-Sanchez, M., Sarkar, S., Underwood, B., Winslow, A., and Rubinsztein, D. C. (2009) Mammalian macroautophagy at a glance. *J Cell Sci* **122**, 1707-1711

171. Noda, T., and Ohsumi, Y. (1998) Tor, a phosphatidylinositol kinase homologue, controls autophagy in yeast. *J Biol Chem* **273**, 3963-3966

172. Scott, R. C., Schuldiner, O., and Neufeld, T. P. (2004) Role and regulation of starvation-induced autophagy in the Drosophila fat body. *Dev Cell* **7**, 167-178

173. Zinszner, H., Kuroda, M., Wang, X., Batchvarova, N., Lightfoot, R. T., Remotti, H., Stevens, J. L., and Ron, D. (1998) CHOP is implicated in programmed cell death in response to impaired function of the endoplasmic reticulum. *Genes Dev* **12**, 982-995

174. Bunkenborg, J., Garcia, G. E., Paz, M. I., Andersen, J. S., and Molina, H. (2010) The minotaur proteome: avoiding cross-species identifications deriving from bovine serum in cell culture models. *Proteomics* **10**, 3040-3044

175. Oravcova, J., Bohs, B., and Lindner, W. (1996) Drug-protein binding sites. New trends in analytical and experimental methodology. *J Chromatogr B Biomed Appl* **677**, 1-28

176. Wright, D. E., Wang, C. Y., and Kao, C. F. (2012) Histone ubiquitylation and chromatin dynamics. *Front Biosci (Landmark Ed)* **17**, 1051-1078

177. Wang, H., Wang, L., Erdjument-Bromage, H., Vidal, M., Tempst, P., Jones, R. S., and Zhang, Y. (2004) Role of histone H2A ubiquitination in Polycomb silencing. *Nature* **431**, 873-878

178. Olsen, J. V., Macek, B., Lange, O., Makarov, A., Horning, S., and Mann, M. (2007) Higher-energy C-trap dissociation for peptide modification analysis. *Nat Methods* **4**, 709-712

179. Huang da, W., Sherman, B. T., and Lempicki, R. A. (2009) Systematic and integrative analysis of large gene lists using DAVID bioinformatics resources. *Nat Protoc* **4**, 44-57

180. Hsu, J. L., Huang, S. Y., Chow, N. H., and Chen, S. H. (2003) Stable-isotope dimethyl labeling for quantitative proteomics. *Anal Chem* **75**, 6843-6852

181. Maere, S., Heymans, K., and Kuiper, M. (2005) BiNGO: a Cytoscape plugin to assess overrepresentation of gene ontology categories in biological networks. *Bioinformatics* **21**, 3448-3449

182. Montojo, J., Zuberi, K., Rodriguez, H., Kazi, F., Wright, G., Donaldson, S. L., Morris, Q., and Bader, G. D. (2010) GeneMANIA Cytoscape plugin: fast gene function predictions on the desktop. *Bioinformatics* **26**, 2927-2928

183. Delgado-Escueta, A. V. (2007) Advances in genetics of juvenile myoclonic epilepsies. *Epilepsy Curr* **7**, 61-67

184. Ganesh, S., Tsurutani, N., Suzuki, T., Hoshii, Y., Ishihara, T., Delgado-Escueta, A. V., and Yamakawa, K. (2004) The carbohydrate-binding domain of Lafora disease protein targets Lafora polyglucosan bodies. *Biochem Biophys Res Commun* **313**, 1101-1109

185. Wang, W., Parker, G. E., Skurat, A. V., Raben, N., DePaoli-Roach, A. A., and Roach, P. J. (2006) Relationship between glycogen accumulation and the laforin dual specificity phosphatase. *Biochem Biophys Res Commun* **350**, 588-592

186. Moreno, D., Towler, M. C., Hardie, D. G., Knecht, E., and Sanz, P. (2010) The laforin-malin complex, involved in Lafora disease, promotes the incorporation of K63-linked ubiquitin chains into AMP-activated protein kinase beta subunits. *Mol Biol Cell* **21**, 2578-2588

187. Mittal, S., Dubey, D., Yamakawa, K., and Ganesh, S. (2007) Lafora disease proteins malin and laforin are recruited to aggresomes in response to proteasomal impairment. *Hum Mol Genet* **16**, 753-762

188. Turnbull, J., Epp, J. R., Goldsmith, D., Zhao, X., Pencea, N., Wang, P., Frankland, P. W., Ackerley, C. A., and Minassian, B. A. (2014) PTG depletion rescues malin-deficient Lafora disease in mouse. *Ann Neurol*

189. Bantscheff, M., Schirle, M., Sweetman, G., Rick, J., and Kuster, B. (2007) Quantitative mass spectrometry in proteomics: a critical review. *Anal Bioanal Chem* **389**, 1017-1031

190. Boersema, P. J., Foong, L. Y., Ding, V. M., Lemeer, S., van Breukelen, B., Philp, R., Boekhorst, J., Snel, B., den Hertog, J., Choo, A. B., and Heck, A. J. (2010) In-depth qualitative and quantitative profiling of tyrosine phosphorylation using a combination of phosphopeptide immunoaffinity purification and stable isotope dimethyl labeling. *Mol Cell Proteomics* **9**, 84-99

191. De Baere, I., Derua, R., Janssens, V., Van Hoof, C., Waelkens, E., Merlevede, W., and Goris, J. (1999) Purification of porcine brain protein phosphatase 2A leucine carboxyl methyltransferase and cloning of the human homologue. *Biochemistry* **38**, 16539-16547

192. Tolstykh, T., Lee, J., Vafai, S., and Stock, J. B. (2000) Carboxyl methylation regulates phosphoprotein phosphatase 2A by controlling the association of regulatory B subunits. *EMBO J* **19**, 5682-5691

193. Longin, S., Zwaenepoel, K., Martens, E., Louis, J. V., Rondelez, E., Goris, J., and Janssens, V. (2008) Spatial control of protein phosphatase 2A (de)methylation. *Exp Cell Res* **314**, 68-81

194. Lee, J. A., and Pallas, D. C. (2007) Leucine carboxyl methyltransferase-1 is necessary for normal progression through mitosis in mammalian cells. *J Biol Chem* **282**, 30974-30984

195. Sontag, J. M., Nunbhakdi-Craig, V., and Sontag, E. (2013) Leucine carboxyl methyltransferase 1 (LCMT1)-dependent methylation regulates the association of protein phosphatase 2A and Tau protein with plasma membrane microdomains in neuroblastoma cells. *J Biol Chem* **288**, 27396-27405

196. Sontag, E., Hladik, C., Montgomery, L., Luangpirom, A., Mudrak, I., Ogris, E., and White, C. L., 3rd. (2004) Downregulation of protein phosphatase 2A carboxyl methylation and methyltransferase may contribute to Alzheimer disease pathogenesis. *J Neuropathol Exp Neurol* **63**, 1080-1091

197. Jackson, J. B., and Pallas, D. C. (2012) Circumventing cellular control of PP2A by methylation promotes transformation in an Akt-dependent manner. *Neoplasia* **14**, 585-599

CURRICULUM VITAE

Punitee Garyali

EDUCATION

1999-2005	M.B.B.S. Mahatma Gandhi Institute of Medical Sciences, Sewagram, India
2006-2008	M.Tech. Biological Sciences and Bioengineering Indian Institute of Technology, Kanpur, India
2009-2014	Ph.D. Biochemistry and Molecular Biology, Indiana University, Indianapolis, IN

RESEARCH AND TRAINING EXPERIENCE

2005-2006	Practicing Physician: Bee Enn Charitable Hospital, Jammu, India
2006-2008	Graduate Research Assistant: Indian Institute of Technology Kanpur, Laboratory of Dr. Subramanian. Ganesh.
2008-2009	Technical Trainee: Dr. Reddy's Laboratories, Hyderabad, India.
2009-2014	Graduate Research Assistant: Indiana University School of Medicine. Laboratory of Dr. Peter Roach.

HONORS AND AWARDS

1999	Merit Scholarship by National Scholarship Scheme, Government of NCT, Delhi, India
1999	6th Rank in All-India Medical Entrance Examination, Mahatma Gandhi Institute of Medical Sciences, India
2000	University Award in Biochemistry
2000	1st Rank in Seminar of Academy of Basic Medical Sciences, Sewagram
2000-2002	Honors in Biochemistry, Microbiology, Pharmacology, Forensic Medicine
2003	Completed Problem Solving for Better Health sponsored by Dreyfus Health Foundation, New York, USA and Health Action by People, Thiruvananthpuram, India, Mahatma Gandhi Institute of Medical Sciences, Sewagram, India.
2004	Completed training in Basic Neonatal Care and Resuscitation, Sewagram, India
2006-2008	Research Assistantship by Department of Biotechnology, Government of India.
2009-2010	Fellowship by IBMG, Indiana University
2010-2014	Research Assistantship, Indiana University

2014   Erica Daniel Kepner Award for Scientific Achievement, Indiana University-Honorable Mention Award

SERVICES

2011-2013   IUSM Graduate Student Mentor Program

CONFERENCES ATTENDED

1. Continuing Medical Education (CME), Physiology and Pathology, Mahatma Gandhi Institute of Medical Sciences, Sewagram, India, 2000
2. Problem Solving for Better Health Problem Solving for Better Health sponsored by Dreyfus Health Foundation, New York, USA and Health Action by People, Thiruvananthpuram, India, Mahatma Gandhi Institute of Medical Sciences, Sewagram, India, 2003
3. Brain Awareness Symposium, Indian Institute of Technology, Kanpur, India, 2007
4. The laforin-malin complex suppresses the cellular toxicity of misfolded proteins implicated in neurological disorders. **Garyali, P.**, Siwach, P., Singh, Ganesh, S. All India Cell Biology Conference BHU, Varanasi, 2007
5. EMBO International Workshop on development and disease, Indian Institute of Technology Kanpur, India, 2008
6. Role of malin E3 Ubiquitin Ligase in Lafora disease. **Garyali, P.**, Roach, P.J. Biochemistry Retreat, Indiana University, 2012

PUBLICATIONS

1. **Garyali, P.**, Siwach, P., Singh, P.K., Puri, R., Mittal, S., Sengupta, S., Parihar, R., Ganesh, S. 2009. The malin-laforin complex suppresses the cellular toxicity of misfolded proteins by promoting their degradation through the ubiquitin-proteasomal system. *Human Molecular Genetics.* 18 (4): 688-700.
2. **Garyali, P.,** Segvich, D.M., DePaoli-Roach, A.A., Roach, P.J. 2014. Protein degradation and quality control in cells from laforin and malin knockout mice. *Journal of Biological Chemistry*. Published online on June 9, *in press*.
3. **Garyali, P.,** DePaoli-Roach, A.A., Roach, P.J., Mosley, A.L. Mouse skeletal muscle ubiquitin proteome. *Manuscript in preparation*.
4. **Garyali, P.,** Mosley, A.L. Proteomic analysis of enriched diGly peptides. *Manuscript in preparation*.
5. DePaoli-Roach, A.A., Contreras, C., Segvich, D.M., **Garyali, P.,** Roach, P.J. Decreased glycogen accumulation in *Epm2a* and *Epm2b* knockout mice abolishes lafora bodies and restores neuronal, proteosome and autophagy functions. *Manuscript in preparation*.